

L
2010

LIBRARY
Michigan State
University

This is to certify that the
dissertation entitled

ORTHOGONAL DECOMPOSITION METHODS FOR
MODAL ANALYSIS

presented by

UMAR FAROOQ

has been accepted towards fulfillment
of the requirements for the

Ph.D. degree in Mechanical Engineering



Major Professor's Signature

12/18/2009

Date

MSU is an Affirmative Action/Equal Opportunity Employer

PLACE IN RETURN BOX to remove this checkout from your record.
TO AVOID FINES return on or before date due.
MAY BE RECALLED with earlier due date if requested.

DATE DUE	DATE DUE	DATE DUE

ORTHOGONAL DECOMPOSITION METHODS FOR MODAL ANALYSIS

By

Umar Farooq

A DISSERTATION

Submitted to
Michigan State University
in partial fulfillment of the requirements
for the degree of

DOCTOR OF PHILOSOPHY

Mechanical Engineering

2009

ABSTRACT

ORTHOGONAL DECOMPOSITION METHODS FOR MODAL ANALYSIS

By

Umar Farooq

The output-only class of experimental modal analysis has recently gained tremendous popularity. The distinct advantage of using these methods is the measurement of responses only, without the need of input measurements. On the other hand, the proper orthogonal decomposition (POD) for some time, has been recognized as a standard empirical modal analysis scheme. This work is an attempt to apply some generalizations of POD to tie the gap between output-only modal analysis and decomposition methods.

The state-variable modal decomposition (SVMD) is a generalization of POD method developed in this work. It enables frequency, damping, and mode-shape estimations from free-response ensemble data for generally damped linear multi-degree-of-freedom systems. The method extracts modal parameter information from an eigenvalue problem that is formed by correlations of state-variable ensembles. Numerical simulations are presented to show the method's efficacy for a broad range of damping levels present in the systems.

The smooth orthogonal method (SOD) is another generalization of the POD method that has shown good parameter estimation characteristics from free responses in the past. Extension of the SOD and SVMD decomposition methods for randomly excited systems is also addressed in this work. This work shows that the SOD and SVMD eigenvalue problems formulated from white noise induced response data can be tied to the unforced structural eigenvalue problem, and thus can be used for modal parameter estimation. Numerical simulations for lightly damped vibratory system are

explored. Simulations show that for light damping, satisfactory results are obtained for estimating both system frequencies and modal vectors.

Experimental investigation of the SVMD method for the free response case is conducted in order to help understand practical considerations regarding the method. Using various experimental setups, issues related to optimal data-length and filter settings are explored. Modal coordinates are evaluated, together with modal vectors/frequencies, to qualitatively eliminate the spurious modes obtained during decomposition.

The decomposition quality is quantified next by means of two new tools. The spectrum assurance and the spectrum difference criteria are first evaluated on numerical examples. These methods are then investigated in real life experiments to quantify the quality of modal coordinates and identification results. We observe that both tools used together help establish the true system modes and eliminate spurious modes. The effect of time record length used in the identification process is studied via numerical examples.

Lastly, a comparison of decomposition based methods is made with the common time-domain identification schemes using numerical simulations as well as actual experiments. While the comparison highlights the strengths and weaknesses of the compared methods, it also shows that the orthogonal decomposition based methods are, in essence, equally competitive with the time-domain methods.

Dedicated to
To the greatest Gift of God to the world,
Prophet Muhammad (SAWW)
To my parents, for their unconditional and imperishable love,
My parents Sahibzada Ishtiaq Hussain and Mrs. Shaheen Ishtiaq
My nieces Huda and Warda

ACKNOWLEDGMENTS

This work would not have been possible had my advisor Dr. Brian Feeny not inspired me to do so. I would like to extend my deepest and fondest gratitude to him for his support, encouragement and tutelage through thick and thin during this journey.

My guidance committee deserves special appreciation. I am indebted to Dr. Hassan Khalil, Dr. Alan Haddow, and Dr. Steve Shaw for their time, help and useful suggestions to bring improvements in this work.

I would like to thank my late grandfathers Sahibzada Irshad Hussain and Sahibzada Mushtaq Hussain, and my siblings Yasir Waqas and Huma Ishtiaq for their unflagging support and continuous prayers that has helped me survived through the hard times.

I would also like to thank my friends and colleagues for their endless support during my years at Michigan State University. I value the friendship of Shahin Nudehi, Elliot Motato, Jeff Rhoads, Jimmy Issa, Nick Miller and Brian Olson and cherish the technical discussions with them.

A word of thank for Dr. Gökcek who instilled in me the importance of writing technical papers. I appreciate his guidance in that matter.

I would also like to thank Dr. David Chelidze for introducing the beautiful SOD scheme to me that was motivation of this work.

Last but not the least, I would like to thank our graduate secretary Aida Montalvo, and my room mates M. Waqas Ali and Farooq Rauf for their help and support.

TABLE OF CONTENTS

LIST OF TABLES	x
LIST OF FIGURES	xii
1 Introduction	1
1.1 Background	1
1.1.1 Analytical modal analysis	2
1.1.2 Experimental modal analysis	3
1.1.3 Classification of signals	3
1.2 Output-only modal analysis	4
1.3 Proper orthogonal decomposition and output-only time domain methods	5
1.4 Preview of this thesis	7
1.5 Contributions of this work	10
2 State Variable Modal Decomposition of Free Responses	13
2.1 Introduction	13
2.2 Nonsymmetric state-variable modal decomposition	14
2.2.1 State-variable linear vibration model	14
2.2.2 Decomposition strategy	15
2.3 Numerical examples	17
2.3.1 Proportionally damped example	18
2.3.2 Generally damped example	19
2.3.3 Step size selection	20
2.4 Robustness under noise	21
2.5 Summary	25
3 Random Response	27
3.1 Introduction	27
3.2 Smooth orthogonal decomposition	28
3.2.1 Smooth orthogonal decomposition and modal analysis for free vibration	28

3.2.2	Smooth orthogonal decomposition for systems under random excitation	30
3.2.2.1	Smooth orthogonal decomposition and random excitation	30
3.2.2.2	White noise	31
3.3	Numerical example	32
3.4	State-variable modal decomposition for systems under random excitation	38
3.4.1	State-variable modal decomposition and random excitation . .	38
3.4.2	Numerical example	40
3.5	Summary	42
4	Experimental Investigation	44
4.1	Introduction	44
4.1.1	Assumptions	45
4.2	A single-degree-of-freedom experiment	47
4.3	Clamped-free beam experiment	50
4.3.1	Filtering effects	54
4.3.2	Identification results	55
4.3.3	Modal coordinates	58
4.4	Limitations on the number of sensors and active modes	64
4.4.1	Sensitivity analysis	64
4.4.2	Numerical example	67
4.4.3	A free-free linear beam experiment	68
4.4.3.1	Identification by SVMMD	70
4.5	Summary	73
5	Quantitative Assessment of Identification	75
5.1	Use of modal coordinates to evaluate decomposition results	75
5.2	Quantitative assessment of modal coordinate FRF	77
5.2.1	Introduction	77
5.2.2	The spectrum assurance criterion (SAC)	77
5.2.3	Spectrum difference (SD)	78
5.3	Numerical simulations	79

5.3.1	Correct frequency and damping estimates in both FRFs, with noise contamination in one of the FRFs	80
5.3.2	Correct frequency in both FRFs, with incorrect damping in the tested FRF	82
5.3.3	Correct damping in both FRFs, with incorrect frequency in the tested FRF	84
5.3.4	Lightly damped vs. heavily damped systems	86
5.3.5	Summary of trends	88
5.4	Experimental data	90
5.4.1	Large sampling N=12,000	92
5.4.2	Smaller sampling N=1000	95
5.4.3	Comments and summary	99
5.5	Time record length	100
5.5.1	Results	101
5.5.1.1	High damping	101
5.5.1.2	Low damping	103
5.5.2	Summary of trends	104
5.6	Summary	106
6	Comparison with Other Identification Methods	110
6.1	Introduction	110
6.2	Time-domain modal identification methods	111
6.2.1	Ibrahim time domain method	111
6.2.2	Eigensystem realization algorithm	114
6.2.2.1	A note on obtaining Markov parameters in ERA	116
6.3	Numerical simulations	117
6.3.1	Free response: A three DOF discrete system example	117
6.3.1.1	Noise effects	119
6.3.2	Forced response: A sixteen DOF system example	120
6.3.2.1	Noise effects	121
6.4	Clamped-free cantilever beam experiment	123
6.4.1	Identification results	125
6.5	Summary	130

7	Conclusions	134
7.1	Synopsis	134
7.1.1	Free response	134
7.1.2	Random response	135
7.1.3	Experiments	136
7.1.4	Quantitative evaluation	136
7.1.5	Comparison to other methods	137
7.2	Recommendations for use of the decomposition methods	138
7.3	Future work	139
7.3.1	Damping estimation for random excitation	140
7.3.2	Continuous systems	140
7.3.3	Nonlinear systems	141
	BIBLIOGRAPHY	144

LIST OF TABLES

3.1	System frequencies estimated from smooth orthogonal decomposition (SOD) with white noise forcing compared against structural eigen frequencies in Eq. 3.3	33
3.2	Estimated SOD modes compared against system modes using the modal assurance criterion	34
3.3	Percentage error computation (SOD) for all modes	37
3.4	System frequencies estimated from state variable decomposition (SVMD) with white noise forcing compared against structural eigen frequencies in Eq. (3.3)	41
3.5	System damping ratios estimated from the state-variable decomposition (SVMD) with white noise forcing compared against structural damping ratios in Eq. (3.3)	42
4.1	Estimated modal parameters from the decomposition method compared against theoretical and classical experimental methods	49
4.2	Estimated modal parameters from the decomposition method for a linear beam free response compared against the undamped structural eigen frequencies and the FFT for data consisting of first $N = 12,000$ sample values.	56
4.3	Experimental system frequencies (Hz.) estimated from SVMD for a linear beam free response compared against the undamped structural eigen frequencies and the FFT values for data consisting of first $N = 1000$ sample points.	56
4.4	Experimental modal damping estimated from the SVMD method for the linear beam free response for first $N = 1000$ sample values. Only the first three damping estimates are experimentally estimated by “pure mode” log decrement method.	57
4.5	Modal parameters estimation from reduced number of sensors compared against the theoretical eigenvalue problem for a three DOF discrete system with 8 bit quantization noise.	68

4.6	Modal frequency estimation for an experimental free-free beam using a number of sensors that is less than active frequencies compared against the theoretical undamped values.	70
5.1	Estimated modal parameters from the decomposition method for a linear beam free response for first $N = 12,000$ sample values.	92
6.1	Estimated modal parameters from various decomposition methods compared against the theoretical eigenvalue problem for a 3 DOF discrete system example	118
6.2	Modal parameters estimation from various decomposition methods compared against the theoretical eigenvalue problem for a 3 DOF discrete system with 8-bit quantization noise.	119
6.3	System frequencies estimated from decomposition methods with white noise forcing compared against structural eigen frequencies	122
6.4	Experimental system frequencies (Hz.) estimated from various decomposition methods for a linear beam free response compared against the undamped structural eigen frequencies	126
6.5	Experimental modal damping estimated from various decomposition methods for the linear beam free response. Only first three damping estimates are computed by using dominantly single mode log decrement method	126

LIST OF FIGURES

2.1	The acceleration of mass one, computed from applying the finite difference matrix \mathbf{D} to the displacement ensemble with noise. Upper is the underdamped example, and lower is the overdamped example. Images in this dissertation are presented in color	22
2.2	The damping factor estimate for first mode for various levels of noise. The solid line (—) shows system damping while dashed line (- -) presents the estimated damping. The horizontal axis indicates the value b representing the uniform noise in the range $\pm 1/2^b$	24
2.3	The modal frequency estimate for first mode for various levels of noise. The solid line (—) shows modal frequency while dashed line (- -) presents the estimated frequency. The horizontal axis indicates the value b representing the uniform noise in the range $\pm 1/2^b$	24
3.1	The mass-spring-damper model. The dashpots are figurative to represent the presence of damping, and do not accurately correspond to the example damping matrix.	32
3.2	A comparison between mode shapes from the structural eigenvalue problem (solid lines) and those estimated from the smooth orthogonal decomposition ('o' symbols). The sensor locations refer to the mass indices. The location 0 represents the wall attachment. The modes are in ascending order by modal frequency.	35
3.3	The frequency estimates improve as N gets large. The solid line (-) represents the true frequency (rad/sec) and (—*) are the estimated frequencies (rad/sec). The percent error in frequency estimation computed at $N = 10^4$ for modes 1 to 8 are 1.2%, 0.17%, 0.12%, 0.02%, 0.11%, 0.22%, 0.01% and 0.31% respectively also shown in Table 1.	36
3.4	The maximum singular values of \mathbf{XX}^T/N (m^2), \mathbf{VV}^T/N (m/s^2) and \mathbf{XF}^T/N (N-m). The dashed line (-●) represents values of \mathbf{XX}^T/N , the dashed line (-*) represents the values of \mathbf{VV}^T/N and the line (-★) represents values of \mathbf{XF}^T/N . We can see by $N = 10^4$ samples, $\mathbf{XF}^T/N \ll (\mathbf{XX}^T/N, \mathbf{VV}^T/N)$ and is perhaps negligible for this and larger values of N	37

3.5	The undamped natural frequency estimate starts to deteriorate for high damping. The solid line (—) represents the true frequency (rad/sec) and (—*) is the estimated frequency (rad/sec). Here samples size is $N = 10^5$	38
3.6	The MAC values comparison for SVMD for random excitation. MAC value of 1 shows vectors match up. Modes are not in any particular sequence	41
4.1	The experimental setup for study by Rhoads et. al	47
4.2	The impulse response of SDOF beam experiment for study by Rhoads et. al	49
4.3	The truncated sample points to obtain a “clean” signal for analysis of the study by Rhoads et. al	50
4.4	The FFT log plot of the SDOF beam experiment	51
4.5	The experimental setup of a 16 DOF clamped-free beam	51
4.6	The beam acceleration snapshots of the acceleration ensemble of a 16 DOF clamped-free beam with its mean removed.	52
4.7	The linear FFT plot of a 16 DOF clamped-free beam. Only first six modes are shown.	53
4.8	The frequency response of the second order high-pass filter for the 16 DOF beam experiment.	54
4.9	SVMD is compared for the first beam mode against the theoretical mode. SVMD is shown with + mark, theoretical mode is shown with the solid line —.	58
4.10	SVMD is compared for the second beam mode against the theoretical mode. SVMD is shown with + mark, the theoretical mode is shown with the solid line —.	59
4.11	SVMD is compared for the third beam mode against the theoretical mode. SVMD is shown with + mark, the theoretical mode is shown with the solid line —.	59

4.12	SVMD is compared for the fourth beam mode against the theoretical mode. SVMD is shown with + mark, the theoretical mode is shown with the solid line —.	60
4.13	SVMD is compared for the fifth beam mode against the theoretical mode. SVMD is shown with + mark, the theoretical mode is shown with the solid line —.	61
4.14	SVMD modal coordinates are shown for the first 5 beam modes. Modal coordinates indicate the quality of the decomposition, and can be used to distinguish between computational and actual modes.	62
4.15	SVMD modal coordinates are shown for the third beam mode. Modal coordinates can be used to distinguish between computational and actual modes. Actual mode is shown in dotted (- -), whereas spurious is shown in solid line (—).	63
4.16	The FFT of an acceleration time history channel of the experimental free-free beam. Eight active frequencies are visible within the Nyquist range.	69
4.17	Mode shapes obtained by the SVMD of the experimental free-free beam.	71
4.18	First four state-variable modal coordinates plot of the experimental free-free beam.	72
4.19	FFT of the first state-variable modal coordinate of the experimental free-free beam.	72
5.1	The low noise FRF plot with $\delta = \vartheta * \eta$ representing strength of uniform random noise signal amplitude. Here ϑ value is 1. The dotted line represents FRF plot with no noise $\vartheta = 0$ and is shown for comparison purpose only.	81
5.2	The high noise FRF plot with $\delta = \vartheta * \eta$ representing strength of uniform random noise signal amplitude. Here ϑ value is 4. The dotted line represents FRF plot with no noise $\vartheta = 0$ and is shown for comparison purpose only.	82

5.3	The SAC estimates for frequency identification for various levels of noise. The solid line (—) shows the amplitude SAC while dashed line (- -) presents the amplitude of complex version of the SAC. The horizontal axis indicates the value ϑ representing the uniform random noise coefficient. When noise level increases, the estimates deteriorate significantly.	83
5.4	The spectrum difference estimates for frequency identification for various levels of noise. The horizontal axis indicates the value ϑ representing the uniform random noise coefficient. When noise level increases, the estimates deteriorate.	84
5.5	The SAC values for various estimates of identified damping ratios. The solid line (—) shows the amplitude SAC while dashed line (- -) presents the amplitude of complex version of SAC. The damping estimate error ratio ζ_2/ζ_1 ranges from -100 % at 0.001 to +100 % at 2 with ζ_1 being 0.08 at 1.	85
5.6	The spectrum difference values for various estimates of identified damping ratios. The damping estimate error ratio ζ_2/ζ_1 ranges from -100 % at 0.001 to +100 % at 2 with ζ_1 being 0.08 at 1.	86
5.7	The SAC values for various estimates of identified frequency values. The solid line (—) shows the amplitude SAC while dashed line (- -) presents the amplitude of the complex version of SAC. The frequency estimate error ratio ω_2/ω_1 ranges from -100 % at 0.0 to +200 % at 3.	87
5.8	The spectrum difference values for various estimates of identified frequency values. The frequency estimate error ratio ω_2/ω_1 ranges from -100 % at 0.0 to +200 % at 3.	88
5.9	The amplitude SAC values for various estimates of identified damping values. The solid line (—) shows the amplitude SAC while dashed line (- -) presents the amplitude of the complex version of SAC. The reference system damping ratio is chosen as $\zeta_1 = 0.02$	89
5.10	The spectrum difference values for various estimates of identified damping ratios. The reference system damping ratio is chosen as $\zeta_1 = 0.02$	89
5.11	The SAC values for various estimates of identified damping values. The solid line (—) shows the amplitude SAC while dashed line (- -) presents the amplitude of the complex version of SAC. The reference system damping ratio is chosen as $\zeta_1 = 0.2$	90

5.12	The spectrum difference (SD) values for various estimates of identified damping ratios. The reference system damping ratio is chosen as $\zeta_1 = 0.2$	91
5.13	The amplitudes of complex SAC values computed for each FRF generated from the SVMD estimates compared against FRFs from modal coordinates.	93
5.14	The $r = 1$ - SD values computed for each FRF generated from the SVMD estimates compared against FRFs from modal coordinates. For ease of visualization, values of SD subtracted from 1 are plotted instead.	93
5.15	The amplitudes of complex SAC values computed for each FRF generated from the FFT estimates compared against FRFs from modal coordinates. The estimates are ordered to match sequence by SVMD for ease of comparison.	94
5.16	The $r = 1$ - SD values computed for each FRF generated from the FFT estimates compared against FRFs from modal coordinates. The estimates are ordered to match the sequence of SVMD. For ease of visualization, values of SD subtracted from 1 are plotted instead. . . .	95
5.17	The amplitude of complex SAC values computed for each FRF generated from the SVMD estimates compared against FRFs from modal coordinates.	96
5.18	The $r=1$ -SD values computed for each FRF generated from the SVMD estimates compared against FRFs from modal coordinates. The estimates are not ordered in any particular sequence. For ease of visualization, values of SD subtracted from 1 are plotted instead.	97
5.19	The amplitude of complex SAC values computed for each FRF generated from the FFT estimates compared against FRFs from modal coordinates. The estimates are ordered to match sequence by SVMD for ease of comparison.	98
5.20	The $r=1$ -SD values computed for each FRF generated from the FFT estimates compared against FRFs from modal coordinates. The estimates are ordered to match the sequence of SVMD. For ease of visualization, values of SD subtracted from 1 are plotted instead.	98

5.21	The percent error in estimation of frequency parameters against various lengths of data for a 3 DOF underdamped system. Each time record is normalized by its modal period. The quantization noise level is 10 bits.	102
5.22	The percent error in estimation of damping values against various lengths of data for a 3 DOF underdamped system. Each time record is normalized by its modal period. The quantization noise level is 10 bits.	103
5.23	The percent error in estimation of frequency parameters against various lengths of data for a 3 DOF underdamped system. Each time record is normalized by its modal period. The maximum error appears in the first mode. The quantization noise level is 6 bits.	104
5.24	The percent error in estimation of damping values against various lengths of data for a 3 DOF underdamped system. Each time record is normalized by its modal period and the maximum error appears in the first mode. The quantization noise level employed is 6 bits.	105
5.25	The percent error in estimation of frequency parameters against various lengths of data for a 3 DOF underdamped system. Each time record is normalized by its modal period. The quantization noise level employed is 6 bits.	106
5.26	The percent error in estimation of damping values against various lengths of data for a 3 DOF underdamped system. Each time record is normalized by its modal period. The quantization noise level employed is 6 bits.	107
5.27	The percent error in estimation of frequency parameters against various lengths of data for a 3 DOF underdamped system. Each time record is normalized by its modal period. The quantization noise level employed is 10 bits.	108
5.28	The percent error in estimation of damping values against various lengths of data for a 3 DOF underdamped system. Each time record is normalized by its modal period. The quantization noise level employed is 10 bits.	109
6.1	The mass-spring-damper model. The dashpots are figurative to represent the presence of damping, and do not accurately correspond to the example damping matrix.	120

6.2	The MAC values for all SVMD modes. MAC value of 1 shows vectors match up. Modes are not in any particular sequence	123
6.3	The MAC values for all sixteen modes for SOD. MAC value of 1 shows vectors match up. Modes are not in any particular sequence	124
6.4	The MAC values for all ITD modes. MAC value of 1 shows vectors match up. Modes are not in any particular sequence	124
6.5	The MAC values for all mass-weighted POD modes. MAC value of 1 shows vectors match up. Modes are not in any particular sequence . .	125
6.6	Identification methods are compared for the first beam mode. POD is shown with dotted line - -, SOD is shown with crosses \times , SVMD with circles \circ , and ITD with the solid line —.	127
6.7	Identification methods are compared for the second beam mode. POD is shown with dotted line - -, SOD is shown with crosses \times , SVMD with circles \circ , and ITD with the solid line —.	128
6.8	Identification methods are compared for the third beam mode. SOD is shown with crosses \times , SVMD with circles \circ , and ITD with the solid line —.	129
6.9	Identification methods are compared for the fourth beam mode. SOD is shown with crosses \times , SVMD with circles \circ , and ITD with the solid line —.	130
6.10	Identification methods are compared for the fifth beam mode. SOD is shown with crosses \times , SVMD with circles \circ , and ITD with the solid line —.	131
6.11	The log plot of POVs shown. The plot shows about 4 significant modes.	131
6.12	SOD and POD mode shape identification for a higher mode with the system excited in a way to get a dominant 3rd order beam mode response. SOD is shown with the solid line —, and POD is shown with a dotted line - -.	132
7.1	The modal coordinates plot for ω_2 and their phase space are plotted for 10 second simulation time.	142
7.2	The modal coordinates plot for ω_2 and their phase space are plotted for simulation time of 400 seconds.	143

Introduction

1.1 Background

Modal analysis is a procedure that describes the inherent dynamic behavior of a structure in terms of its dynamic properties, namely the natural frequencies, damping ratios and mode shape characteristics. Modal analysis is viewed as an efficient tool geared towards understanding and optimizing structural characteristics for a large class of noise and vibration applications, thereby resulting in, for example, lighter, stronger, and safer structures, and superior performances. Simply put, modal analysis is the study of the natural vibration characteristics of structures [1].

Modal analysis applications cover a broad range of objectives [2] including:

- Identification and assessment of vibrations phenomena
- Validation, correction and updating of the analytical dynamical models.
- Development of experimentally based dynamic models.
- Estimation of the dynamic behavior of both individual components and/or assembled structures.
- Design of systems such that resonances are avoided.

- Optimization of the dynamic properties of structures (mass, stiffness, damping) and model integration with other dynamic areas, such as acoustics and fatigue.
- Estimation of applied forces from the measured responses.
- Prediction of the responses due to complex and/or multiple excitations.
- Structural health monitoring, damage detection and structural integrity assessment.
- Prediction of the effect of structural modifications, for instance, the inclusion of damping in finite element models and updating of finite element models.

1.1.1 Analytical modal analysis

Two kinds of modal analysis techniques exist: analytical and experimental. When performed analytically, modal analysis utilizes the mathematical model of a structure's dynamic behavior to compute the modal parameters. The mathematical model is either a set of differential equations obtained by classical principles such as Newton's laws, Lagrange's equations, or numerical techniques such as finite element models (FEMs), that could be used to derive an eigenvalue problem. This eigenvalue problem produces a set of mode shapes each with an associated natural frequency and a modal damping value. The mode shapes can be used to define a coordinate change that decouples the system into individual oscillators with characteristic modal frequencies and damping ratios. These modal parameters provide a complete description of the structure's dynamic behavior. To perform this kind of analysis, complete information of the system, for example, mass, damping, stiffness, and forcing functions, is assumed to be available.

1.1.2 Experimental modal analysis

Unlike analytical modal analysis, experimental modal analysis is used to determine the modal parameters by actual testing. There are two ways of performing experimental modal analysis: Classical or traditional modal analysis, and operational or output-only modal analysis. In classical modal analysis, a set of frequency response functions (or impulse response functions) is computed, from a set of measured input forces and output responses of a structure [3–6], that are then processed to determine the modal parameters. In the output-only modal analysis, as the name indicates, only the output responses are measured and the excitation and operating forces are unmeasured inputs. There are various output-only approaches; but typically, an eigenvalue problem is constructed that produces modal parameter estimates strictly based on the obtained data.

Next, we will briefly note the types of signals utilized in the experimental modal analysis.

1.1.3 Classification of signals

All signals can be broadly classified into either stationary or non-stationary categories. A stationary signal is one whose distributions remain constant in their statistical parameters (for instance amplitude distribution and standard deviation) over time (or space) [7, 8]. Another definition of stationary signals (in wide-sense) implies a signal whose power spectrum does not change with time [9]. Stationarity implies that the ensemble will look just the same if the time origin is shifted.

Stationary signals are further divided into deterministic and random signals. Random signals are unpredictable in their instantaneous frequency content and/or their amplitude level, but their statistical characteristics are still relatively uniform over time. Examples of random signals are rain falling on a roof, noise from waterfalls, jet engine noise, turbulence in pump flow patterns and cavitation, vibration of ship hulls

due to flow of water along the hull, and the noise from an air-conditioning system [9–11].

All signals that are not stationary category can be considered non-stationary. For non-stationary and/or nonlinear signals, promising methods have been developed for structural analysis, such as Hilbert-Huang transform [12–16] and wavelet analysis [17–26]. The interested reader is referred to these works for understanding these methods.

The discussion contained in this work is limited to stationary random signals, and transient and decaying signals that may result from short duration non-stationary phenomena with clearly defined beginnings and ends. This would for instance comprise impulse and white noise forcing functions.

1.2 Output-only modal analysis

The output-only (or response-only or operational) modal analysis has gained popularity over recent years (see for example [27–36]). Advantages of output-only analysis over traditional modal analysis are the following. I) In many real life applications, the nature of input forcing prevents its measurement (for instance earthquake excitation, wind excitations, or traffic loads on structures) and output-only analysis eliminates the need to measure inputs. II) The construction of complex frequency response functions or transfer matrix functions in traditional experimental modal analysis requires an experienced engineer to correlate various response rows (or columns) to correctly identify the system modes, and is cumbersome when the modes are not well separated. III) Contrary to traditional modal analysis, in many cases output-only analysis can eliminate the need of stand-alone testing for the structure at various locations (or components).

The output-only methods can be either time or frequency based. A non-exhaustive

list of time domain based output-only methods includes, the Ibrahim time domain method [27, 37–41], a series of methods based on Prony’s method [3, 42], such as the complex exponential method [28, 43]; its single-input, multiple-output extension called the least square complex exponential method [29] and its multi-input, multi-output extension called the polyreference complex exponential method [30], the eigen-system realization algorithm [31, 44, 45], the independent component analysis [46, 47], and the stochastic subspace identification methods [32]. Frequency based output-only methods include the orthogonal polynomial methods [33, 34], the complex mode indicator function [35], and the recent frequency domain decomposition [36].

For a more detailed survey of modal parameter identification methods, reader is referred to the findings of [43, 48–51] that also include historical references such as [42] and [52–54].

1.3 Proper orthogonal decomposition and output-only time domain methods

The proper orthogonal decomposition (POD) produces modes that optimize the signal energy distribution in a set of measured time series. POD can be classified as an output-only method (at least for structural applications) since it requires only the time histories of the coordinate’s outputs without the need of measuring the inputs. POD has emerged as a standard tool that has been applied to turbulence, structures, and many other types of systems. POD has been used, for example, to characterize spatial coherence in turbulence and structures [55–61], to evaluate the dimensions of the dynamics [57–60, 62], to detect modal interactions [63, 64], to produce empirical modes for reduced order models [65–71], and in system identification [72–75]. The POD is similar to Karhunen-Loeve decomposition [76, 77], or more appropriately Kosambi-Karhunen-Loeve decomposition [78], principal components analysis [79], and

singular value decomposition [80]. All of these tools have been compared for structural applications [81]. The similar biorthogonal decomposition has also been applied to fluids and plasmas [82, 83].

POD is easily applied to discrete systems, or systems with discrete measurements $x_i(t_j)$, where $i = 1, \dots, M$ are the sensor indices, and $j = 1, \dots, N$ are the time sample indices. An ensemble matrix is formed as $\mathbf{X}^T = [\mathbf{x}_1, \dots, \mathbf{x}_M]$, where the vectors \mathbf{x}_i have elements of time samples $x_i(t_j)$. So each row of \mathbf{X} is a sampled history of one sensor on the structure. Then the matrix $\mathbf{R} = \mathbf{X}\mathbf{X}^T/N$ is formed. If the means of the signals are all zero, then \mathbf{R} is a covariance matrix. Otherwise, it is referred to as a correlation matrix, and the method can still be applied. The eigenvectors of \mathbf{R} are the proper orthogonal modes (POMs), and the eigenvalues are the proper orthogonal values (POVs).

If the mass distribution is uniform, the POD produces the normal modes of a structure [84–87], including 2-D structures [88]. If the mass distribution is not uniform, but known, or if the stiffness matrix is known, the POD can be weighted to produce the normal modes [84]. POD can be used for modal analysis if the damping is light, and if the system is either impulse excited or randomly excited [89]. The proper orthogonal modes (POMs) then converge to the linear normal modes, and the proper orthogonal values (POVs) provide the mean squared values of the modal coordinates. Proper orthogonal modal coordinates can be used to obtain information on frequencies and damping ratios.

Another POD based decomposition technique is the complex orthogonal decomposition (COD) [90]. Here, the ensemble \mathbf{X} of oscillatory signals is expanded into the complex domain to form an ensemble \mathbf{Z} of complex analytic signals. This is done non-uniquely [91] by the Fast Fourier Transform (FFT) [92] or Hilbert transform [91, 93]. Then a complex Hermitian correlation matrix $\mathbf{R} = \mathbf{Z}\bar{\mathbf{Z}}^T/N$ is formed. (A complex Hermitian matrix was also formed in the frequency domain for modal analysis [94].)

The complex Hermitian matrix \mathbf{R} has real eigenvalues (COVs) and generally complex eigenvectors (COMs). The COVs represent mean squared amplitudes of complex modal oscillations. The COMs can be interpreted as complex modes, representing generally a mix of traveling and standing wave behaviors, which can be extracted and quantified. As such, the COD can characterize the modal content of systems with mixed standing and traveling wave behavior. This renders that COD is also applicable for structural analysis of non-stationary signals. Initial indications are that the complex modes can be efficiently extracted. Much like POD for general systems, the COMs will not produce complex linear normal modes except under special circumstances. But the ongoing work suggests that the COD provides an optimized and systematic characterization of generally oscillatory behavior.

A recent addition to the time domain output-only family is smooth orthogonal decomposition (SOD) [95] that has shown good results for modal analysis of lightly damped structures in free response case. The SOD method, described in more detail later, is also viewed as a variant of the proper orthogonal decomposition method being evaluated for structural modal analysis. The SOD method is applicable in blind source separation [96], fatigue damage identification [97, 98], and was recently presented as a generalized modal analysis scheme [99]. However, the method has room for development as will be shown later in section 3.2.

1.4 Preview of this thesis

The current work extends the POD method for the modal parameter estimation of structural systems under free response as well as under random excitation, using state-variables [100–102]. The current work takes motivation from the SOD method, and modifies the existing POD method to estimate modal frequencies and damping ratios in addition to the linear normal modes as originally estimated by the POD. Similar

to the SOD, the state-variable modal decomposition method (SVMD) falls under the time-domain category and exploits the frequency content “hidden” in the time period considered.

The orthogonal decomposition-based method SVMD (and also SOD) carries some advantages. For example, SVMD does not involve the possibility of oversized state matrices (at least in the noise-free case) and their spurious modes (as in the Ibrahim time domain and the schemes based on Prony’s method); the estimation of initial states (for instance in stochastic subspace identification methods); or the construction of generalized block Hankel matrices (as in the eigensystem realization algorithm); or spectral density functions (as in the frequency domain decomposition). SVMD thereby invokes minimum assumptions and is simpler in construction.

The main idea of the SVMD method is presented in chapter 2. There, we derive the method from a state variable perspective and formulate the parameter estimation as a nonsymmetric, generalized eigenvalue problem. The data-based eigenvalue problem is related to the generalized eigenvalue problem associated with free-vibration solutions of the state-variable formulation of linear multi-degree-of-freedom systems in that chapter. For linear free-response data, the inverse-transpose of the eigenvector matrix approximate to the state-variable modal eigenvectors, and the eigenvalues of the nonsymmetric eigenvalue problem approximate those of the state-variable model. As such, the eigenvalues lead to estimates of frequencies and modal damping. The method handles damping ratios ranging from low to “moderately high” values, and the estimation is carried out regardless of whether damping is modal or nonmodal, and whether the modes are real or complex. Numerical simulations are presented for both damping cases. The issue of robustness under noise is also addressed. The resemblance of the method with POD can be easily seen by the eigenvalue problem construction.

For vibratory systems subjected to random excitations, modal parameter estima-

tion is addressed in Chapter 3. Primarily the extension to the SOD method is shown. This work shows that under certain conditions, the SOD eigenvalue problem formulated from white noise induced response data can be tied to the unforced structural eigenvalue problem, and thus can be used for modal parameter estimation. Using output response ensembles only, the generalized eigenvalue problem is formed to estimate eigen frequencies and modal vectors for an eight-degree-of-freedom lightly damped vibratory system. The estimated frequencies are compared against system frequencies obtained from structural eigenvalue problem and the estimated modal vectors are checked using the modal assurance criterion. Numerical simulations are presented for lightly damped structures whose output has been corrupted with noise. Simulations show that for light damping, satisfactory results are obtained for estimating both the system frequencies and the modal vectors. Then, formulation of SVMD for random response is briefly addressed. The same example is used for SVMD eigenvalue problem and the results show very similar identification values for system frequencies and mode shapes.

An experimental investigation for the free response cases is conducted in chapter 4. This gives insight into practical considerations and the issues that may arise if the decomposition method is to be implemented in the real world. Modal analysis is performed for both single and multi-degree-of-freedom systems and two experiments are reported. In the single-degree-of-freedom case a beam is sensed with a strain gauge whereas in the multi-degree-of-freedom cases, accelerometers are employed. In that way, ensemble matrices are observed to be obtained in multiple ways with no impact on the results. The effect of time-record length on the detection of modal parameters is explored. Modal coordinates are computed. Together with the modal parameters and mode shapes, modal coordinates could prove to be an effective tool to efficiently separate actual modes from the spurious ones. Analysis done in this chapter also underscores the advantages and limitations of using the state variable modal

decomposition method by evaluating yet another multi-degree-of-freedom system with issues surrounding filtering and reduced observability for such systems.

Two new tools are developed in chapter 5 to quantitatively assess the decomposition results. Numerical studies are conducted first to explore the strengths and sensitivity of these tools. Employing frequency response functions, these tools provide a quantitative means of evaluating the modal coordinates and the identification results. Then, by using these tools, the actual and fictitious modes are separated in the experiments with a greater degree of authority than the previous qualitative assessments.

It is natural to compare the decomposition methods with other time domain modal identification schemes. This comparison is conducted in chapter 6. The selection of time domain methods is based on their impact, historical significance and/or their relevance to the current experimental modal analysis. Methods are compared both using numerical simulations (with and without presence of noise in the system), and using actual experimental data. The same data set is used by each method for effective comparison. Two numerical simulations for free response and random response cases are conducted. The same multi-degrees-of-freedom experiment explored in chapter 4 is evaluated for comparison. These studies help in understanding the strength and weaknesses of various modal identification methods.

Lastly, we conclude in chapter 7 with some observations and potential directions to future work. Extension of the decomposition method to nonlinear systems and/or the use of nonlinear normal modes is addressed.

1.5 Contributions of this work

This work is an effort to tie up the current gap between various time domain methods and the orthogonal decomposition methods (like POD) for modal parameter estima-

tion. We summarize the contributions of this work as below.

- The state-variable modal decomposition method is a novel identification scheme that ties a data-based non-symmetric eigenvalue problem to the state-space form of the ordinary differential equations for multi-degree-of-freedom structural systems. It is a response-only method that enables frequency, damping ratios and mode shape estimates for free vibration problems. The method is applicable for both modal and nonmodal damping cases without the need for measuring the forcing inputs. The method produces good modal parameters estimates in low noise cases.
- Modal parameter identification was extended to the random response case for both smooth orthogonal decomposition and the state-variable decomposition method. In numerical simulations, for the systems subjected to random excitation, the decomposition based methods SOD and SVMD, showed good identification characteristics for lightly damped systems. Identification was still good when the response was contaminated with random noise at the output.
- The SVMD method was evaluated for free vibration experimental tests. Both single-degree and multi-degree-of-freedom systems were explored. By testing under conditions that may deviate from ideal theoretical assumptions, insight into the importance of data-length for analysis and filtering effects was gained. Modal coordinates for SVMD together with the SVMD modal vectors were seen as a valuable way of detecting system modes from “fictitious” modes and determining the quality of the decomposition. Multiple experimental tests verified that SVMD is a viable method for modal parameter identification.
- A quantitative analysis of the parameter estimates that are obtained by the decomposition method was achieved by formulating two new tools. To gain confidence in decomposition results, to eliminate the spurious modes and to

reinforce the visual feel obtained through the modal coordinates, the spectrum assurance and the spectrum difference criteria were developed. These criteria were evaluated first through numerical studies. Certain benchmark cases were numerically simulated and sensitivity to the system parameters was established. Then, we applied these tools to our experimental results and gained further insight on eliminating spurious modes. The effect of the data record length in the identification by the decomposition method of a system corrupted with noise was also evaluated via a numerical study. High and low damping cases were explored and a trend was established in determining the correct data length for a given test run.

- A comparison of decomposition based methods SVMD/SOD with other popular output-only modal analysis methods was performed. The methods were compared by conducting tests on free and forced response numerical simulations and the actual experimental tests. The same set of data was used for each scheme to maintain consistency in the comparisons. In this way, the strengths and the weaknesses of each scheme were matched.

State Variable Modal Decomposition of Free Responses

2.1 Introduction

This chapter presents a method of decomposing free-response ensemble data into modal components, while enabling frequency, damping, and mode-shape estimation for generally damped linear multi-degree-of-freedom systems. The basic idea is a generalization of proper orthogonal decomposition (POD) [55–57], with similarity also to smooth orthogonal decomposition (SOD) [95] and complex orthogonal decomposition (COD) [90]. Below, the application of these methods to modal analysis is reviewed, and the niche of the new method is staged.

The approach presented here is a generalized eigen decomposition based on state-variable ensembles. We will tie this decomposition strategy to state-variable models of generally damped linear vibration systems to reveal a method of obtaining frequency, damping, and mode shape information, without access to input measurements. The method will be illustrated with numerical examples.

2.2 Nonsymmetric state-variable modal decomposition

In this section, we summarize the state-variable modeling of vibration systems. The decomposition equation is presented, and then tied to the state-variable model.

2.2.1 *State-variable linear vibration model*

The state-variable model of linear vibration systems is used on systems with nonproportional (non-Rayleigh [103]) and nonmodal (non-Caughey [104]) damping to obtain damped vibration modes [105, 106]. The equations of motion for free vibrations are

$$\mathbf{M}\ddot{\mathbf{x}} + \mathbf{C}\dot{\mathbf{x}} + \mathbf{K}\mathbf{x} = \mathbf{0}, \quad (2.1)$$

where \mathbf{x} is an $n \times 1$ array of displacements, \mathbf{M} , \mathbf{C} , and \mathbf{K} , are the $n \times n$ mass, damping, and stiffness matrices, and the dots indicate time derivatives. Then defining a $2n \times 1$ state vector $\mathbf{y}^T = [\dot{\mathbf{x}}^T, \mathbf{x}^T]$, and introducing the equation $\mathbf{M}\dot{\mathbf{x}} - \mathbf{M}\dot{\mathbf{x}} = \mathbf{0}$, yields unforced equations of motion of the form

$$\mathbf{A}\dot{\mathbf{y}} + \mathbf{B}\mathbf{y} = \mathbf{0}, \quad (2.2)$$

where

$$\mathbf{A} = \begin{bmatrix} \mathbf{0} & \mathbf{M} \\ \mathbf{M} & \mathbf{C} \end{bmatrix}, \quad \mathbf{B} = \begin{bmatrix} -\mathbf{M} & \mathbf{0} \\ \mathbf{0} & \mathbf{K} \end{bmatrix}. \quad (2.3)$$

\mathbf{A} and \mathbf{B} are $2n \times 2n$ and symmetric, but are neither positive nor negative definite.

Assuming a response of the form $\mathbf{y} = e^{\alpha t} \underline{\phi}$, the eigenvalue problem

$$\alpha \mathbf{A} \underline{\phi} + \mathbf{B} \underline{\phi} = \mathbf{0} \quad (2.4)$$

in general yields complex eigenvalues α and eigenvectors $\underline{\phi}$, with $\underline{\phi} = [\mathbf{v}^T, \mathbf{w}^T]^T$, where $n \times 1$ vector partition \mathbf{v} corresponds to characteristic shapes of velocity states, and partition \mathbf{w} represents characteristic shapes in displacement (complex modes). By the construction of \mathbf{y} , $\mathbf{v} = \alpha \mathbf{w}$. The vectors $\underline{\phi}$ are orthogonal with respect to matrices \mathbf{A} and \mathbf{B} . The latter does not imply that the vectors \mathbf{w} are orthogonal with respect to \mathbf{M} and \mathbf{K} . In fact, they are not.

2.2.2 Decomposition strategy

The decomposition strategy is based on the free-response state-variable ensemble $\mathbf{Y} = [\mathbf{V}^T, \mathbf{X}^T]^T$, where \mathbf{X} is a displacement ensemble, and $\mathbf{V} = \mathbf{X}\mathbf{D}^T \approx \dot{\mathbf{X}}$ is an approximate velocity ensemble, like the SOD [95]. An example of an $(N - 2n_d) \times N$ matrix of centered finite differences, with $n_d = 1$ for half the span of the finite difference, is

$$\mathbf{D} = \frac{1}{2\Delta t} \begin{bmatrix} -1 & 0 & 1 & 0 & \dots & 0 \\ 0 & -1 & 0 & 1 & \dots & 0 \\ \vdots & \ddots & \ddots & \ddots & \ddots & \vdots \\ 0 & \dots & \dots & -1 & 0 & 1 \end{bmatrix}, \quad (2.5)$$

where Δt represents the sampling time. Thus \mathbf{V} is $n \times (N - 2n_d)$, and so the first and last n_d columns of \mathbf{X} are dropped so that \mathbf{Y} has compatible partitions.

We then take the derivative $\mathbf{W} = \mathbf{Y}\mathbf{D}^T \approx \dot{\mathbf{Y}}$, this time using an $(N - 4n_d) \times (N - 2n_d)$ difference matrix \mathbf{D} . The first and last n_d time samples of \mathbf{Y} are then dropped so that the dimensions of \mathbf{Y} and \mathbf{W} are both $2n \times N - 4n_d$. We form a correlation matrix $\mathbf{R} = \mathbf{Y}\mathbf{Y}^T / (N - 4n_d)$ and a nonsymmetric matrix $\mathbf{N} = \mathbf{Y}\mathbf{W}^T / (N - 4n_d)$.

The $2n \times 2n$ eigenvalue problem is then

$$\alpha \mathbf{R} \underline{\psi} = \mathbf{N} \underline{\psi}. \quad (2.6)$$

Rewriting this eigenvalue problem, $\alpha \mathbf{Y}\mathbf{Y}^T \underline{\psi} = \mathbf{Y}\mathbf{W}^T \underline{\psi}$. Making use of Eq. (2.2), $\mathbf{W} \approx \dot{\mathbf{Y}} = -\mathbf{A}^{-1}\mathbf{B}\mathbf{Y}$, and we have

$$\alpha \mathbf{Y}\mathbf{Y}^T \underline{\psi} \approx -\mathbf{Y}\mathbf{Y}^T \mathbf{B}^T \mathbf{A}^{-T} \underline{\psi}. \quad (2.7)$$

We expect $\mathbf{Y}\mathbf{Y}^T$ to be invertible. This is true if all displacement measurements are independent and if $N - 4n_d > n$.

As such, $\alpha \underline{\psi} \approx -\mathbf{B}^T \mathbf{A}^{-T} \underline{\psi}$. In matrix form

$$\mathbf{\Psi} \mathbf{\Lambda} \approx -\mathbf{B}^T \mathbf{A}^{-T} \mathbf{\Psi}, \quad (2.8)$$

where $\mathbf{\Lambda}$ is a diagonal matrix of eigenvalues. Taking the inverse-transpose, $\mathbf{\Psi}^{-T}\mathbf{\Lambda}^{-1} \approx -\mathbf{B}^{-1}\mathbf{A}\mathbf{\Psi}^{-T}$, whence $\mathbf{B}\mathbf{\Psi}^{-T} \approx -\mathbf{A}\mathbf{\Psi}^{-T}\mathbf{\Lambda}$, and hence

$$-\mathbf{A}^{-1}\mathbf{B}\mathbf{\Psi}^{-T} \approx \mathbf{\Psi}^{-T}\mathbf{\Lambda}. \quad (2.9)$$

Letting $\mathbf{U} = \mathbf{\Psi}^{-T}$, the data eigenvalue problem leads to

$$-\mathbf{A}^{-1}\mathbf{B}\mathbf{U} \approx \mathbf{U}\mathbf{\Lambda}, \quad (2.10)$$

which is a generalized eigenvalue problem with matrices \mathbf{A} and \mathbf{B} , the solution of which determines the unknowns \mathbf{U} and $\mathbf{\Lambda}$. The matrix form of the structural eigenvalue problem of Eq. (2.4) is

$$-\mathbf{A}^{-1}\mathbf{B}\mathbf{\Phi} = \mathbf{\Phi}\mathbf{\Gamma}, \quad (2.11)$$

a generalized eigenvalue problem with the same matrices \mathbf{A} and \mathbf{B} , the solution of which determines the unknowns $\mathbf{\Phi}$ and $\mathbf{\Gamma}$. The eigenvalue problems of Eqs. (2.10) and (2.11) have the same solution (within the modal normalization constants), indicating that $\mathbf{\Phi} \approx \mathbf{U} = \mathbf{\Psi}^{-T}$ and $\mathbf{\Gamma} = \mathbf{\Lambda}$. (The same logic is seen in SOD analysis of linear vibration systems [95].)

$\mathbf{\Psi}$ and $\mathbf{\Lambda}$ are $2n \times 2n$ matrices, corresponding to $2n$ eigenvectors and $2n$ eigenvalues, for an n -degree-of-freedom system. If the eigenvectors are complex, they come in conjugate pairs. That is, a conjugate pair of eigenvectors and eigenvalues represents one mode. If the eigen solution is real, an eigenvector characterizes a response configuration decaying at a rate contained in the corresponding eigenvalue. If, in fact, the damping is “modal” (Caughey) [104], there will be n independent displacement partitions \mathbf{v} among the $2n$ eigenvectors, which correspond to the n more familiar synchronous normal modes.

Thus, we expect the eigenvalues of Eq. (2.6) to approximate the state-variable eigenvalues, containing information about damping and frequency. The inverse of the modal matrix from Eq. (2.6) resembles the complex linear normal modal matrix of

the state-variable system Eq. (2.4), and contains velocity and displacement partitions. The only approximation in the method is in $\dot{\mathbf{X}} \approx \mathbf{X}\mathbf{D}^T$ and $\dot{\mathbf{Y}} \approx \mathbf{Y}\mathbf{D}^T$. Hence we expect reasonable estimations when noise is limited and the step size is sufficiently small compared to characteristic time scales.

2.3 Numerical examples

For comparison, we use the example shown in [84] for POD and [95] for SOD. We will treat underdamped and overdamped examples for both proportional and generalized damping. The mass and stiffness matrices are

$$\mathbf{M} = \begin{bmatrix} 2 & 0 & 0 \\ 0 & 1 & 0 \\ 0 & 0 & 1 \end{bmatrix}, \mathbf{K} = \begin{bmatrix} 2 & -1 & 0 \\ -1 & 2 & -1 \\ 0 & -1 & 1 \end{bmatrix} \quad (2.12)$$

and the initial conditions are $\mathbf{x}(0) = (1, 0, 0)^T$, and $\mathbf{v}(0) = (0, 0, 0)^T$. The undamped natural frequencies of the system are $\omega_1 = 0.4209$, $\omega_2 = 1.000$, and $\omega_3 = 1.6801$. In each simulation, the time responses for each mass displacement and velocity were numerically computed. Here, we used a step size $\Delta t = 0.004977$ and a sample size $N = 3000$. This time record closely matches one period of the lowest-frequency mode. We generated the state variable response from $\mathbf{y}(t) = \Phi \mathbf{q}_0 e^{\alpha t}$ where $\mathbf{q}_0 = \Phi^T \mathbf{A} \mathbf{y}(0)$. To emulate an experiment, we kept the displacement ensemble \mathbf{X} from the displacement partition of the ensemble generated from sampling $\mathbf{y}(t)$. We approximated $\dot{\mathbf{X}} \approx \mathbf{V} = \mathbf{X}\mathbf{D}^T$, and built the state-variable data ensemble \mathbf{Y} . The ensemble $\mathbf{W} = \mathbf{Y}\mathbf{D}^T$ (independent from displacement modal vector \mathbf{u}) was then formed and the endpoints were truncated to obtain compatible matrix dimensions. The eigenvalue problem Eq. (2.6) was formulated using \mathbf{Y} and \mathbf{W} .

2.3.1 *Proportionally damped example*

In this example we chose the damping matrix to be proportional to just the mass matrix, such that $\mathbf{C} = c\mathbf{M}$.

First, we consider an underdamped example with $c = 0.5$. The system eigenvalues are complex, of the form $-\zeta_j\omega_j \pm i\omega_j\sqrt{1-\zeta_j^2}$. These values are $\alpha_1 = \bar{\alpha}_1 = 0.25 + 0.3386i$, $\alpha_3 = \bar{\alpha}_4 = 0.25 + 0.9682i$, $\alpha_5 = \bar{\alpha}_6 = 0.25 + 1.6614i$. The modal damping factors are then $\zeta_1 = 0.5940$, $\zeta_2 = 0.2500$ and $\zeta_3 = 0.1488$. The lowest-frequency mode has a damped frequency of $\omega_{d1} = 0.3386$. Our time record specified above spans 81% of the associated oscillations period.

From the decomposition eigenvalues, estimates of the damping factors and natural frequencies are identical to that of system to more than four significant figures. For proportional damping three out of six of the displacement partitions of the state-variable modal vectors are independent. The corresponding independent displacement eigenvectors were normalized to real form of unit length as $\mathbf{u}_1^T = (0.3602, 0.5928, 0.7204)^T$, $\mathbf{u}_2^T = (-0.7071, 0.0, 0.7071)^T$ and $\mathbf{u}_3^T = (0.2338, -0.8524, 0.4676)^T$. All agree with the linear normal modes (LNMs) to 4th decimal place.

Now we consider an overdamped example with $c = 2.5$, leading to two real and four complex structural eigenvalues. The complex eigenvalues are $\alpha_1 = \bar{\alpha}_1 = 1.25 + 1.1227i$, whereas the real pairs are $(2.427, 0.073)$ and $(2.000, 0.500)$, which have modal damping factors of $\zeta_1 = 2.9701$, $\zeta_2 = 1.2500$ and $\zeta_3 = 0.7440$. The decomposition method also yielded one complex and two real eigenvalues from which damping factors and natural frequencies are identical to those of the structural problem. Also, the corresponding independent displacement eigenvectors, normalized to real form of unit length agreed with the linear normal modes (LNMs) to the fourth decimal place.

2.3.2 Generally damped example

We will consider underdamped and overdamped examples. For the underdamped example the damping matrix was

$$\mathbf{C} = \begin{bmatrix} 1.2 & -0.9 & 0 \\ -0.9 & 1.2 & -0.3 \\ 0 & -0.3 & 0.3 \end{bmatrix} \quad (2.13)$$

Then $\mathbf{KM}^{-1}\mathbf{C} \neq \mathbf{CM}^{-1}\mathbf{K}$, rendering the system to be nonmodally damped [104]. In the case of nonmodal damping, the definition of a modal damping factor is slightly ill posed since we trying to estimate the modal damping from the system that is non-modally damped. Besides, the system cannot be decoupled into individual oscillators of the form

$$\ddot{q}_i + 2\zeta_i\omega_i\dot{q}_i + \omega_i^2q_i = 0 \quad (2.14)$$

Nonetheless, the frequency of damped oscillation is the imaginary part of the eigenvalue. The eigenvalues obtained from the structural-model eigenvalue problem Eq. (2.4) are complex, and are $\alpha_1 = \bar{\alpha}_2 = 0.7620 + 1.4190i$, $\alpha_3 = \bar{\alpha}_4 = 0.2474 + 1.006i$, $\alpha_5 = \bar{\alpha}_6 = 0.0405 + 0.4218i$. Using the magnitude of the eigenvalue as “ ω_j ”, and comparing the real part to “ $\zeta_j\omega_j$ ” produces numbers for $\tilde{\zeta}_j$, and $\tilde{\omega}_j$. In this case $\tilde{\zeta}_1 = 0.0957$, $\tilde{\zeta}_2 = 0.2388$, and $\tilde{\zeta}_3 = 0.4731$, and $\tilde{\omega}_1 = 0.4238$, $\tilde{\omega}_2 = 1.0360$, and $\tilde{\omega}_3 = 1.6107$.

The modal decomposition method eigenvalues are found to be nearly identical to the system structural eigenvalues, and the “damping factors” and “natural frequencies” are identical to fourth decimal place. All unit length normalized displacement partitions of the corresponding complex eigenvectors, $\mathbf{w}_1^T = \bar{\mathbf{w}}_2^T = (-0.3674 + 0.0317i, -0.5901 - 0.0129i, -0.7197 - 0.0056i)^T$, $\mathbf{w}_3^T = \bar{\mathbf{w}}_4^T = (0.6517 + 0.1358i, 0.0499 - 0.1539i, -0.7908 + 0.1022i)^T$, $\mathbf{w}_5^T = \bar{\mathbf{w}}_6^T = (-0.3526 + 0.1499i, 0.9224 - 0.0431i, -0.3469 - 0.2670i)^T$, agreed with the LNMs to the fourth

decimal place.

Now a highly overdamped example is considered. The damping matrix was chosen as

$$\mathbf{C} = \begin{bmatrix} 6.0 & -4.5 & 0 \\ -4.5 & 7.5 & -3.0 \\ 0 & -3.0 & 3.0 \end{bmatrix} \quad (2.15)$$

The structural modal eigenvalue problem (2.4) produces four real and two complex eigenvalues. The complex eigenvalues are $\alpha_1 = \bar{\alpha}_1 = 0.1858 + 0.4165i$, whereas the real pairs are (9.8853, 0.2432) and (2.6180, 0.3820). The real pairs were matched to produce the correct undamped modal frequency estimates but in reality could pose problems if “true” frequency information is unknown. The “damping factors” are $\tilde{\zeta}_1 = 0.4073$, $\tilde{\zeta}_2 = 1.5000$ and $\tilde{\zeta}_3 = 3.2665$ and corresponding “modal frequencies” are $\tilde{\omega}_1 = 0.4561$, $\tilde{\omega}_2 = 1.000$, and $\tilde{\omega}_3 = 1.5504$.

The decomposition method also produces four real and two complex eigenvalues that are nearly identical to the structural eigenvalues. The displacement partitions of the six eigenvectors are $\mathbf{w}_1^T = \bar{\mathbf{w}}_2^T = (0.4717 - 0.0829i, 0.5784 + 0.0054i, 0.6728 + 0.0534i)^T$, $\mathbf{w}_3^T = (0.5365, 0, -0.8439)^T$, $\mathbf{w}_4^T = (0.1989, 0, -0.9800)^T$, $\mathbf{w}_5^T = (-0.2792, 0.8869, -0.3680)^T$, and $\mathbf{w}_6^T = (0.1098, -0.7683, -0.6305)^T$, which agreed with the LNMs to the 4th decimal place.

2.3.3 Step size selection

The differentiation step size is a parameter of the method. If the step size is too large, it results in erroneous parameter estimates and gets worse in over damped cases. If the step size is too small, it results in noise amplification. This implies that the sampling resolution needs to be chosen appropriately to fully capture the features of the transient time response, and in turn to accurately estimate the system parameters, particularly for very highly damped (or very fast) systems. For choosing the sample time, important features of the response are the characteristic settling time, $\tau_{1j} = 4/\zeta_j\omega_j$, and the oscillation period, $\tau_{2j} = 2\pi/\omega_{dj}$. It was concluded by

numerous simulations that any step size that lies within 5% of the minimum (over j) of τ_{1j} and τ_{2j} would give reasonable resolution and hence serves our purpose. For data obtained through experiments, the settling time criterion might be good enough to approximate the step size. Time records should be appropriately chosen with regard to the maximum of τ_{1j} and τ_{2j} . This information may not be available *a-priori*, but provides a rough rule of thumb for the required time resolution.

2.4 Robustness under noise

To emulate a 10-bit quantization noise in digitization [91], we set up random fluctuations. The MATLAB function “rand” was used to generate an ensemble of uniformly distributed random numbers between $\pm 2^{-10}x_0$, where x_0 is the maximum initial condition. ‘Rand’ emulates white noise. We verified that the spectrum of our random data was uniformly distributed. The root mean squared value was very close to $2^{-10}x_0/\sqrt{3}$. The random ensemble was added to the displacement matrix \mathbf{X} . We then took numerical derivatives of the new \mathbf{X} to build \mathbf{V} and subsequently our ensemble matrices. All the above mentioned cases were studied under noisy data with a step size of 0.0049767 and $N = 3000$. To reduce noise amplification from differentiation over short time steps, we used a differentiation step size of 32 ($n_d = 16$). This value was selected after some trials on step sizes and was found to be better than others. Examples of finite-difference mass accelerations with noise are shown in Fig. (2.1) for the proportionally underdamped and overdamped examples. The figure also shows how much time record was used in all examples.

For the proportionally damped, underdamped example of $c = 0.5$, the errors in the estimated damping factors and natural frequencies were 0.82%, 0.57% and 0.17%, and 0.09%, 0.05% and 0.01%, respectively. The corresponding complex independent displacement eigenvectors normalized to real form agreed with

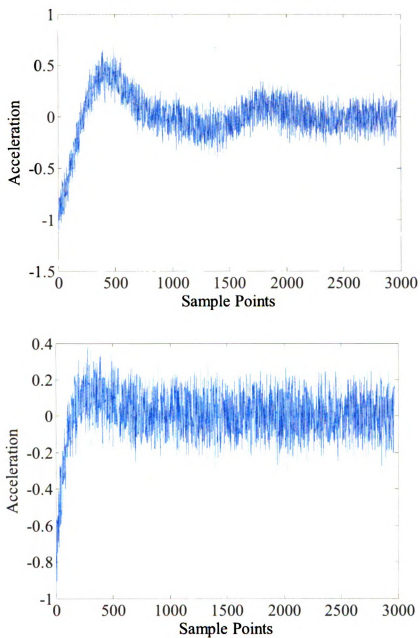


Figure 2.1: *The acceleration of mass one, computed from applying the finite difference matrix \mathbf{D} to the displacement ensemble with noise. Upper is the underdamped example, and lower is the overdamped example. Images in this dissertation are presented in color*

the LNMs to the 4th decimal place. For the overdamped case of $c = 2.5$, two eigenpairs were overdamped and one was underdamped. We were able to get

good estimates of the underdamped eigenvalues and also the slow part of the system eigenvalues. The underdamped system frequency and damping had 1.8% and 0.56% errors respectively. The slow eigenvalues were 0.0752 and 0.4903, with corresponding vectors $(0.3576, 0.5925, 0.7218)^T$ and $(0.7021, -0.0067, -0.7120)^T$ that are comparable against state-variable model eigenvalues (0.073 and 0.500) and the vectors $(0.3602, 0.5928, 0.7204)^T$ and $(0.7071, 0.0, -0.7071)^T$ respectively. For the state-variable model, the slow and fast eigen-pairs correspond to the same eigenvector and thus are easy to visualize, the decomposition estimates the vector associated with the slow eigenvalues within reasonable accuracy. The identified eigenvectors associated with the fast eigenvalues were $(0.3930, 0.5925, 0.7033)^T$ and $(0.7312, 0.1141, -0.6725)^T$ that may still be reasonable. But the fast eigenvalues, even with faster sampling and a larger differentiation step size, were corrupted by noise and gave erroneous results. This means we were unable to get good estimates of ζ_j and ω_j for the overdamped system. From the slow eigenvalues though, we can estimate modal time constants and given the system frequencies (e.g. by FEM), we can still estimate damping ratios with reasonable accuracy.

In the generally damped examples, for the underdamped case of Eq. (2.13), the errors in the estimated damping factors and natural frequencies were 0.52%, 0.04% and 0.67%, and 0.04%, 0.11% and 0.13%, respectively. The displacement partitions of the six complex eigenvectors agreed with the LNM to the 3rd decimal place. For overdamped case of Eq. (2.15), the same interpretation about fast and slow eigenvalues holds as described in case of proportionally damped overdamped case.

Lastly, we consider the effect of increasing the noise level. Here the system is chosen to be modally under damped with $\mathbf{C} = 0.5\mathbf{M}$. We used a differentiation step size of 32 ($n_d = 16$). As the noise bit level was incremented (doubling the noise level), the error typically increased, until at five bits, the error in the worst mode (highest damping factor) was 55% Fig. (2.2) and Fig. (2.3).

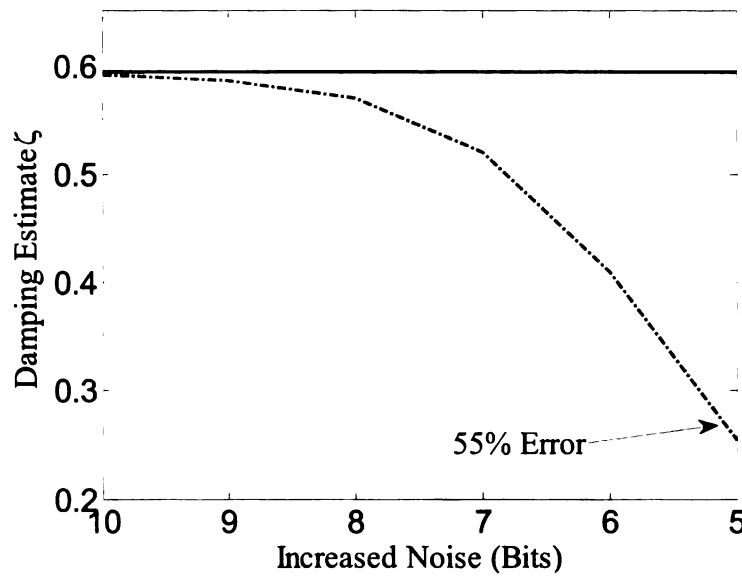


Figure 2.2: The damping factor estimate for first mode for various levels of noise. The solid line (—) shows system damping while dashed line (- -) presents the estimated damping. The horizontal axis indicates the value b representing the uniform noise in the range $\pm 1/2^b$.

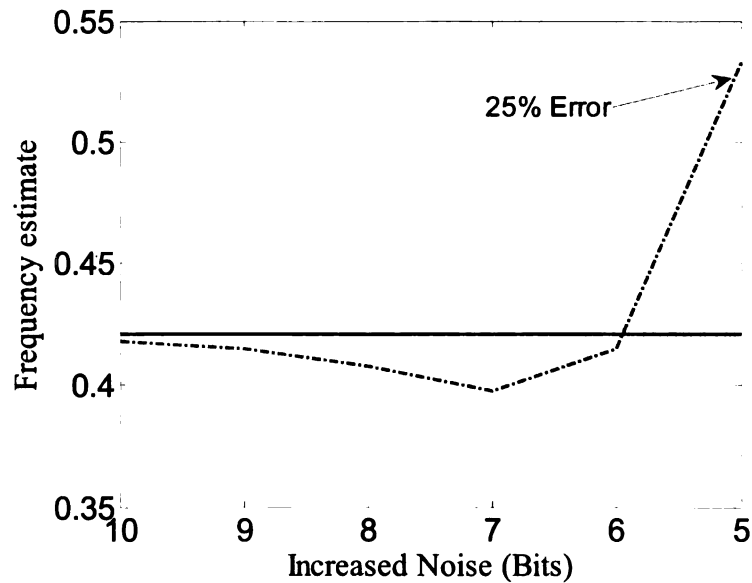


Figure 2.3: The modal frequency estimate for first mode for various levels of noise. The solid line (—) shows modal frequency while dashed line (- -) presents the estimated frequency. The horizontal axis indicates the value b representing the uniform noise in the range $\pm 1/2^b$.

That some frequency estimates improved with noise is probably random happenstance. We briefly looked into varying the number of data. The results were similar with $N = 3730$ (a full response cycle of the lower mode damped response), and the results deteriorated, primarily for the lowest mode, when N was increased to 9000. The suspected reason is that, with the modal damping factor of 0.5940, the modal response was settled for most of the time record, and therefore the lowest modal data was dominated by the noise. In fact, one of the better results came with $N = 1865$, representing a half cycle of lower mode response. For further lower values of N , results deteriorated. It seems that the time record should include at least a half cycle of the mode to be identified, but also for modes with significant damping, the time record should not be too long. Observations with various step sizes were also made. When noise is present, longer differentiation step sizes are beneficial at larger noise levels. However, the differentiation step size promotes error if it is a “large” fraction of the response period of the mode to be identified. These are simple observations from a few numerical experiments. More is explained when we conduct the experiments in next chapters.

These examples suggest that the decomposition method is robust under low levels of noise that might be seen in experiments. In multiple simulations, we found that examples with damping factors up to around $\zeta = 0.8$ were successful. With higher damping we could estimate slow time constants but not ζ_j and ω_j . In many experiments, accelerometers are used so displacement signals will be less prone to high frequency noise since accelerations are integrated to obtain \mathbf{X} and \mathbf{V} .

2.5 Summary

We have proposed a method for extracting modal information from free responses of generally damped linear multi-degree-of-freedom systems. A generalized nonsymmet-

ric eigenvalue problem was posed, involving “correlations” of state-variable ensembles. The resulting eigenvalues and eigenvectors can be complex in general. The eigenvalues hold information of damping and frequency, while the eigenvectors indicate the mode shapes associated with the state-variable model.

The method is applicable to free multi-modal responses with small or “large” damping, and with modal or nonmodal damping in noise-free cases (even for overdamped systems). In the noisy cases, however, we were successfully able to identify frequencies and damping factors when damping factors had values up to $\zeta = 0.8$. To obtain modal parameters under these conditions, the system input need not be measured; only the response is measured.

We applied this scheme to several numerical examples, for which accurate estimates of modal parameters (frequency, damping factor or decay rate, and mode shapes) were possible regardless of the damping value. The sampling rate should be sufficiently smaller than the shortest characteristic time interval, defined by decay time or oscillation period. For nonmodally damped systems, the eigenvalues can accurately quantify the decay rates, damped frequencies, and mode shapes, including complex modes. In the presence of noise, large damping factors could not be extracted, but the slow decay rates were still estimated. Numerical examples suggest that there is an optimal choice of the differentiation time step, and the time record, for extracting modal frequencies and damping in the presence of noise.

Random Response

3.1 Introduction

*R*andom excitation is one of the five common types of excitations that is applied to the test structures for modal analysis (the others being transient (impact, step or chirp), stepped-sinusoidal, slow sine sweeps, and periodic). A great deal of literature exists on experimental modal analysis for randomly excited systems. Such analysis requires deriving FRFs from random excitations (see for example [4, 6]). Here we focus on the modal analysis of randomly excited systems, where only the response needs to be measured and the inputs do not need to be measured.

We will primarily focus on the SOD analysis for systems under random excitation. We will begin by reviewing the SOD method for free response and will extend the theory to the random response. Next, we will present a numerical example for a lightly damped, linear multi-degree-of-freedom system. Then, we will show that the SVM analysis of random response holds quintessential similarity with the SOD, that will be augmented with the same numerical example.

3.2 Smooth orthogonal decomposition

3.2.1 *Smooth orthogonal decomposition and modal analysis for free vibration*

The “smooth orthogonal decomposition” (SOD) [95] can be applied to lightly damped symmetric vibration systems with inhomogeneous mass distributions to find structural modes. First, an $n \times N$ ensemble matrix \mathbf{X} of displacements is obtained from N time samples of n displacement signals. Then an ensemble $\mathbf{V} \approx \dot{\mathbf{X}}$ of velocities is formed. This can be done by finite difference through a matrix \mathbf{D} , such that $\mathbf{V} = \mathbf{X}\mathbf{D}^T$ where \mathbf{X} is an ensemble of displacements (in structures case). Next the velocity covariance matrix $\mathbf{S} = \mathbf{V}\mathbf{V}^T/N_v$ is formed, where N_v is the number of velocity samples. If the finite difference covers two adjacent samples, such that $v_i(t_j) = x_i(t_{j+1}) - x_i(t_j)$, then $N_v = N - 1$, if $v_i(t_j) = x_i(t_{j+1}) - x_i(t_{j-1})$, then $N_v = N - 2$, and so on. Keeping the displacement data that correspond to the calculated velocity data, the ensemble \mathbf{X} is pared down to the same dimensions as \mathbf{V} . The matrix $\mathbf{R} = \mathbf{X}\mathbf{X}^T/N_v$ is then formed, representing a covariance matrix if the mean of the displacement data is zero.

Then the SOD is based on a generalized eigenvalue problem cast as

$$\lambda \mathbf{R} \underline{\psi} = \mathbf{S} \underline{\psi}. \quad (3.1)$$

For a free multi-modal response with light damping, the eigenvalues λ approximate the frequencies squared, and the inverse-transpose of the modal matrix $\underline{\Psi}$ approximates the linear modal matrix.

To see this, consider first the symmetric undamped vibration system of the form

$$\mathbf{M}\ddot{\mathbf{x}} + \mathbf{K}\mathbf{x} = \mathbf{0}, \quad (3.2)$$

which is associated with the eigenvalue problem $-\omega^2 \mathbf{M} \underline{\phi} + \mathbf{K} \underline{\phi} = \mathbf{0}$, which in matrix form is

$$\mathbf{K} \underline{\Phi} = \mathbf{M} \underline{\Phi} \underline{\Lambda}, \quad (3.3)$$

where $\mathbf{\Lambda}$ is a diagonal matrix of eigenvalues and the columns of $\mathbf{\Phi}$ are the eigenvectors. The eigenvalues and eigenvectors provide the modal frequencies and the mode shapes.

The SOD eigenvalue problem Eq. (3.1) can be written as $\lambda \mathbf{X} \mathbf{X}^T \underline{\psi} = \mathbf{V} \mathbf{V}^T \underline{\psi}$, or

$$\lambda \mathbf{X} \mathbf{X}^T \underline{\psi} = \mathbf{X} \mathbf{D}^T \mathbf{D} \mathbf{X}^T \underline{\psi}. \quad (3.4)$$

Close examination [95] shows that $\mathbf{D}^T \mathbf{D} \mathbf{X}^T \approx -\ddot{\mathbf{X}}^T$. If the system damping is negligible, then from the symmetric vibration model of Eq. (3.2), we would find $-\ddot{\mathbf{X}}^T = \mathbf{X}^T \mathbf{K} \mathbf{M}^{-1}$. Hence, Eq. (3.4) becomes $\lambda \mathbf{X} \mathbf{X}^T \underline{\psi} = \mathbf{X} \mathbf{X}^T \mathbf{K} \mathbf{M}^{-1} \underline{\psi}$. In matrix form,

$$\mathbf{X} \mathbf{X}^T \mathbf{\Psi} \mathbf{\Lambda} = \mathbf{X} \mathbf{X}^T \mathbf{K} \mathbf{M}^{-1} \mathbf{\Psi}. \quad (3.5)$$

Assuming $\mathbf{X} \mathbf{X}^T$ is invertible (n modes are active and $N_v \geq n$), we have $\mathbf{\Psi} \mathbf{\Lambda} = \mathbf{K} \mathbf{M}^{-1} \mathbf{\Psi}$. Taking the inverse transpose and noting symmetry, $\mathbf{\Psi}^{-T} \mathbf{\Lambda}^{-1} = \mathbf{K}^{-1} \mathbf{M} \mathbf{\Psi}^{-T}$, and hence

$$\mathbf{K} \mathbf{\Psi}^{-T} = \mathbf{M} \mathbf{\Psi}^{-T} \mathbf{\Lambda}. \quad (3.6)$$

Comparing equations (3.6) and (3.3), the eigenvalue problem of SOD has reduced to the eigenvalue problem Eq. (3.3) of the undamped vibration system. The SOD modal matrix is thus related to the structural linear modal matrix as $\mathbf{\Phi} = \mathbf{\Psi}^{-T}$. Chelidze and Zhou [95] derived this relationship starting with an optimization representation of the eigenvalue problem.

SOD is applicable for symmetric, but otherwise general, mass and stiffness distributions. SOD directly produces estimates of the modal frequencies from the eigenvalue problem. Insight to modal participation is not directly obtained, but can come from analysis of the modal coordinates, dependent on how modal vectors are normalized. Limitations of SOD are that SOD is restricted to lightly damped systems, and it has not been justified or studied for random excitations. Also, sufficient numbers of sensed displacements are needed.

3.2.2 Smooth orthogonal decomposition for systems under random excitation

Previously, proper orthogonal decomposition for modal analysis was justified for random excitation [89]. Here the SOD will be justified for white noise excitation.

3.2.2.1 Smooth orthogonal decomposition and random excitation

Consider the symmetric vibration system neglecting damping,

$$\mathbf{M}\ddot{\mathbf{x}} + \mathbf{K}\mathbf{x} = \mathbf{f}(t), \quad (3.7)$$

where $\mathbf{f}(t)$ is a random excitation. In terms of the sampled ensemble matrices, $\mathbf{M}\ddot{\mathbf{X}} + \mathbf{K}\mathbf{X} = \mathbf{F}$, with \mathbf{F} representing the ensemble matrix of the sampled $\mathbf{f}(t)$, and therefore $\mathbf{D}^T \mathbf{D} \mathbf{X}^T \approx -\ddot{\mathbf{X}}^T = \mathbf{X}^T \mathbf{K} \mathbf{M}^{-1} - \mathbf{F}^T \mathbf{M}^{-1}$. Hence, from the matrix form of (3.4)

$$\frac{1}{N} \mathbf{X} \mathbf{X}^T \Psi \Lambda = \frac{1}{N} \mathbf{X} \mathbf{X}^T \mathbf{K} \mathbf{M}^{-1} \Psi - \frac{1}{N} \mathbf{X} \mathbf{F}^T \mathbf{M}^{-1} \Psi. \quad (3.8)$$

The elements in the matrix $\frac{1}{N} \mathbf{X} \mathbf{X}^T$ represent cross correlations (with zero delay) between responses, and are expected to be nonzero. The elements in the matrix $\mathbf{L} = \frac{1}{N} \mathbf{X} \mathbf{F}^T$ represent cross correlations (with zero delay) between responses and random inputs. In other words, the elements L_{ij} are the means of the products $x_i(t)f_j(t)$. If their expected values are zero, then this term can be neglected, and the decomposition eigenvalue problem would then converge, as N gets large, to

$$\frac{1}{N} \mathbf{X} \mathbf{X}^T \Psi \Lambda = \frac{1}{N} \mathbf{X} \mathbf{X}^T \mathbf{K} \mathbf{M}^{-1} \Psi, \quad (3.9)$$

which is the same as Eq. (3.5), and thus reduces to the undamped structural eigenvalue problem if $\mathbf{X} \mathbf{X}^T$ is invertible. Under this condition, the SOD, even with random excitation, would produce the modal frequencies and mode shapes of the system. Thus we are interested in conditions for which $\mathbf{L} \rightarrow \mathbf{0}$ as N gets large.

Elements of \mathbf{L} have the form

$$L_{ij} = \frac{1}{N} \sum_{k=1}^N \sum_{l=1}^m \int_{-\infty}^{\infty} h_{il}(\tau) f_l(t_k - \tau) d\tau f_j(t_k), \quad (3.10)$$

where $h_{il}(t)$ is an element of the impulse response matrix, between $\mathbf{f}(t)$ and \mathbf{x} . In this form $h_{il}(t)$ is a linear combination of modal coordinate impulse response functions, each sinusoidal with a modal frequency. Interchanging the order of sums,

$$\begin{aligned} L_{ij} &= \sum_{l=1}^m \int_{-\infty}^{\infty} h_{il}(\tau) \frac{1}{N} \sum_{k=1}^N f_l(t_k - \tau) f_j(t_k) d\tau \\ &= \sum_{l=1}^m \int_{-\infty}^{\infty} h_{il}(\tau) C_{jl}^f(\tau) d\tau \end{aligned} \quad (3.11)$$

where $C_{jl}^f(\tau)$ is the cross correlation between the forcing functions associated with coordinates j and l .

3.2.2.2 White noise

Here there are two useful possibilities. One is that the forcing on all coordinates are statistically independent. For example, independent bombardment of each coordinate by random turbulence fluctuations might qualify. Then $C_{jl}^f(\tau) = R_j^f(\tau) \delta_{jl}$, where $R_j^f(\tau)$ is the autocorrelation of the j th forcing term. If the forcing functions are modeled as white noise, then $C_{jl}^f(\tau) = \gamma_j \delta(\tau) \delta_{jl}$, where $\delta(\tau)$ is the Dirac delta function, and δ_{jl} is the Kronecker delta.

Another possibility is that each forcing term is dependent, for example in random base excitation. Then $f_j(\tau) = \hat{\gamma}_j f(\tau)$, and hence $C_{jl}^f(\tau) = \hat{\gamma}_{jl} R_f(\tau)$. If the forcing function is modeled as white noise, then $C_{jl}^f(\tau) = \gamma_{jl} \delta(\tau)$.

In either of these white noise cases, we have the form $L_{ij} = \sum_{l=1}^m \int_{-\infty}^{\infty} h_{il}(\tau) \gamma_{jl} \delta(\tau) d\tau = \sum_{l=1}^m h_{il}(0) \gamma_{jl}$. For a typical vibration system, the impulse response function will be such that $h_{il}(0) = 0$, whence $L_{ij} = 0$. Thus, for white noise, the response and excitation are uncorrelated, and the matrix form of the SOD eigenvalue problem of Eq. (3.4) represents the undamped structural eigenvalue problem of Eq. (3.3) for large N . As such, the SOD should produce estimates of the modal frequencies and mode shapes of the undamped model under white noise excitation. The natural excitation algorithm (referred to as NExT) [107,108] also arrives at a

similar conclusion albeit in a different way. There, it was shown that for a system subjected to uncorrelated white noise inputs, the cross correlation between various outputs would be a sum of complex exponential functions of the same form as the sum of impulse response functions of the original system. Thus, NExT would accommodate using output-only methods for modal parameter identification in case of independent (uncorrelated) white noise forcing.

3.3 Numerical example

We simulated the eight-degree-of-freedom linear vibratory system shown in Fig. 3.1. The system observes light modal damping and was excited by white noise applied to the first mass with zero initial conditions. The mass and stiffness matrices are given

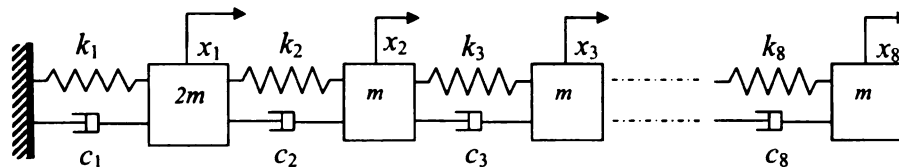


Figure 3.1: *The mass-spring-damper model. The dashpots are figurative to represent the presence of damping, and do not accurately correspond to the example damping matrix.*

as

$$\mathbf{M} = \begin{bmatrix} 2 & 0 & 0 & 0 & 0 & 0 & 0 & 0 \\ 0 & 1 & 0 & 0 & 0 & 0 & 0 & 0 \\ 0 & 0 & 1 & 0 & 0 & 0 & 0 & 0 \\ 0 & 0 & 0 & 1 & 0 & 0 & 0 & 0 \\ 0 & 0 & 0 & 0 & 1 & 0 & 0 & 0 \\ 0 & 0 & 0 & 0 & 0 & 1 & 0 & 0 \\ 0 & 0 & 0 & 0 & 0 & 0 & 1 & 0 \\ 0 & 0 & 0 & 0 & 0 & 0 & 0 & 1 \end{bmatrix}, \quad \mathbf{K} = \begin{bmatrix} 2 & -1 & 0 & 0 & 0 & 0 & 0 & 0 \\ -1 & 2 & -1 & 0 & 0 & 0 & 0 & 0 \\ 0 & -1 & 2 & -1 & 0 & 0 & 0 & 0 \\ 0 & 0 & -1 & 2 & -1 & 0 & 0 & 0 \\ 0 & 0 & 0 & -1 & 2 & -1 & 0 & 0 \\ 0 & 0 & 0 & 0 & -1 & 2 & -1 & 0 \\ 0 & 0 & 0 & 0 & 0 & -1 & 2 & -1 \\ 0 & 0 & 0 & 0 & 0 & 0 & -1 & 1 \end{bmatrix}, \quad (3.12)$$

and the damping matrix is chosen to be $\mathbf{C} = c\mathbf{M}$, where $c = 0.01$.

The system was simulated for 1000 seconds (later on we found out this time to be equal to 34 periods of the fundamental mode) with SIMULINK toolbox in Matlab, which uses a fixed-step Dormand Prince (a member of family of Runge-Kutta methods) differential equation solver [109] to evaluate the response of the system. White noise forcing was generated using the Gaussian white noise generator function that generates discrete-time normally distributed random numbers with sampling time step matching the solver step size chosen as 0.1, resulting in generation of 10,000 data points. The forcing was observed to have a mean approaching zero. Both displacement and forcing matrices were saved to the Matlab workspace for further processing. The excitation was applied to the first mass only.

In the decomposition, the \mathbf{V} ensemble was formed with centered finite differences with a total step of two samples, such that difference matrix \mathbf{D} was $N_v \times N$, and $\mathbf{V} = \mathbf{X}\mathbf{D}^T$ was $n \times N_v$, where $N_v = N - 2$. From the data decomposition eigenvalues, estimates of the natural frequencies are compared to the true modal frequencies in Table 3.1.

Table 3.1: *System frequencies estimated from smooth orthogonal decomposition (SOD) with white noise forcing compared against structural eigen frequencies in Eq. 3.3*

SOD	Structural EVP	% Error
0.1816	0.1838	1.19
0.5275	0.5266	0.17
0.8133	0.8143	0.12
1.0963	1.0966	0.02
1.3875	1.3859	0.11
1.6449	1.6412	0.22
1.8368	1.8366	0.01
1.9524	1.9586	0.31

The modal assurance criterion [110, 111] is a useful tool for testing whether the estimated modes are consistent with the system modes. The normalized inner products (squared) between estimated and true modes are seen in Table 3.2. Values of

Table 3.2: *Estimated SOD modes compared against system modes using the modal assurance criterion*

Mode	1	2	3	4	5	6	7	8
1	0.9993	0.0001	0.0001	0.0001	0.0000	0.0002	0.0004	0.0003
2	0.0003	0.9998	0.0004	0.0005	0.0001	0.0008	0.0019	0.0012
3	0.0003	0.0000	0.9994	0.0013	0.0002	0.0022	0.0051	0.0035
4	0.0003	0.0002	0.0003	0.9999	0.0005	0.0056	0.0127	0.0094
5	0.0000	0.0001	0.0001	0.0004	1.0000	0.0006	0.0022	0.0011
6	0.0003	0.0007	0.0023	0.0057	0.0005	0.9999	0.0279	0.0136
7	0.0008	0.0017	0.0051	0.0136	0.0018	0.0256	0.9997	0.0307
8	0.0005	0.0008	0.0021	0.0070	0.0012	0.0145	0.0296	0.9999

near unit magnitude indicate modal vectors that nearly line up.

For visualization, the modal vectors from smooth orthogonal decomposition and the structural eigenvalue problem are compared in Fig. 3.2.

With random excitation, results are expected to converge as N increases. For this example, we increased N , with the time step fixed at 0.1, and plotted the estimated frequencies in Fig. 3.3 (Table 3.3 shows the percent errors). Increasing N improves the frequency estimates. The period of the lowest-frequency mode is about 34 seconds. Estimates of this mode converged within about 10,000 samples, or 1000 seconds (about 30 first-mode cycles of random response).

Important in the convergence is the relative contributions of matrices $\frac{1}{N}\mathbf{X}\mathbf{X}^T$, $\frac{1}{N}\mathbf{V}\mathbf{V}^T$ and $\frac{1}{N}\mathbf{X}\mathbf{F}^T$. The maximum singular values of these matrices are plotted in Fig. 3.4, indicating that $\frac{1}{N}\mathbf{X}\mathbf{F}^T$ approaches zero (while the other matrices' singular values settle to finite values), thereby becoming negligible in Eq. 3.8 for large N .

The example problem studied had a maximum damping ratio of $\zeta = 0.027$ in the system corresponding to fundamental frequency of $\omega_1 = 0.1838$. With increasing damping, the results deteriorated as seen in Fig. 3.5, even with increased sample size

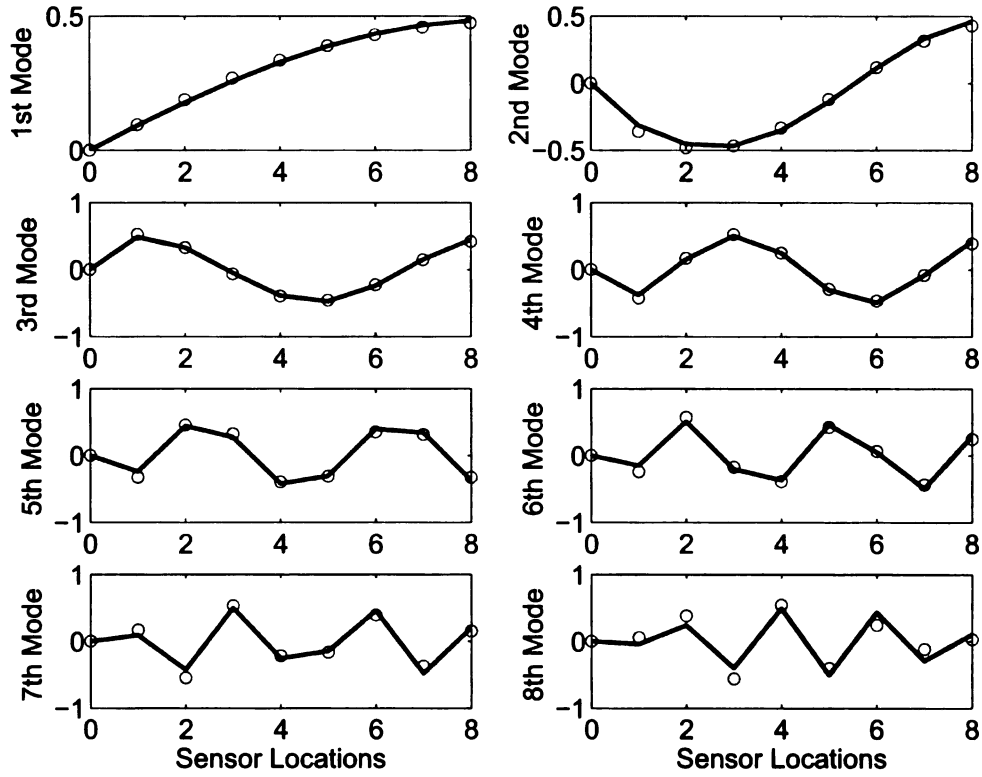


Figure 3.2: A comparison between mode shapes from the structural eigenvalue problem (solid lines) and those estimated from the smooth orthogonal decomposition ('o' symbols). The sensor locations refer to the mass indices. The location 0 represents the wall attachment. The modes are in ascending order by modal frequency.

$N = 10^5$.

When the system had a first-mode damping factor of $\zeta = 0.8$, the error in corresponding frequency estimation was $\approx 8\%$. We also see in the Fig. 3.5, that the frequency estimation is very good for the ideal undamped case, for which the theory was developed.

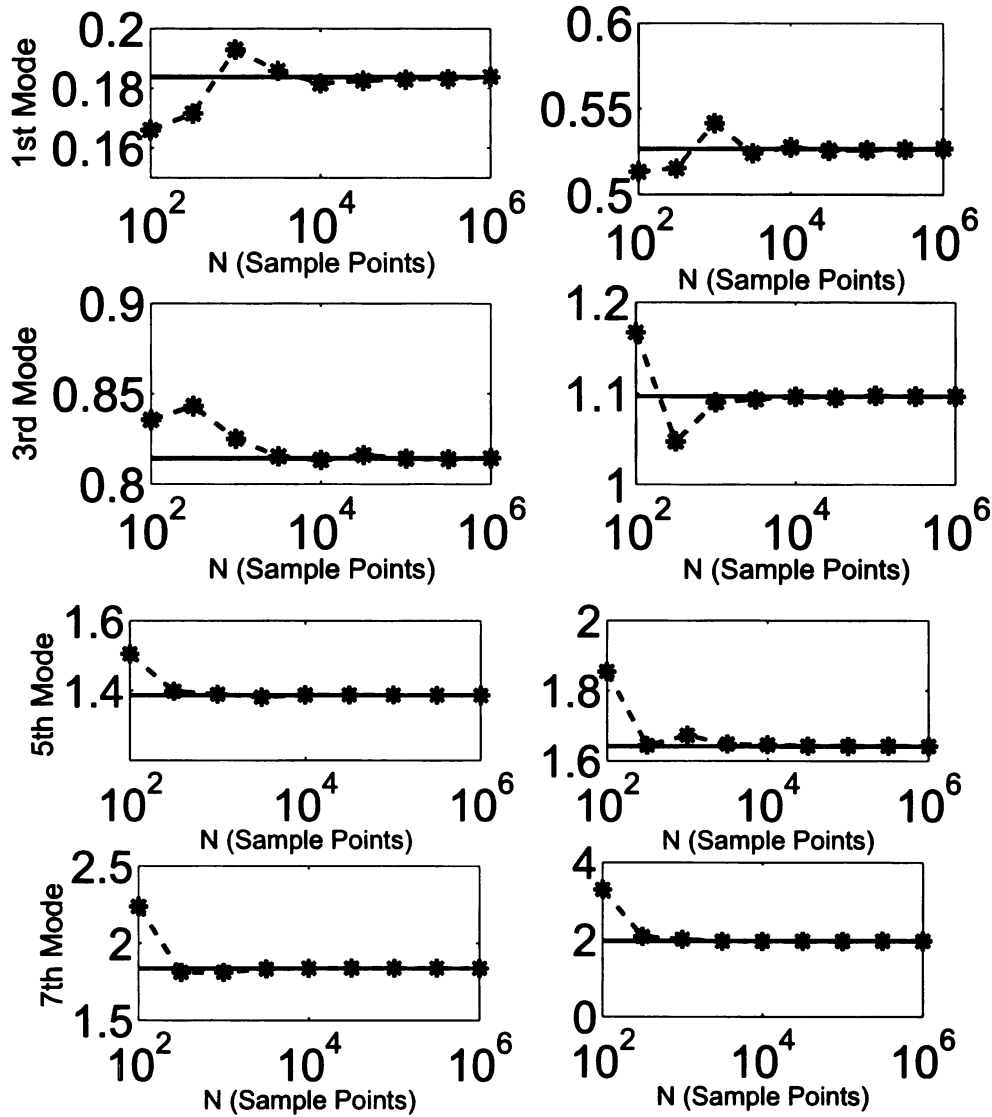


Figure 3.3: The frequency estimates improve as N gets large. The solid line (—) represents the true frequency (rad/sec) and (—*) are the estimated frequencies (rad/sec). The percent error in frequency estimation computed at $N = 10^4$ for modes 1 to 8 are 1.2%, 0.17%, 0.12%, 0.02%, 0.11%, 0.22%, 0.01% and 0.31% respectively also shown in Table 1.

Table 3.3: *Percentage error computation (SOD) for all modes*

Sample Points	10^2	$10^{2.5}$	10^3	$10^{3.5}$	10^4	$10^{4.5}$	10^5	$10^{5.5}$	10^6
ω_1	9.68	6.69	4.95	1.08	1.19	0.70	0.48	0.38	0.00
ω_2	2.54	2.14	2.82	0.49	0.17	0.17	0.11	0.05	0.03
ω_3	2.60	3.53	1.30	0.12	0.12	0.20	0.02	0.07	0.01
ω_4	6.38	4.51	0.57	0.29	0.02	0.11	0.04	0.00	0.00
ω_5	8.60	0.85	0.21	0.39	0.11	0.08	0.06	0.02	0.00
ω_6	12.94	0.13	1.87	0.37	0.22	0.01	0.00	0.01	0.01
ω_7	21.79	1.42	1.45	0.27	0.01	0.05	0.03	0.04	0.00
ω_8	68.04	5.83	2.25	0.39	0.31	0.14	0.07	0.03	0.01

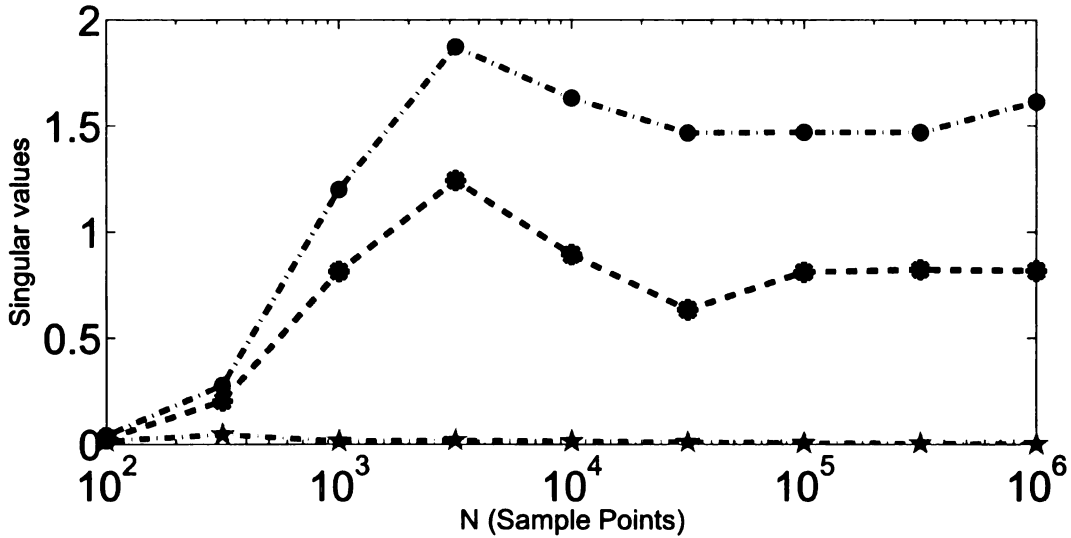


Figure 3.4: *The maximum singular values of \mathbf{XX}^T/N (m²), \mathbf{VV}^T/N (m/s)² and \mathbf{XF}^T/N (N-m). The dashed line (•) represents values of \mathbf{XX}^T/N , the dashed line (•) represents the values of \mathbf{VV}^T/N and the line (•) represents values of \mathbf{XF}^T/N . We can see by $N = 10^4$ samples, $\mathbf{XF}^T/N \ll (\mathbf{XX}^T/N, \mathbf{VV}^T/N)$ and is perhaps negligible for this and larger values of N*

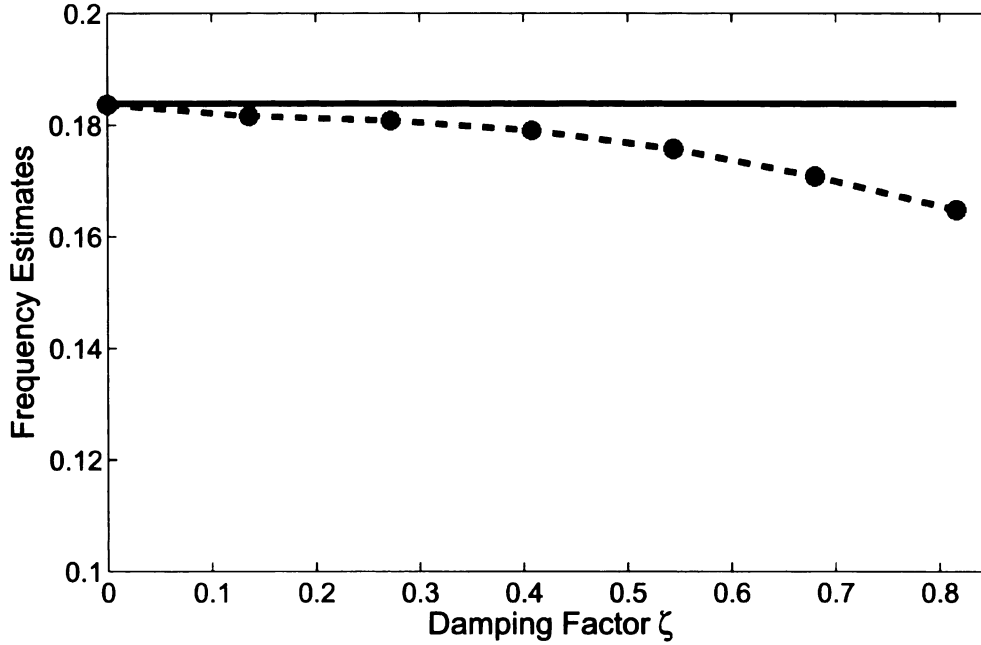


Figure 3.5: *The undamped natural frequency estimate starts to deteriorate for high damping. The solid line (–) represents the true frequency (rad/sec) and (–*) is the estimated frequency (rad/sec). Here samples size is $N = 10^5$*

3.4 State-variable modal decomposition for systems under random excitation

In this section, we explore the SVMD method for random response. We apply the decomposition strategy in the similar way as described in section (2.2.2), and we will see that there is a remarkable resemblance in the SVMD and the SOD analysis of randomly excited systems which will be fully exploited.

3.4.1 State-variable modal decomposition and random excitation

Consider a MDOF damped vibration system,

$$\mathbf{M}\ddot{\mathbf{x}} + \mathbf{C}\dot{\mathbf{x}} + \mathbf{K}\mathbf{x} = \mathbf{f}(t), \quad (3.13)$$

where $\mathbf{f}(t)$ is a random excitation and the matrices \mathbf{M} , \mathbf{C} , and \mathbf{K} represent the system mass, damping and stiffness terms in the usual manner.

We define a state vector $\mathbf{y}^T = [\dot{\mathbf{x}}^T, \mathbf{x}^T]$, and again use the equation $\mathbf{M}\ddot{\mathbf{x}} - \mathbf{M}\dot{\mathbf{x}} = \mathbf{0}$, to obtain forced equations of motion of the form

$$\mathbf{A}\dot{\mathbf{y}} + \mathbf{B}\mathbf{y} = \bar{\mathbf{F}}, \quad (3.14)$$

where

$$\mathbf{A} = \begin{bmatrix} \mathbf{0} & \mathbf{M} \\ \mathbf{M} & \mathbf{C} \end{bmatrix}, \quad \mathbf{B} = \begin{bmatrix} -\mathbf{M} & \mathbf{0} \\ \mathbf{0} & \mathbf{K} \end{bmatrix}, \quad \bar{\mathbf{F}} = \begin{bmatrix} \mathbf{0} \\ \mathbf{F} \end{bmatrix} \quad (3.15)$$

where \mathbf{F} represents the ensemble matrix of the sampled $\mathbf{f}(t)$. Thus similar to section 2.2.2, we use the state-variable ensemble $\mathbf{Y} = [\mathbf{V}^T, \mathbf{X}^T]^T$, where $\mathbf{V} = \mathbf{X}\mathbf{D}^T \approx \dot{\mathbf{X}}$ is the approximate velocity ensemble, and \mathbf{D} is the matrix of centered finite differences.

The vector form of the state-variable eigenvalue problem of Eq. (2.6) is

$$\alpha \mathbf{Y}\mathbf{Y}^T \underline{\psi} = \frac{1}{N} \mathbf{Y}\mathbf{W}^T \underline{\psi} \quad (3.16)$$

Now, taking the derivative $\mathbf{W} = \mathbf{Y}\mathbf{D}^T \approx \dot{\mathbf{Y}}$, and making use of the Eq. (3.14), $\mathbf{W} \approx \dot{\mathbf{Y}} = -\mathbf{A}^{-1}\mathbf{B}\mathbf{Y} + \mathbf{A}^{-1}\bar{\mathbf{F}}$, we get

$$\alpha \frac{1}{N} \mathbf{Y}\mathbf{Y}^T \underline{\psi} \approx -\frac{1}{N} \mathbf{Y}\mathbf{Y}^T \mathbf{B}^T \mathbf{A}^{-T} \underline{\psi} + \frac{1}{N} \mathbf{Y}\bar{\mathbf{F}}^T \mathbf{A}^{-T} \underline{\psi}. \quad (3.17)$$

In matrix form,

$$\frac{1}{N} \mathbf{Y}\mathbf{Y}^T \mathbf{\Psi} \mathbf{\Lambda} = -\frac{1}{N} \mathbf{Y}\mathbf{Y}^T \mathbf{B}^T \mathbf{A}^{-T} \mathbf{\Psi} + \frac{1}{N} \mathbf{Y}\bar{\mathbf{F}}^T \mathbf{A}^{-T} \mathbf{\Psi}. \quad (3.18)$$

We are interested in the conditions when $\mathbf{Y}\bar{\mathbf{F}}^T \mathbf{A}^{-T} \mathbf{\Psi} \approx 0$. Close examination of this matrix reveals

$$\begin{aligned} \frac{1}{N} \mathbf{Y}\bar{\mathbf{F}}^T \mathbf{A}^{-T} \mathbf{\Psi} &= \frac{1}{N} \begin{bmatrix} \mathbf{V} \\ \mathbf{X} \end{bmatrix} [\mathbf{0} \quad \mathbf{F}^T] \mathbf{A}^{-T} \mathbf{\Psi} \\ &= \frac{1}{N} \begin{bmatrix} \mathbf{0} & \mathbf{X}\mathbf{D}^T \mathbf{F}^T \\ \mathbf{0} & \mathbf{X}\mathbf{F}^T \end{bmatrix} \mathbf{A}^{-T} \mathbf{\Psi} \end{aligned} \quad (3.19)$$

The elements of Eq. (3.19) contain the matrices $\mathbf{X}\mathbf{F}^T$ and $\mathbf{X}\mathbf{D}^T\mathbf{F}^T$. Of these matrices, $\mathbf{X}\mathbf{F}^T$ has exactly the same form as the Eq. (3.10) discussed in the section (3.2.2.1) for the SOD forced eigenvalue problem while the other matrix $\mathbf{X}\mathbf{D}^T\mathbf{F}^T$ is much similar but involves a linear combination of terms in \mathbf{F} . This matrix could also be seen as $\mathbf{V}\mathbf{F}^T$ which won't exploit $h_v(0)$, since $h_v(0) \neq 0$. However, by looking at the singular values of $\mathbf{V}\mathbf{F}^T/N$, it was observed in this example (but not shown) that the singular values of $\mathbf{V}\mathbf{F}^T/N$ have similar strength to those of $\mathbf{X}\mathbf{F}^T/N$ and thus may be approximated to $\mathbf{0}$ for larger N values. This is not a proof but gives some evidence of success in approximating $\mathbf{V}\mathbf{F}^T \approx \mathbf{0}$.

Thus, for the white noise cases as detailed in section (3.2.2.2), the response and the excitation are uncorrelated, and the matrix form of the SVMD eigenvalue problem Eq. (3.18) represents the unforced structural eigenvalue problem Eq. (2.11) for large N . Just like SOD, the SVMD should also produce estimates of the modal parameters (frequency and damping), and mode shapes of the MDOF system subjected to white noise excitation.

3.4.2 *Numerical example*

To perform modal parameter identification using SVMD for randomly excited systems, we revisit the same example that was used for SOD random analysis. Since the initial conditions, the simulation time interval, the step sizes, the numerical integration scheme, and the set of data points ($N = 10,000$), are kept exactly the same as the SOD example, the interested reader can draw conclusions about both methods.

For the SVMD decomposition, the ensemble matrices \mathbf{Y} and \mathbf{W} were formed and assembled in the eigenvalue problem. From the data decomposition eigenvalues, estimates of the natural frequencies are compared to the true modal frequencies in Table 3.4.

The modal vectors from state-variable modal decomposition and the structural

Table 3.4: System frequencies estimated from state variable decomposition (SVMD) with white noise forcing compared against structural eigen frequencies in Eq. (3.3)

SVMD	Structural EVP	% Error
0.1826	0.1838	0.65
0.5292	0.5266	0.49
0.8094	0.8143	0.60
1.0967	1.0966	0.00
1.3822	1.3859	0.27
1.6361	1.6412	0.30
1.8275	1.8366	0.49
1.9453	1.9586	0.67

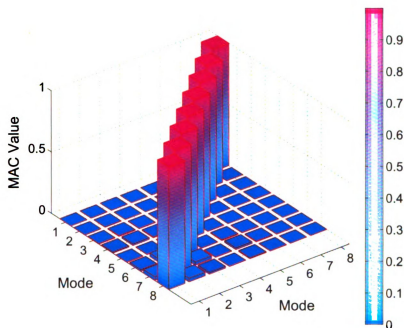


Figure 3.6: The MAC values comparison for SVMD for random excitation. MAC value of 1 shows vectors match up. Modes are not in any particular sequence

eigenvalue problem are compared using the modal assurance criterion in Fig. 3.6.

The frequency and mode shape estimates show the same trend as those seen in the SOD modal identification. Similarly, it was also seen (but not shown) that the estimates improved when the sample size increased. However, SVMD was unable to produce good damping estimates (not shown) that were expected from the theoretical

analysis. This needs further investigation. However, we suspect that this is primarily due to involvement of differentiating of the \mathbf{X} ensemble twice to obtain the velocity and acceleration ensembles. This can be seen by looking at the damping values obtained by the SVMD decomposition that uses the SIMULINK generated acceleration and velocity ensembles (as opposed to generating velocity and acceleration ensembles by differentiating the displacement ensemble) for $N = 10^{4.5}$ samples, as shown in Table 3.5.

Table 3.5: *System damping ratios estimated from the state-variable decomposition (SVMD) with white noise forcing compared against structural damping ratios in Eq. (3.3)*

Damping ratio	Structural EVP	SVMD
ζ_1	0.0272	0.0281
ζ_2	0.0095	0.0101
ζ_3	0.0061	0.0074
ζ_4	0.0046	0.0047
ζ_5	0.0036	0.0038
ζ_6	0.0030	0.0028
ζ_7	0.0027	0.0028
ζ_8	0.0026	0.0027

Further increase of sample points, showed further reduction of the error in damping ratio estimates. Furthermore, system damping ratios up to $\zeta = 0.8$ were estimated within 5% of accuracy.

3.5 Summary

The extension of smooth orthogonal decomposition and the state-variable decomposition methods for modal parameter estimation under random excitation has been presented. Analysis suggests that, for undamped systems, if the expected value of the product between response and excitation variables is zero, then the decomposition methods converge to an equivalent representation of the undamped structural

eigenvalue problem, and therefore should produce estimated modal frequencies and mode shapes for randomly excited structures. This was justified for white noise excitation, and the convergence to the structural eigenvalue problem was demonstrated in a simulation.

In the SOD simulation example, random excitations were applied to a linear eight-degree-of-freedom structural system while damping was kept light. It was shown that the mean of the product of displacement matrix and forcing vector approaches zero as sufficiently large number of samples are captured. This in turn means that the effect of forcing in formulating the eigenvalue problem becomes negligible. Therefore, the smooth orthogonal decomposition eigenvalue problem from data of the randomly forced problem in essence becomes representative of the free structural eigenvalue problem.

The example problem studied was subjected to light damping. As damping increases, the SOD estimation results slowly deteriorated. While this work focused on white-noise excitation, if it can be shown that the mean of product between the response and the forcing approaches zero (in reference to equations (3.8) and (3.10)) for other classes of random excitation, this would broaden the applicability of smooth orthogonal decomposition for randomly excited systems.

For random responses, all of the conclusions reached for smooth orthogonal decomposition also apply to the state-variable modal decomposition and thus any of these methods is equally good candidate for modal frequencies and mode shapes estimates of lightly damped system. The SVMD could not produce good damping estimations unless \mathbf{V} was known accurately, separately from $\mathbf{X}\mathbf{D}^T$. In such case, SVMD estimations got beyond small damping restrictions.

4.1 Introduction

Previous work using numerical studies has shown that for low noise cases, the decomposition based methods work very well in estimating modal parameters for free response and in some cases forced response. However, to implement the decomposition methods in the physical applications, experimental studies must be conducted. These types of studies can be helpful in understanding practical aspects of the identification problem, for instance, proper selection of system model order, issues surrounding number of sensors, linearity, boundary conditions, and effects of filtering. This chapter, thus deals with the experimental verification of the ideas presented in the previous chapters. The experimental studies conducted herein address both the advantages and the limitations of applying the decomposition methods in non-perfect conditions.

In this work, three kinds of experimental studies are conducted. First, a structural system modeled as a single-degree-of-freedom (SDOF) system is investigated in section (4.2) and then a clamped-free beam experiment that presents a structural system modeled as a multi-degree-of-freedom (MDOF) is addressed in section (4.3). Modal analysis is performed on both kinds of experiments using the SVMD method

[100–102]. Practical aspects of data length and effects of filtering are addressed followed by the use of modal coordinates for qualitatively establishing true or spurious modes. Finally, we investigate an experimental study reported in the reference [112] to highlight the limitations on using the decomposition method.

4.1.1 Assumptions

Let, for any arbitrary input $f(t)$, the system output $y(t)$ be given as

$$y(t) = \int_{-\infty}^{+\infty} h(\tau)f(t - \tau)d\tau \quad (4.1)$$

In Eq. (4.1), $h(\tau)$ is a weighting function (impulse response function) defined as the output of the system at any time to a unit impulse applied at a time $\tau = 0$. For the response of the systems detailed herein, the experiments assume the following outline. A rigorous treatment of the subject can be found at, for example in [5, 113, 114].

- The system under study is *linear*. A system is linear if response characteristics are additive and homogeneous, that is, it obeys the *principle of superposition* [115–119]. This means that doubling or halving the inputs would respectively double or half the outputs at any particular frequency. This also suggests that $h(t)$ is not dependent on the input [120].
- The system is *time invariant*, implying that the impulse response function $h(\tau)$ and its Fourier transform $H(\omega)$ do not change whether the input is applied now or the input is delayed t seconds from now. That is

$$h(t, \tau) = h(\tau) \text{ for } -\infty < t < +\infty \quad (4.2)$$

In simple terms, the system parameters (mass, stiffness and damping) are constant.

- The system is considered *stable* such that every possible bounded input produces a bounded output for systems having all of their poles in the left half

plane. This is true if the function $h(\tau)$ is absolutely integrable [120]. To see this,

$$|y(t)| = \left| \int_{-\infty}^{+\infty} h(\tau) f(t - \tau) d\tau \right| \leq \int_{-\infty}^{+\infty} |h(\tau)| |f(t - \tau)| d\tau \quad (4.3)$$

If the input $f(t)$ is bounded by a finite constant R , that is,

$$|f(t)| \leq R \quad \forall t \quad (4.4)$$

then, using the Eq. (4.4) in Eq. (4.3), we see that

$$|y(t)| \leq R \int_{-\infty}^{+\infty} |h(\tau)| d\tau \quad (4.5)$$

Or simply,

$$\int_{-\infty}^{+\infty} |h(\tau)| d\tau < \infty \quad (4.6)$$

Similar conclusion for a MIMO case is presented in [117]. The condition in Eq. (4.6) is deemed both necessary and sufficient [121] (reproduced here without proof) rendering that the system is BIBO (bounded input bounded output) stable. For a detailed discussion on stability in linear systems, please see for example [115–118, 121].

- The system should be *physically realizable*. In other words,

$$h(\tau) = 0 \quad \text{for } \tau < 0 \quad (4.7)$$

This condition asserts that the system would not respond before the excitation is applied. Thus, Eq. (4.1) can be modified to

$$y(t) = \int_0^{+\infty} h(\tau) f(t - \tau) d\tau \quad (4.8)$$

The above conditions are generally true for calculating any FRFs and hence are applicable to the output-only methods' experimentation as well.

4.2 A single-degree-of-freedom experiment

In this section, experimental data of a study conducted by Rhoads et. al [122] is analyzed using the SVM [100] method. The beam experiment was conducted in such a way that the system behaves as a single-degree-of-freedom (SDOF) system since the beam was resonated into its fundamental mode, the excitation turned off and the free response examined, and therefore is used for evaluating the SVM method as a SDOF case. The purpose of the original experiment conducted in Dynamics and Vibrations Research Lab at MSU, was to augment the analysis of parametric amplification in mechanical systems. Modal parameters in the original work were obtained using the classical methods [92] and are used as a benchmark for comparison.

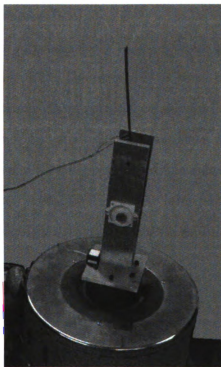


Figure 4.1: *The experimental setup for study by Rhoads et. al*

The experimental setup of Rhoads et. al [122] comprised a cantilever spring steel beam of dimensions ($190 \times 19 \times 0.5 \text{ mm}^3$) vertically mounted on a electromagnetic

shaker (MB Dynamics PM-500) as shown in Fig. 4.1. The base excitation provided by the shaker was measured by a 3-axis accelerometer (Analog Devices ADXL105EM-3). The beam was sensed with two electrical resistance strain gauges (Vishay Micro measurements division, model EA-13-120LZ-120) mounted on either sides of the beam that constitute a half-bridge circuit [123]. A strain gauge signal conditioner (Vishay Micro measurements division, Model 2210) was then employed to amplify and balance the signal strain gauge Wheatstone bridge circuit and after filtering the signal at 100 HZ cut-off frequency, the signal was fed to a data acquisition system (TEAC GX-1 Integrated Recorder) where the strain signals were recorded. For the analysis contained in this work, the system was excited in a different way from Rhoads et. al [122]. Here, instead of the shaker, the excitation was provided by a finger flick that incurs a free-vibration response [124].

Data were acquired for approximately 12.267 seconds and 63814 data points were obtained as shown in Fig. 4.2. The strain data were then recorded in a comma separated value (CSV) format Excel spreadsheet file and subsequently sent to MATLAB for further processing. For analysis purposes, data were truncated down to get $\approx 10,000$ points to obtain a “clean” portion of the signal, since the initial part of the signal was observed to be “choppy”, and the later part contained high frequency noise. Thus, signal samples from $N = 10,000$ to $N = 20,000$ were used as shown in Fig. 4.3.

The experimental frequency obtained by FFT [92] was about 11.49 Hz as seen in Fig. 4.4, with the damping factor obtained using the logarithmic decrement method [125, 126] from a nearly single-mode response being estimated at ≈ 0.0065 . By looking at the Fig. 4.2, we observe that the damping is both viscous and Coulomb. Nonetheless, we can carry out the identification by SVMD on the data. The frequency value obtained via SVMD method is 11.54 Hz. The computed damping factor from SVMD is ≈ 0.0066 . The representative equivalent viscous damping identification is consis-

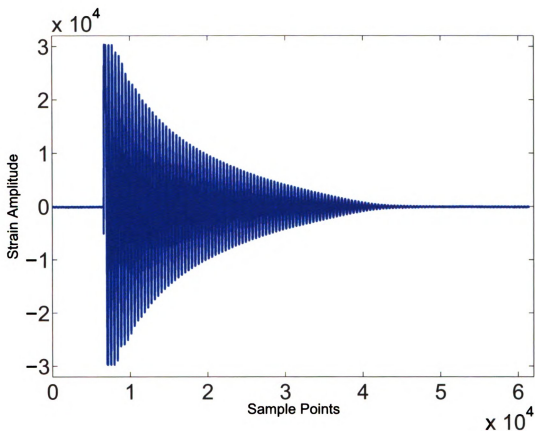


Figure 4.2: *The impulse response of SDOF beam experiment for study by Rhoads et. al*

tent with the log decrement method calculation. The theoretical natural frequency calculated is 11.5 Hz, with mass of the sensor being ignored since it is very small. The associated error values respectively are shown in Table 4.1.

Table 4.1: *Estimated modal parameters from the decomposition method compared against theoretical and classical experimental methods*

Parameter	Theoretical	Classical	Experimental	Methods	SVMD
Frequency (Hz)	11.50		11.49		11.54
Damping Ratio ζ	-		0.0065		0.0066
Error in Frequency	0		0.08%		0.34%
Error in Damping	-		0%		1.53%

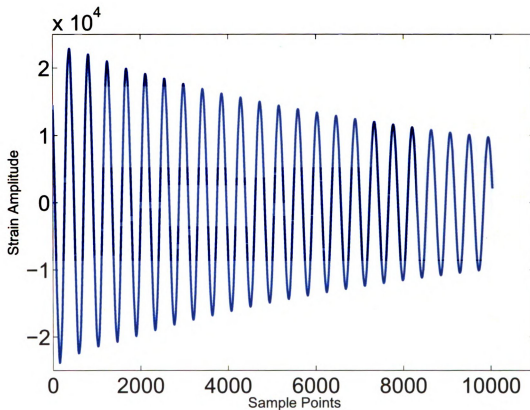


Figure 4.3: *The truncated sample points to obtain a “clean” signal for analysis of the study by Rhoads et. al*

4.3 Clamped-free beam experiment

This section describes the modal parameter estimation of a clamped-free beam using the SVMd method for a free vibration experiment. The system is assumed to follow the assumptions described in section (4.1.1). The experimental setup of the system is described as below.

A $941 \times 52 \times 3 \text{ mm}^3$ clamped-free uniform steel beam as shown in Fig. 4.5 was prepared for the experiment conducted in the Dynamics and Vibrations Research Lab at MSU. The beam was sensed with 16 PCB model number 352B10 accelerometers, each of which weighs 0.7 gm with a sensitivity listed in catalogue at about 10 mV/g (individual sensitivities vary slightly), equally spaced from clamp to the beam tip via beeswax [4]. Beam properties hence are: elastic modulus $E = 190 \times 10^9 \text{ GPa}$, density

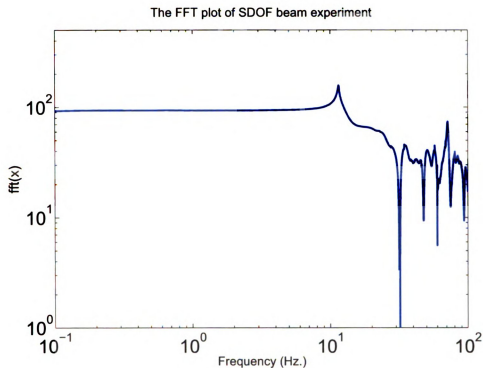


Figure 4.4: *The FFT log plot of the SDOF beam experiment*

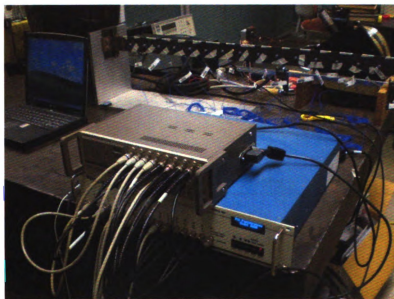


Figure 4.5: *The experimental setup of a 16 DOF clamped-free beam*

$\rho = 7500 \text{ Kg/m}^3$, mass per unit length including the sensors mass $m = 1.1907 \text{ Kg/m}$,
(without the sensors mass $\bar{m} = 1.1787 \text{ Kg/m}$ but mass of the sensors was accounted

for in calculating the theoretical natural frequencies of the system), and moment of inertia $I = 1.17 \times 10^{-10} \text{ m}^4$. Measurement signals from the accelerometers were then processed via signal conditioning amplifier PCB Model number 481A02, the output of which was then fed to a data acquisition system (TEAC GX-1 Integrated Recorder) where the acceleration measurement signals were recorded by passing through a low pass filter and then converted into ASCII.txt format. Further processing of these files was done in Matlab.

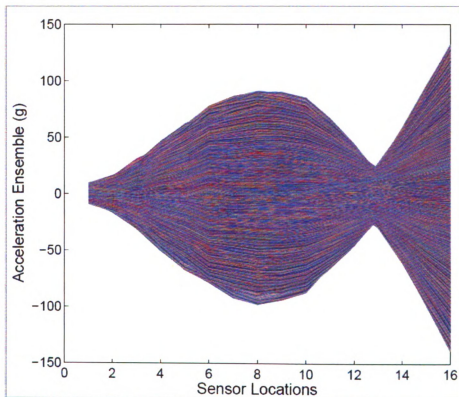


Figure 4.6: *The beam acceleration snapshots of the acceleration ensemble of a 16 DOF clamped-free beam with its mean removed.*

The data were sampled at a rate of 5 kHz. The data were digitally filtered with the cut-off frequency of the low-pass filter set at 0.4 kHz. This value was set well below the Nyquist frequency to avoid aliasing effects. The beam was excited with an impulse, with the resulting response monitored by the accelerometers. Measurement recording time of approximately six seconds was used with sampling step used as $1/F_s$, where F_s

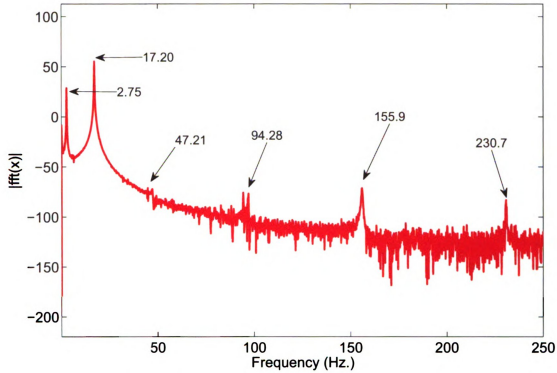


Figure 4.7: The linear FFT plot of a 16 DOF clamped-free beam. Only first six modes are shown.

is the sampling frequency. The number of samples thus obtained were $N = 36,327$. The data were also high-pass filtered to reduce the low frequency noise effects on subsequent integrations of the acceleration signals. As such, the ensemble matrix of acceleration time histories A of size 16×36327 was formed. For uniformity, each acceleration signal was then individually calibrated per its accelerometer sensitivity specifications. Using the Matlab routine “cumtrapz”, the velocity V and displacement X ensembles were obtained numerically. All ensembles were then processed to remove the respective means. On one of the acceleration signals, the FFT algorithm was conducted and is plotted in Fig. 4.7. Next, the correlation matrices $\mathbf{P} = \mathbf{Y}\mathbf{Y}^T$ and $\mathbf{Q} = \mathbf{Y}\mathbf{W}^T$, for the decomposition method SVMD were formed, where $\mathbf{Y} = [\mathbf{v}^T, \mathbf{x}^T]^T$ and $\mathbf{W} = [\mathbf{A}^T, \mathbf{V}^T]^T$ that were obtained by numerically integrating the acceleration ensemble.

4.3.1 Filtering effects

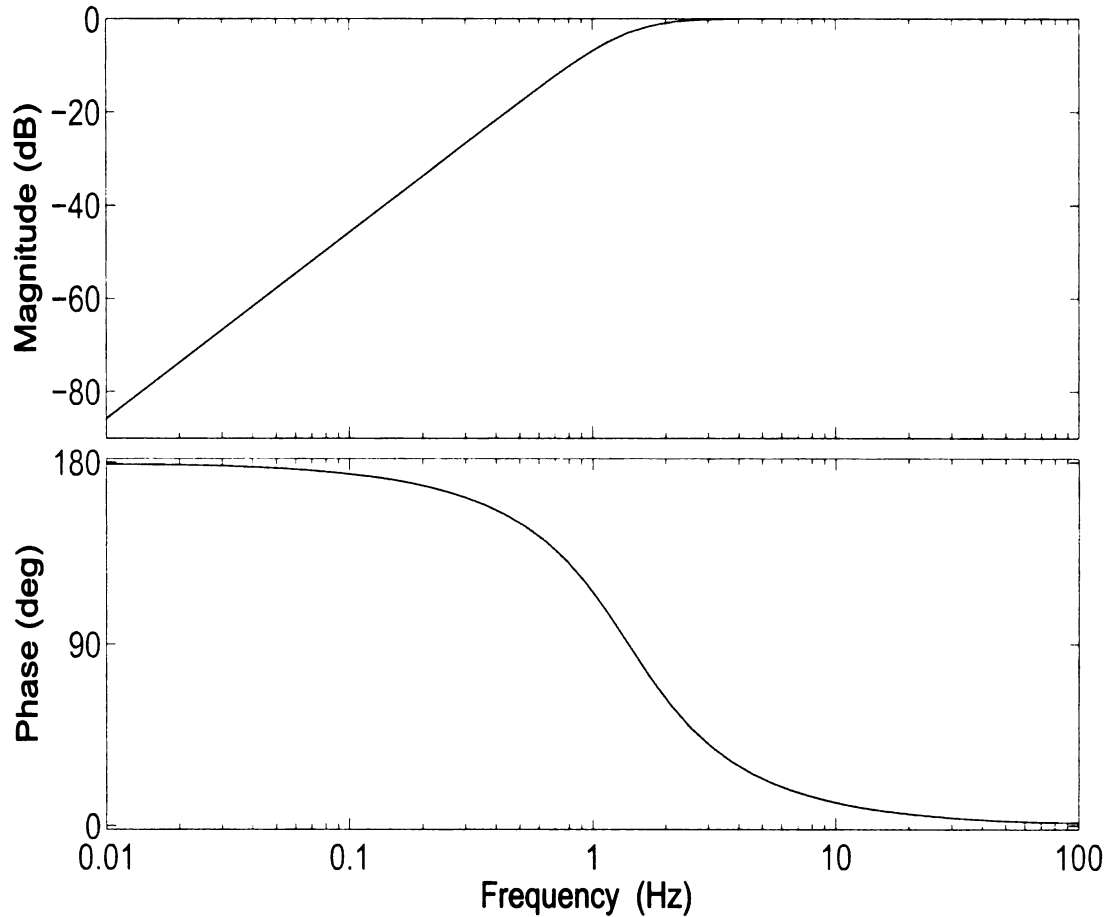


Figure 4.8: *The frequency response of the second order high-pass filter for the 16 DOF beam experiment.*

To remove a low frequency “drift” in the integrated signal ensembles, data were high-pass filtered at a filter frequency of 1.4 Hz. This value was selected at about half of the first natural frequency obtained from the FFT plot Fig. 4.7. Note that the filter frequency was evaluated in the range of 0.5 Hz to 2.0 Hz with no significant change observed in the high frequency estimates, and some improvements seen in the lowest frequency estimate as the filter frequency approached to 0.5 Hz. This suggests that as a limiting case, a maximum of one half of the fundamental frequency by FFT should be employed as the filter frequency.

The frequency response of the second order high-pass filter modeled as a SDOF system is shown in Fig. 4.8. The filter amplitude at twice the break frequency is observed to be 0 dB (1 in the linear case), thus implying that application of the filter does not reduce the estimated frequencies amplitudes. The phase shifting effects caused by this filter can be removed by running the filter “backwards”. In that way, the filter becomes a fourth order system.

The filter was applied prior to, and after each numerical integration of the signals. Thus, to maintain consistency, the acceleration ensemble was filtered thrice, the velocity ensemble twice and the displacement ensemble only once. Cast this way, the filter order became 12 for the ensembles.

4.3.2 *Identification results*

We kept the first $N = 12,000$ points to minimize the contribution of the high frequency noise dominating the decayed signals in the later part of the ensembles. These reduced sized ensemble matrices \mathbf{Y} and \mathbf{W} were then assembled into \mathbf{P} and \mathbf{Q} of the SVMD eigenvalue problem from which the eigenvectors and eigenvalues were extracted. From the acceleration snapshots in Fig. 4.6, we see that the beam acceleration had a dominant second mode, implying that the impulse input, or equivalently the initial conditions, had a stronger effect on the second modal coordinate than the rest [105].

The theoretical frequency values and the values from taking the FFT and the log decrement method are tabulated in Table 4.2. The log decrement method is applied to carefully excited, dominantly single-mode excitation responses (this was obtained by constraining a nodal point while plucking the beam). The SVMD method identified modal frequencies and the respective damping ratios as also presented the same table. The error thus in the frequency estimates is 1.41% and 0.30% respectively.

Since the high modes are expected to damp out rather quickly, for the same experi-

Table 4.2: *Estimated modal parameters from the decomposition method for a linear beam free response compared against the undamped structural eigen frequencies and the FFT for data consisting of first $N = 12,000$ sample values.*

Parameter	Theoretical	Classical Methods	SVMD
ω_1	2.74	2.75	2.78
ω_2	17.16	17.20	17.18
ζ_1	-	0.0048	0.0049
ζ_2	-	0.0040	0.0032

mental run, in order to see the higher modes, data were further pared down to the first $N = 1000$ points with everything else being kept the same. Now the decomposition method was able to estimate the first five modes. The obtained frequency identification results for the first five modes are shown in the Table 4.3. Damping estimates for the first three modes computed on the carefully excited, dominantly “pure mode” responses by the log decrement method are compared against the identification scheme in the Table 4.4.

Table 4.3: *Experimental system frequencies (Hz.) estimated from SVMD for a linear beam free response compared against the undamped structural eigen frequencies and the FFT values for data consisting of first $N = 1000$ sample points.*

Method	Theoretical	FFT	SVMD
ω_1	2.74	2.75	3.01
ω_2	17.16	17.20	17.18
ω_3	48.05	47.21	47.39
ω_4	94.16	94.28	88.96
ω_5	156.66	155.9	153.78

It is clear from these two ($N = 12,000$ and $N = 1000$) data sets that a trade-off exists between the number of modes to be estimated and the accuracy acquired from the estimation. For an estimation of lower modes, a large-time data set is expected to be useful since higher modes generally dissipate quickly, leaving lower modes to dominate most of the recorded response. On the other hand, for the estimation of

Table 4.4: *Experimental modal damping estimated from the SVMD method for the linear beam free response for first $N = 1000$ sample values. Only the first three damping estimates are experimentally estimated by “pure mode” log decrement method.*

Method	Log Decrement	SVMD
ζ_1	0.0048	-0.035
ζ_2	0.0040	0.0040
ζ_3	0.0036	0.018
ζ_4	-	0.0077
ζ_5	-	0.0017

higher modes, a relatively short-time data set could be utilized with the caveat that “short-time” data set begins to err in the lower modal parameter estimates if the time record is short compared to the lower modal periods. This can be observed in the damping estimate of the first mode that was completely “missed” by the decomposition method even though the frequency estimate for that mode remains reasonable in Table 4.4.

Mode shapes are now estimated using the SVMD method using the $N = 1000$ sample points. The eigenvectors obtained from the method are normalized and are plotted separately for each mode in the figures 4.9, 4.10, 4.11, 4.12, and 4.13. These plots in general, accord with the frequency estimates with a distortion observed in the lowest mode. This distortion is speculated to be due to low frequency limit on the PCB sensor (per product specs, sensor’s working range is 2-10,000 Hz, the lower limit being close enough to the fundamental frequency of the beam).

In both the long and short time-record examples, the number of identified modal sets is well less than number, n , of sensors. The remaining identified modes are spurious. The spurious modes are distinct from the estimated true modes and their complex conjugate pairs, and are dominated by noise.

It is conceivable that spurious SVMD frequencies could be similar to the true

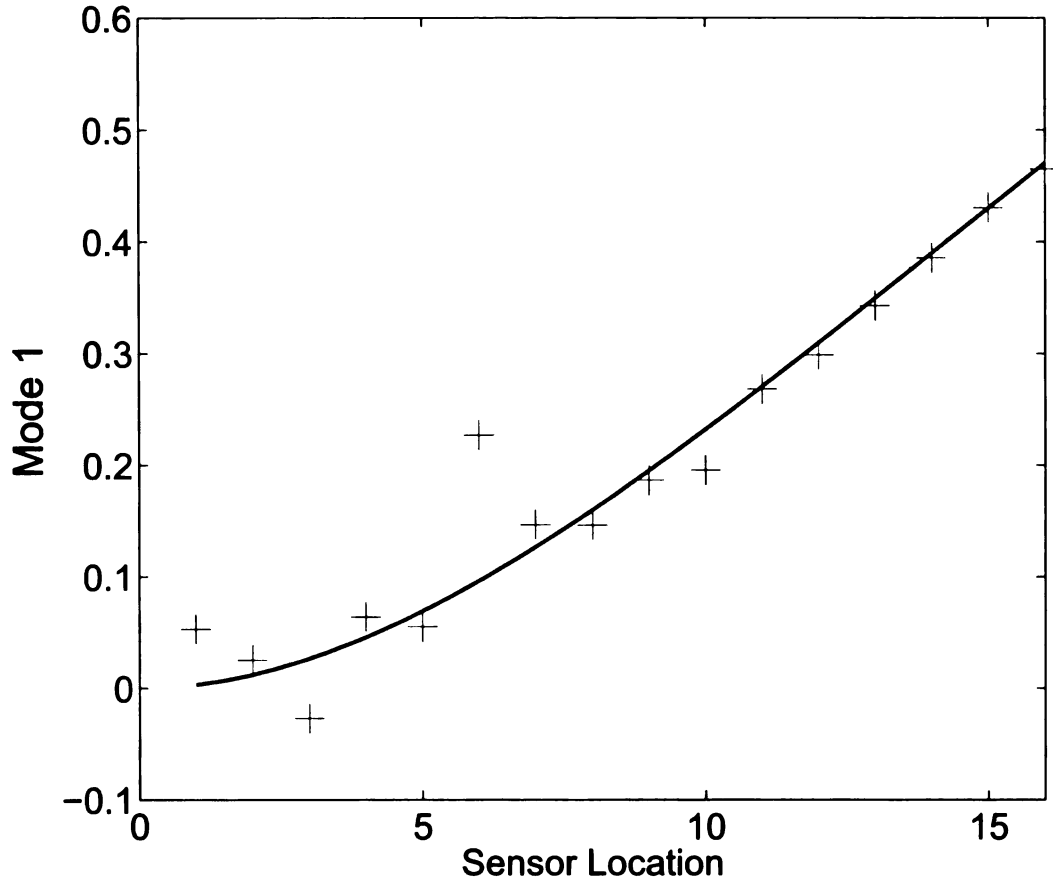


Figure 4.9: *SVMD is compared for the first beam mode against the theoretical mode. SVMD is shown with + mark, theoretical mode is shown with the solid line —.*

frequencies. In this case, the quality of modal coordinates may give a clue to which modes are true.

4.3.3 Modal coordinates

The POD uses proper orthogonal modal coordinates (POCs) to determine the modal frequencies and which modes correspond to which frequencies, as explained in detail in references [84, 85].

$$\mathbf{y}(t) = \sum_{i=1}^n q_i(t) \underline{\psi}_i. \quad (4.9)$$

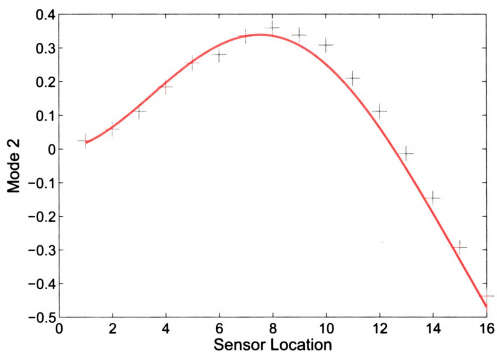


Figure 4.10: *SVMD is compared for the second beam mode against the theoretical mode. SVMD is shown with + mark, the theoretical mode is shown with the solid line —.*

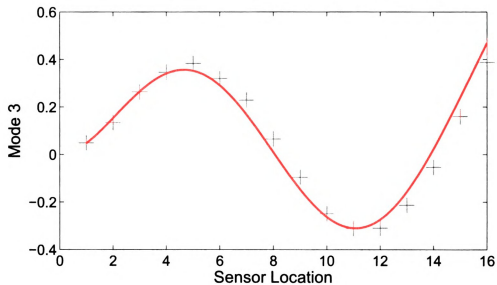


Figure 4.11: *SVMD is compared for the third beam mode against the theoretical mode. SVMD is shown with + mark, the theoretical mode is shown with the solid line —.*

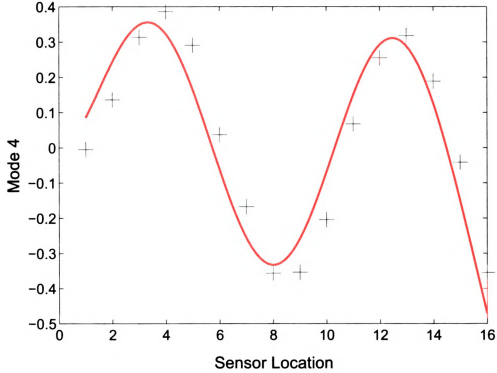


Figure 4.12: *SVMD is compared for the fourth beam mode against the theoretical mode. SVMD is shown with + mark, the theoretical mode is shown with the solid line —.*

where $q_i(t)$ are the SVMD modal coordinates. In matrix form, $\mathbf{X} = \Psi \bar{\mathbf{Q}}$, where elements in the i th row of \mathbf{Q} are the i th SVMD coordinate histories. Noting that for SVMD $\Psi \Psi^{-1} = \mathbf{I}$, the SVMD modal coordinates $\bar{\mathbf{Q}}$ (SVMCs) are now expressed. These are calculated from

$$\mathbf{Y} = \Psi \bar{\mathbf{Q}} \quad (4.10)$$

where columns of Ψ are the inverse-transpose of the eigenvectors obtained by solving SVMD eigenvalue problem (2.6). Thus, modal coordinates $\bar{\mathbf{Q}}$ are simply obtained by

$$\bar{\mathbf{Q}} = \Psi^{-1} \mathbf{Y} \quad (4.11)$$

Alternatively, one can use $\bar{\mathbf{Q}} = \Phi^T \mathbf{Y}$, where Φ is the non-Hermitian matrix of eigenvector matrix obtained by directly solving the SVMD eigenvalue problem (2.6).

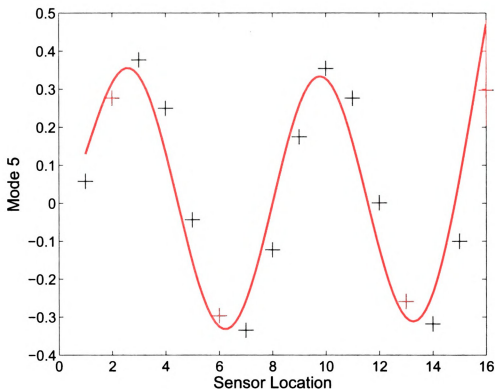


Figure 4.13: *SVMD is compared for the fifth beam mode against the theoretical mode. SVMD is shown with + mark, the theoretical mode is shown with the solid line*

Modal coordinates for the SVMD (SVMCs) are presented in Fig. 4.14. It is shown in the references [84, 85], that the POD directly yields modal dominance and that proper orthogonal modal coordinates give information on modal frequencies. While SVMD gets frequency and damping estimates directly, modal coordinates can indicate the quality of decomposition, and the estimates of the corresponding modal frequencies can be obtained from each modal coordinate time history. For instance, one simple way would be to divide the sampling frequency by a complete cycle of each modal coordinate history. In this particular example, for the first SVMC, the period is not complete (still SVMD got the first mode with data that was less than half of the modal period), but for the higher modes, it is quite easy to calculate the modal frequency. Another way would be to take an FFT of any individual modal coordinate.

As such, frequencies estimated by this way may or may not be as accurate as the ones computed by the SVMd directly, but they do provide a good starting point for further investigations. It appears from Fig. 4.14, that a small quantity of lower modes (mode 1 or 2) has leaked into the higher-modal coordinate histories thus showing a significant low-frequency perturbation on these signals specially in the mode 3 and mode 4.

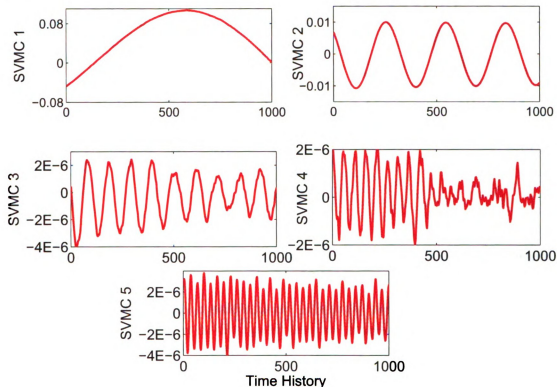


Figure 4.14: SVMd modal coordinates are shown for the first 5 beam modes. Modal coordinates indicate the quality of the decomposition, and can be used to distinguish between computational and actual modes.

With the exception of fourth mode, coordinates are smoothly shaped. A smooth periodic non-noisy modal coordinate history can intuitively indicate an actual mode. For the fourth mode, the latter half of the modal coordinate history is corrupted by noise but the first half is good, so even though borderline, it is still a candidate of an actual mode. Thus, the first half of fourth SVMC was tested, together with

Fig. 4.12 and the frequency estimated by SVMd, it was concluded to be an actual system mode. (Later we will see another way of analyzing these candidates) Also, if

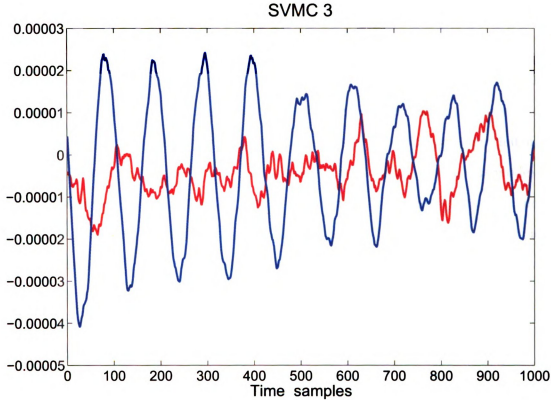


Figure 4.15: SVMd modal coordinates are shown for the third beam mode. Modal coordinates can be used to distinguish between computational and actual modes. Actual mode is shown in dotted (—), whereas spurious is shown in solid line (—).

spurious frequencies are estimated by the SVMd, modal coordinates can “visually” help determine the real modes from fictitious ones. As an example, this is seen in Fig. 4.15 where modal frequencies estimated by the SVMd are close (47.39 and 44.81 Hz), but the modal coordinates clearly indicate the noisy, hence the spurious frequency estimate (shown in the figure as the solid line).

4.4 Limitations on the number of sensors and active modes

In the theoretical development of the SVMD method (section 2.2), it was implicitly assumed that sufficient number of measurement sensors are always available for obtaining the time series data for modal parameter estimation. This number at the minimum is greater than or equal to the system frequencies. In real life cases however, structural systems are composed of infinite degrees-of-freedom, and as such only a limited number of sensors can be applied to any system. We have seen that if the number of sensors n is greater than the number of active modes, spurious modes are present. Conversely, in a situation, where the number of available sensors would be less than the active (dominant) system modes, the SVMD may run into problems. To see this, we will conduct a sensitivity analysis followed by a numerical simulation and an actual experimental test in the following sections.

4.4.1 *Sensitivity analysis*

If the number of sensors employed for identification is less than active/dominant frequencies present in the system, the identified frequencies may deviate from the actual frequencies. To explore this, in this section we analyze an oscillatory system with a harmonic frequency that is contaminated by a small amplitude noise perturbation frequency with only one sensor being used by the system. We are interested in the conditions under which the SVMD identification of the harmonic signal would produce results with minimum or (in ideal case) no estimate deviations. The analysis is carried out by constructing the SVMD eigenvalue problem by this under-sensed system and by obtaining an approximate solution of system eigenvalues.

Consider the harmonic response of a signal containing two frequencies ω_1 and ω_2 such that the amplitude A_2 of ω_2 is very small as compared to the amplitude A of ω_1 , i.e $A_2 = \epsilon A$. Then

$$x(t) = A \cos \omega_1(t) + \epsilon A \cos \omega_2(t) \quad (4.12)$$

Taking the derivative twice, we obtain

$$\dot{x}(t) = -\omega_1 A \sin \omega_1(t) - \epsilon A \omega_2 \sin \omega_2(t) \quad (4.13)$$

$$\ddot{x}(t) = -\omega_1^2 A \cos \omega_1(t) - \epsilon A \omega_2^2 \cos \omega_2(t) \quad (4.14)$$

Forming the \mathbf{Y} and \mathbf{W} matrices, we get

$$\mathbf{Y} = \begin{bmatrix} \dot{x} \\ x \end{bmatrix} = \begin{bmatrix} -\omega_1 A \sin \omega_1 t - \omega_2 \epsilon A \sin \omega_2 t \\ A \cos \omega_1 t + \epsilon A \cos \omega_2 t \end{bmatrix} \quad (4.15)$$

$$\mathbf{W} = \begin{bmatrix} \ddot{x} \\ \dot{x} \end{bmatrix} = \begin{bmatrix} -\omega_1^2 A \cos \omega_1 t - \omega_2^2 \epsilon A \cos \omega_2 t \\ -\omega_1 A \sin \omega_1 t - \omega_2 \epsilon A \sin \omega_2 t \end{bmatrix} \quad (4.16)$$

Thus, the key non-symmetric matrices $\mathbf{Y}\mathbf{Y}^T$ and $\mathbf{Y}\mathbf{W}^T$ are obtained as

$$\mathbf{Y}\mathbf{Y}^T = \begin{bmatrix} \left\{ \begin{array}{c} \omega_1^2 A^2 \sin^2 \omega_1 t \\ + \omega_2^2 \epsilon^2 A^2 \sin^2 \omega_2 t \\ + 2\omega_1 \omega_2 \epsilon A^2 \sin \omega_1 t \sin \omega_2 t \end{array} \right\} & \left\{ \begin{array}{c} -\omega_1 A^2 \sin \omega_1 t \cos \omega_1 t \\ -\omega_1 \epsilon A^2 \sin \omega_1 t \cos \omega_2 t \\ -\omega_2 \epsilon A^2 \sin \omega_2 t \cos \omega_1 t \\ -\epsilon^2 \omega_2 A^2 \sin \omega_2 t \cos \omega_2 t \end{array} \right\} \\ \left\{ \begin{array}{c} -\omega_1 A^2 \sin \omega_1 t \cos \omega_1 t \\ -\omega_1 \epsilon A^2 \sin \omega_1 t \cos \omega_2 t \\ -\omega_2 \epsilon A^2 \sin \omega_2 t \cos \omega_1 t \\ -\epsilon^2 \omega_2 A^2 \sin \omega_2 t \cos \omega_2 t \end{array} \right\} & \left\{ \begin{array}{c} A^2 \cos^2 \omega_1 t \\ + \epsilon^2 A^2 \cos^2 \omega_2 t \\ + 2\epsilon A^2 \cos \omega_1 t \cos \omega_2 t \end{array} \right\} \end{bmatrix} \quad (4.17)$$

and

$$\mathbf{Y}\mathbf{W}^T = \left[\begin{array}{c} \left\{ \begin{array}{l} \omega_1^3 A^2 \sin \omega_1 t \cos \omega_1 t \\ + \omega_2^2 \omega_1 \epsilon A^2 \sin \omega_1 t \cos \omega_2 t \\ + \omega_2^3 \epsilon^2 A^2 \sin \omega_2 t \cos \omega_2 t \\ + \omega_1^2 \omega_2 \epsilon A^2 \sin \omega_2 t \cos \omega_1 t \end{array} \right\} \\ \left\{ \begin{array}{l} -\omega_1^2 A^2 \cos^2 \omega_1 t \\ -\omega_2^2 \epsilon A^2 \cos \omega_1 t \cos \omega_2 t \\ -\epsilon \omega_1^2 A^2 \cos \omega_1 t \cos \omega_2 t \\ -\omega_2^2 \epsilon^2 A^2 \cos^2 \omega_2 t \end{array} \right\} \end{array} \right\} \left\{ \begin{array}{l} \omega_1 A^2 \sin^2 \omega_1 t \\ + \omega_2^2 \epsilon^2 A^2 \sin^2 \omega_2 t \\ + 2\omega_1 \omega_2 \epsilon A^2 \sin \omega_2 t \sin \omega_1 t \end{array} \right\} \\ \left\{ \begin{array}{l} -\omega_1 A^2 \sin \omega_1 t \cos \omega_1 t \\ -\omega_1 \epsilon A^2 \sin \omega_1 t \cos \omega_2 t \\ -\omega_2 \epsilon A^2 \sin \omega_2 t \cos \omega_1 t \\ -\epsilon^2 \omega_2 A^2 \sin \omega_2 t \cos \omega_2 t \end{array} \right\} \end{array} \right] \quad (4.18)$$

Multiplying both sides by $\frac{\Delta t}{N}$ and approximating the summations as integrals, we note that all of the trig identities can be solved/approximated. Substituting these values in the SVMD eigenvalue problem and simplifying, we obtain

$$\begin{aligned} & \left[\begin{array}{cc} \frac{\omega_1^2 A^2 + \omega_2^2 \epsilon^2 A^2}{2} & 0 \\ 0 & \frac{A^2 + \epsilon^2 A^2}{2} \end{array} \right] \Phi \Lambda \\ &= \left[\begin{array}{cc} 0 & \frac{(\omega_1^2 A^2 + \omega_2^2 \epsilon^2 A^2)}{2} \\ \frac{(\omega_1^2 A^2 + \omega_2^2 \epsilon^2 A^2)}{2} & 0 \end{array} \right] \Phi \end{aligned} \quad (4.19)$$

that further simplifies to

$$\Lambda \Phi = \left[\begin{array}{cc} 0 & 1 \\ \frac{(\omega_1^2 A^2 + \omega_2^2 \epsilon^2 A^2)}{(A^2 + \epsilon^2 A^2)} & 0 \end{array} \right] \Phi = \left[\begin{array}{cc} 0 & 1 \\ \frac{(\omega_1^2 + \omega_2^2 \epsilon^2)}{(1 + \epsilon^2)} & 0 \end{array} \right] \Phi \quad (4.20)$$

The identified eigenvalues of this system are

$$\lambda^2 = \frac{(\omega_1^2 + \omega_2^2 \epsilon^2)}{(1 + \epsilon^2)} \quad (4.21)$$

We observe that if the noise perturbation amplitude is small, that is if $\epsilon \approx 0$, then the eigenvalues are approximately ω_1^2 and the SVMD correctly identifies the system frequency. However, if ϵ is significant, the eigenvalues estimation suffers greatly. This would be the case where either the system may have high noise amplitudes, or the system may have many active/dominant modes such that the frequency amplitudes cannot be correlated (i.e A and A_2 are independent, as opposed to the assumption made earlier in this analysis where frequency amplitudes were related).

Addition of a third frequency perturbation to the original signal approximately results in $\lambda^2 = \frac{(\omega_1^2 + \omega_2^2\epsilon^2 + \omega_3^2\epsilon^2)}{(1 + \epsilon^2 + \epsilon^2)}$, that further deviates the SVMD identification from the actual frequency.

This analysis is of a simple system that underscores the repercussions of having limited availability of the sensors and significance of low noise amplitude on the signals when using the SVMD for modal parameter identification. Next, we will present two examples to verify the analysis.

4.4.2 *Numerical example*

In this example, we again simulate the numerical three degree-of-freedom mass-spring-damper example using modal damping ($c = 0.01\mathbf{M}$) shown in section (2.3) with a small difference as explained below.

The system uses $N = 2000$ data points, with time step $\Delta t = 0.01$, is corrupted with 8 bit quantization noise, and uses a differentiation step size of 32 ($n_d = 16$). The response is constructed in the similar way shown in section 2.3 from $\mathbf{y}(t) = \Phi\mathbf{q} = \Phi\mathbf{q}_0 e^{\alpha t}$ where $\mathbf{q}_0 = \Phi^T \mathbf{A}\mathbf{y}(0)$.

While constructing the modal amplitudes $\mathbf{q}(t)$, we added a perturbation frequency $\omega = 2\omega_3$, with an amplitude of order $\epsilon = 0.1$ to the third frequency signal. This way the system has four frequencies with only three sensors. The estimated parameters are shown in table 4.5.

Table 4.5: *Modal parameters estimation from reduced number of sensors compared against the theoretical eigenvalue problem for a three DOF discrete system with 8 bit quantization noise.*

Method	System		SVMD	
Ω_i	<i>Freq.</i>	<i>Damp.</i>	<i>Freq.</i>	<i>Damp.</i>
ω_1	0.4209	0.0119	0.4208	0.0125
ω_2	1.0000	0.0050	0.9958	0.0050
ω_3	1.6801	0.0030	1.7844	0.0054

Modal identification of the first two modes is very good. We see that the third mode is “off”. The approximation of Eq. (4.21) estimates the undamped system frequency at $\omega_3 = 1.7049$, that was not achieved due to presence of damping and noise in the system. (When we ran a simulation for undamped case, SVMD estimated $\omega_3 = 1.7483$ that is closer to the predicted value).

It is clear from this simulation study that the decomposition method at best, is **only** as good as the number of sensors available to it.

4.4.3 A free-free linear beam experiment

In the works of references [86, 112], a linear steel beam was explored to gain insight into **the** POD method. We will use the same beam data to understand the observability **issues** surrounding the SVMD method¹.

In the experiment conducted, a $12.7 \times 12.7 \times 1500 \text{ mm}^3$ uniform steel beam with **free-free** boundary conditions was prepared to experimentally compare its normal **modes** with the extracted POMs. The beam was horizontally hung with two soft **strings** attached at the ceiling and the vibration responses in the horizontal direction **were** measured under the impulse hammer impact excitation (at one free end) applied **in the** same direction. This way, at least eight beam modes were excited. The number **of** beam modes were controlled by adjusting the Nyquist frequency of measurement

¹Special thanks to Dr. S. Han for providing experimental data for this study.

[112] and by using an anti-aliasing filter. To measure the response of the system, six equally spaced accelerometers were attached along the length of the beam. These accelerometers had varying sensitivities, a discussion of which can be seen in [86]. These also made the structure non-homogeneous since they weighed differently and carried significant mass as compared to the beam (the heaviest sensor was reported to be about 3% of the beam mass). The signals were then simultaneously fed into the B&K 2035 FFT signal analyzer (it uses 2048 sampling points) with 8-channel input module. The time record was used as 1 second, hence the sampling frequency was 2048 Hz. The acceleration time response histories and the power spectral densities of the six beam sensor responses can be seen in [112].

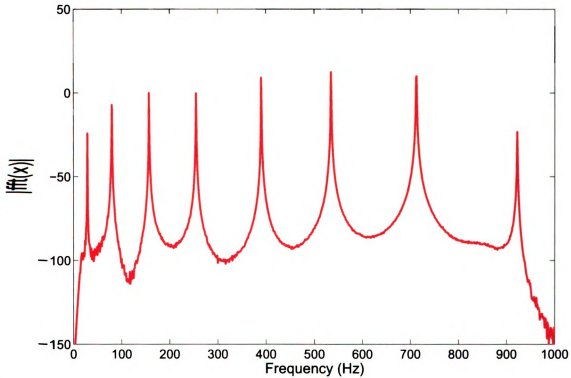


Figure 4.16: The FFT of an acceleration time history channel of the experimental free-free beam. Eight active frequencies are visible within the Nyquist range.

Even though the plot shown in [112], shows seven frequencies, there exists yet another frequency within the Nyquist range (= 1024 Hz) of frequencies that can be

observed by applying an FFT over one of the acceleration time histories (6th sensor chosen here but it is an arbitrary choice) as shown in the Fig. 4.16.

4.4.3.1 Identification by SVMD

The SVMD is now applied on this free-free beam experiment. For this particular example, acceleration ensemble was integrated twice in SIMULINK to get the velocity and displacement ensembles (it resulted in a slightly better identification this way, instead of using the usual MATLAB numerical integration “cumtrapz” scheme). As noted in section 4.3.1, filter application is important and again, the high-pass filter frequency was selected at 14.5 Hz that is approximately half of the beams’ first natural frequency. Then the SVMD eigenvalue problem was formulated and the frequency estimation results computed that are shown in the Table 4.6.

Table 4.6: *Modal frequency estimation for an experimental free-free beam using a number of sensors that is less than active frequencies compared against the theoretical undamped values.*

Method	System	SVMD
Ω_i	<i>Freq.</i>	<i>Freq.</i>
ω_1	29.32	30.19
ω_2	80.83	76.54
ω_3	158.46	158.16
ω_4	261.94	248.40
ω_5	391.30	-
ω_6	546.53	610.71

Parameter identification is reasonable up to three or may be four modes. Identification for the third frequency seems very good but that is probably a random happenstance. SVMD is not able to identify even the fifth and sixth modes (that were expected if we are using 6 sensors, but since all of the 8 beam modes are active/dominant, the decomposition suffers in identification as discussed in section

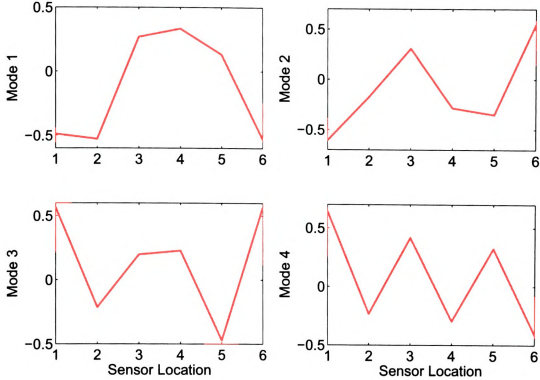


Figure 4.17: Mode shapes obtained by the SVMD of the experimental free-free beam.

4.4.1). Mode shapes for the first four modes are shown in Fig. 4.17. Mode shapes do not reveal a smooth shape and are difficult to interpret if used alone. The mode shape for the third frequency also augments our suspicion that the accurate estimate for the third frequency is only random. Perhaps the only consolation for mode shapes is that POD (and SOD) also reveal the same modal content (not shown). SVMD modal coordinates are also shown in Fig. 4.18 and appear to be giving meaningful information for perhaps the first two modes only (Zooming “in” into the time axis of the higher modes did not show any different results). Rather surprisingly, an FFT computation of the first state-variable modal coordinate is able to detect system frequencies very well as shown in Fig. 4.19 in which the first mode is about 70 dBs above the rest. In fact, these frequencies were precisely the same as identified in reference [112] as the experimental system frequencies. In [112], the authors reported that POD (on

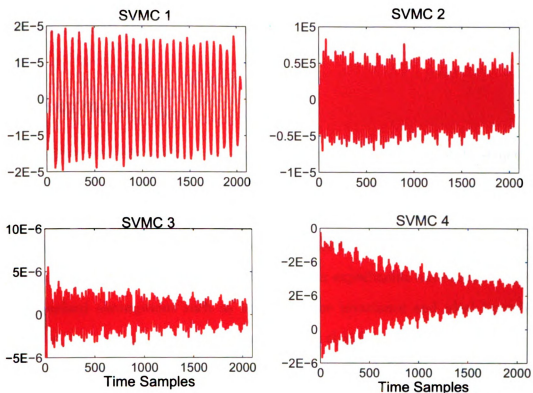


Figure 4.18: First four state-variable modal coordinates plot of the experimental free-free beam.

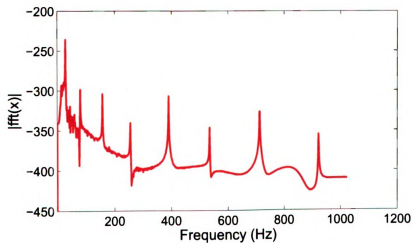


Figure 4.19: FFT of the first state-variable modal coordinate of the experimental free-free beam.

acceleration signals) was able to get better mode shapes on higher modes where the acceleration signals were more significant.

4.5 Summary


We have experimentally evaluated the modal parameter identification of the structural systems using the state-variable modal decomposition method. Two experimental studies are conducted that incorporate identification for the two systems modeled as SDOF and MDOF system, respectively. The identified systems are then matched against the theoretical results. It is possible that our experiments have some deviation from standard assumptions such as linearity, time invariance and ideal boundary conditions, and as such identification can result in significant errors.

The decomposition method showed good results for both SDOF and MDOF cases. For the MDOF case, a greater number of sensors was used than the active/dominant frequencies present in the system and the system frequencies, damping ratios and mode shapes were obtained. We observed that data length can be slightly manipulated to either identify greater number of modes or increase accuracy in lower modal identification. The trend observed was that short-time data results in higher modes estimates whereas longer-time data is good for lower modes estimates. Some spurious modes may appear in parameter identification that by using the modal coordinates together with the modal vectors can be visually separated. The observations stated herein were gained by testing multiple experimental test beams. It was also observed that low frequency noise issue can be addressed by an appropriate filter selection.

To highlight the limitations of the decomposition method, identification was performed on another experimental data from previous works. It was learnt that if number of active/dominant system modes is greater than the number of sensors available, the SVMD method may not be able to accurately identify except maybe a

limited number of modal parameters. In that case, modal coordinates and modal vectors could still be used as a valuable tool for parameter identification at least in qualitative sense.

Quantitative Assessment of Identification

e have seen modal decomposition methods as a way of estimating system parameters. We have also seen that modal coordinates obtained from the decomposition methods shed light on decomposition results in a qualitative manner. We will now focus on developing tools to provide further insight on the quality of identification results. Furthermore, in this chapter, by employing these new tools, we hope to explore some limitations and issues that the decomposition techniques may inherently possess.

5.1 Use of modal coordinates to evaluate decomposition results

Modal coordinates are a useful measure to describe the quality of decomposition methods. Works of Feeny [85] and Chelidze [95] for instance, bear testimony to this statement. While modal coordinates, in general, could be very useful in qualitative examination of decomposition effectiveness, there, however lies a caveat in using this measure alone.

Interpretation of pictorial presentations involves user's judgement that is quite

acceptable if the user is experienced and could easily distinguish between actual and spurious results. However, sometimes a “feel” may not be altogether conclusive especially when the user is not fully experienced in correlating the results. In some extreme cases, this may potentially lead to erroneous conclusions. Therefore, there is a need of a quantitative tool applicable to modal coordinates to determine the quality of decomposition. This would be useful in practical situations, where interpretation of the results may be critical.

Since our interest mostly is in manipulation of the modal coordinates that are inherently decoupled, we focus on system response of SDOF systems. Typically, we would introduce the frequency response function (FRF). The FRF of a system is approximated by taking the Fourier transform (FT) of the input and output of the impulse response of the system. If we assume that the impulse is nearly ideal, we can estimate the FRF from the response only to an unknown scaling constant.

The well known form of a normalized FRF for an ideal mass-spring-damper system as a function of frequencies is

$$H(\omega) = \frac{1}{1 - (\omega/\omega_n)^2 + i2\zeta\omega/\omega_n} \quad (5.1)$$

Note that, for experiments, the FRF would either be generated from taking the FFT of a modal coordinate that will be termed H , or by using estimated frequency and damping, in that case it will be termed as H_o .

We will now use this FRF to introduce two criteria that will be helpful in determination of the decomposition quality. Assuming that the decomposed modal coordinate behaves as a linear SDOF system, the features of its approximate FRF are to be compared to $H(\omega)$ based on extracted system parameters ω_n and ζ .

5.2 Quantitative assessment of modal coordinate FRF

5.2.1 Introduction

We will propose two tools to quantify modal coordinates quality from the decomposition. These are termed as the spectrum assurance criterion and the spectrum difference criterion and are explored below.

5.2.2 The spectrum assurance criterion (SAC)

The spectrum assurance criterion (SAC) bears similarities with the modal assurance criterion (MAC) [111]. While the MAC compares the relative consistency between mode shapes of target modal vector with the ideal modal vector by using inner products, the SAC uses inner products to compare frequency response functions (FRFs). The FRF formed from the modal coordinates is matched against an ideal frequency response that is generated from the damping and frequency estimates obtained from the decomposition or by other means such as FFT. By using the FRFs, the spectrum assurance criterion (SAC) is defined as

$$SAC = \frac{\{|\underline{H}|^T |\underline{H}_o|\}^2}{|\underline{H}|^T |\underline{H}| |\underline{H}_o|^T |\underline{H}_o|} \quad (5.2)$$

where $|\underline{H}|$ represents the magnitude of reference frequency response function vector \underline{H} that is obtained from the modal coordinate spectrum sampled in the ω space, and $|\underline{H}_o|$ represents the magnitude of constructed (actual or obtained) frequency response function vector \underline{H}_o also sampled in the ω space. In this sense, the vectors \underline{H} and \underline{H}_o are obtained from $\underline{H}(\omega)$ and $\underline{H}_o(\omega)$ and thus the elements in those vectors are function evaluations at sampled frequencies, i.e, $H_i = H_i(\omega_i)$ and $H_{oi} = H_o(\omega_i)$. The value $|\underline{H}|^T |\underline{H}_o|$ is an inner product between the magnitudes of the FRFs \underline{H}_o and \underline{H} .

The SAC is a discrete version of the operation

$$SAC = \frac{\langle |H(\omega)|, |H_o(\omega)| \rangle^2}{\langle |H(\omega)|, |H(\omega)| \rangle \langle |H_o(\omega)|, |H_o(\omega)| \rangle} \quad (5.3)$$

where $\langle f, g \rangle = \int_0^\Omega f(\omega)g(\omega) d\omega$ and the integration limits define the frequency domain of the spectrum.

Alternatively, a slightly modified form of Eq. (5.2) could also be used that incorporates complex vectors.

$$SAC|_c = \left| \frac{\{|\underline{H}^* \underline{H}_o|\}^2}{\{\underline{H}^*\}\{\underline{H}\}\{\underline{H}_o^*\}\{\underline{H}_o\}} \right| \quad (5.4)$$

where the superscript * denotes the Hermitian operation. This form can also be seen as a discrete version of the continuous-variable criterion given by

$$SAC|_c = \left| \frac{\langle H^*(\omega), H_o(\omega) \rangle^2}{\langle H^*(\omega), H(\omega) \rangle \langle H_o^*(\omega), H_o(\omega) \rangle} \right| \quad (5.5)$$

The ratio of inner product values obtained lies between 0 and 1, with 1 being the most matching value.

5.2.3 Spectrum difference (SD)

Another measure in parallel to the SAC is the mean of difference between spectrum amplitudes. With this measure, in contrast to the SAC, values approaching zero would indicate that a true mode has been extracted with correct parameter estimates. For each frequency vector of length \overline{N} that is twice the system bandwidth, the mean value of the difference between obtained and referenced FRFs is presented as

$$SD = \frac{1}{2} \left(\frac{\frac{1}{\overline{N}} \sum_{i=1}^{\overline{N}} \{|H_i| - \overline{a}|H_{oi}|\}}{\overline{H}_i} \right) \quad (5.6)$$

where \bar{a} represents the normalized area under the curve of the amplitude of the either FRFs H or H_o , obtained from $\bar{a} = \frac{\int |H(\omega)| d\omega}{\int |H_o(\omega)| d\omega}$ and $\overline{H_i} = \frac{1}{\overline{N}} \sum_{i=1}^{\overline{N}} \{|H_i|\}$. The values of SD range from 0 (perfect estimates) to 1 (no match).

5.3 Numerical simulations

For the purpose of demonstration, a few case studies on numerically simulated data will be shown first. These numerical examples address systems with combinations such as

1. Correct frequency and correct damping (with and without noise).
2. Correct frequency but incorrect damping.
3. Incorrect frequencies, but correct damping
4. Lightly damped systems vs. heavily damped (peaked vs. flat frequency response)

The spectrum assurance and spectrum difference criteria are now applied to a simulation study that incorporates the cases (1-4) stated above. Two FRFs are generated representing the idealized system and the actual or measured system respectively. For this study the natural frequency of the ideal system is chosen as $\omega_1 = 1$ rad/sec and damping ratio is $\zeta_1 = 0.08$ unless specified otherwise. The frequency samples are equally spaced between a frequency range of 0.01 to 3.1 rad/sec resulting in 310 sample points. This frequency range corresponds to twice the bandwidth of the system (about three times the system frequency). This range was chosen to incorporate contributions of target system and residual effects from other modes, if any.

The construction of the measured system (for instance FRFs estimated from modal coordinates) is similar. In the cases to follow, we will vary the parameters of the measured system and address the cases one by one.

Note that, in most simulation studies to follow, the range of parameter (frequency or damping) estimates in identification is considerably wider than those estimated in the actual physical experiments. This is done to gain an understanding of the applicability domain of these two criteria and such establish an “acceptable” level for these criteria. The identification in physical experiments is expected to be in a much smaller domain.

5.3.1 Correct frequency and damping estimates in both FRFs, with noise contamination in one of the FRFs

The motivation of this set of tests is to evaluate the effect of noise in a system (this could be measurement, instrumentation or process noise). Results from this analysis will provide the information in a case where the decomposition method would have correctly identified values of frequency and damping ratio. However, the presence of noise in the system could distort the FRF estimated from the modal coordinate time history, and hence the SAC and SD could deteriorate.

The complex random noise vector η is generated by the MATLAB function “rand” for the already established range of frequencies. The mean of this vector is adjusted to be close to zero with a range of $\pm 1 \pm i$. The expected root mean squared (RMS) value of the amplitude of the noise signal $\alpha = \sqrt{2/3}$ which is very close to the root mean squared value obtained from our data.

Next, we introduce noise coefficient values ϑ . The coefficient ϑ values range from 0 (no noise) to 4 (high noise). The noise vector is scaled by ϑ , such that the total noise vector is $\delta = \vartheta * \eta$. The noise vector samples δ_i are added to the samples of the frequency response H_i to produce a noise contaminated response function. The SAC and SD computations are thus computed between the noisy and the reference FRFs. Sample low and high noise signal values added to the FRFs are shown in Fig. 5.1 and Fig. 5.2 respectively.

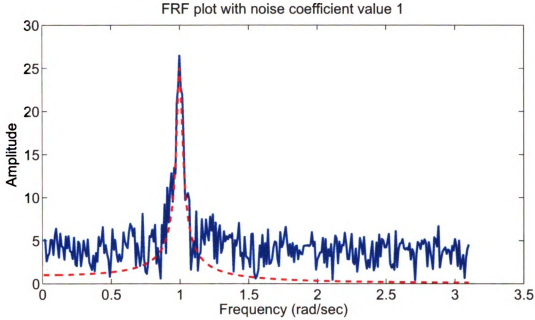


Figure 5.1: *The low noise FRF plot with $\delta = \vartheta * \eta$ representing strength of uniform random noise signal amplitude. Here ϑ value is 1. The dotted line represents FRF plot with no noise $\vartheta = 0$ and is shown for comparison purpose only.*

The normal and complex version of the SAC and SD criteria are evaluated by comparing ideal FRF with the noise added FRF and are shown in Fig. 5.3 and Fig. 5.4 respectively. The values shown for both criteria are very good for low noise cases. However, for increased values of noise, both criteria suffer though spectral difference seems to settle down at a fixed value for greater noise content. The SAC value is near 1 for low noise values in Fig. 5.3, while the SD value is near zero in Fig. 5.4. Also note that the complex version of the SAC seems more sensitive in revealing the modal coordinates than the normal SAC. The complex SAC and the SD performances are similar.

From the results, we establish that even if the decomposition methods correctly identify modal parameters, the effect of noise in modal coordinates could adversely affect the confidence level achieved in identification. If noise level is kept low however, the identification results would be well synchronized with the quantification assess-

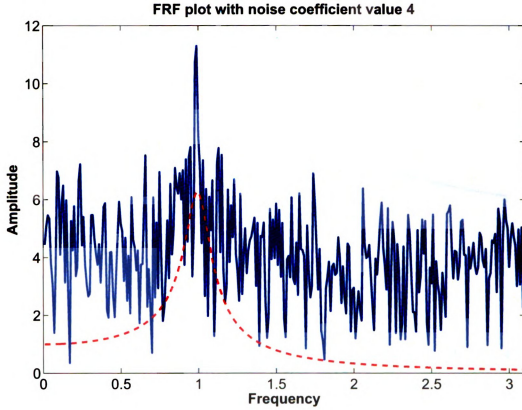


Figure 5.2: The high noise FRF plot with $\delta = \vartheta * \eta$ representing strength of uniform random noise signal amplitude. Here ϑ value is 4. The dotted line represents FRF plot with no noise $\vartheta = 0$ and is shown for comparison purpose only.

ment tools. We also conclude that if a modal coordinate is dominated by noise, for example with a spurious mode, the SAC and SD will produce indicative values.

5.3.2 Correct frequency in both FRFs, with incorrect damping in the tested FRF

In this section and next, we will explore the cases where one of the parameters has been identified correctly while the other has not. Thus, keeping the reference values constant, we will vary the estimation values of the tested FRFs and evaluate the effect on the SAC and SD criteria for such a change. The results from this study will provide insight on sensitivity of the SAC and SD tools on these individual parameters.

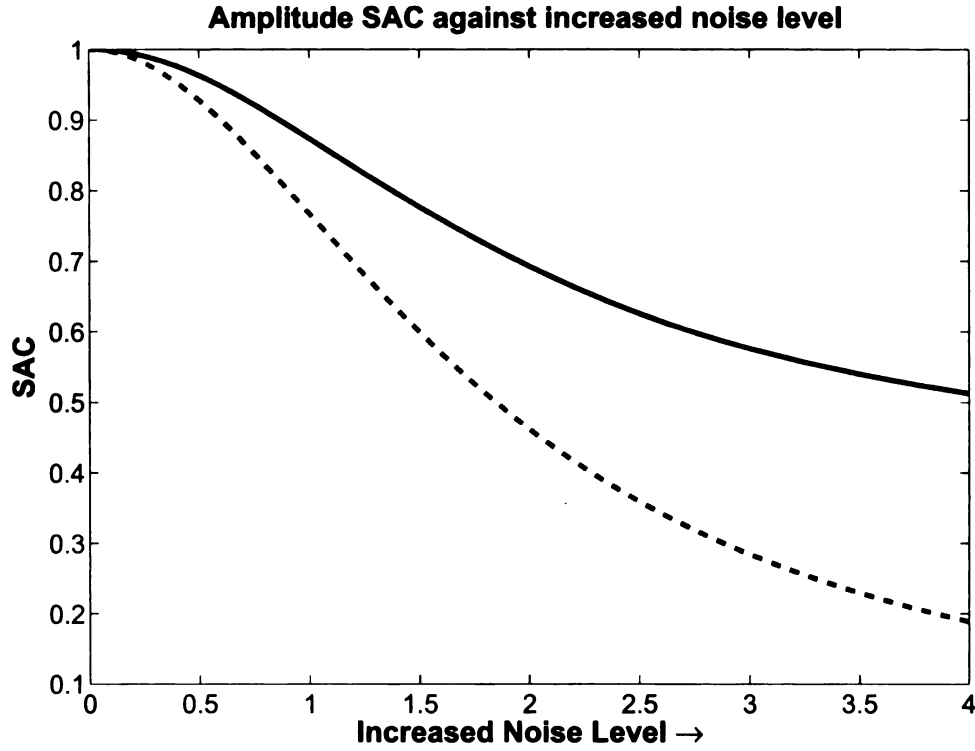


Figure 5.3: *The SAC estimates for frequency identification for various levels of noise. The solid line (—) shows the amplitude SAC while dashed line (- -) presents the amplitude of complex version of the SAC. The horizontal axis indicates the value ϑ representing the uniform random noise coefficient. When noise level increases, the estimates deteriorate significantly.*

The FRF for the measured system is generated by assuming that the decomposition method has identified the frequency content correctly but has identified the wrong damping ratios. This, in real life, would generally be the case for high damping values (SVMD works well for low or moderately damped systems) or low damping with high percentage error.

The damping estimates are presented as ratios of ζ_2/ζ_1 with $\zeta_1 = 0.08$ being the reference value. The error in estimates vary from -100% to $+100\%$ corresponding to ratios of 0 to 2 in the plots shown in Fig. 5.5 and Fig. 5.6 for SAC and spectrum difference estimates respectively.

It can be inferred from the plots that both the SAC and spectrum difference seem

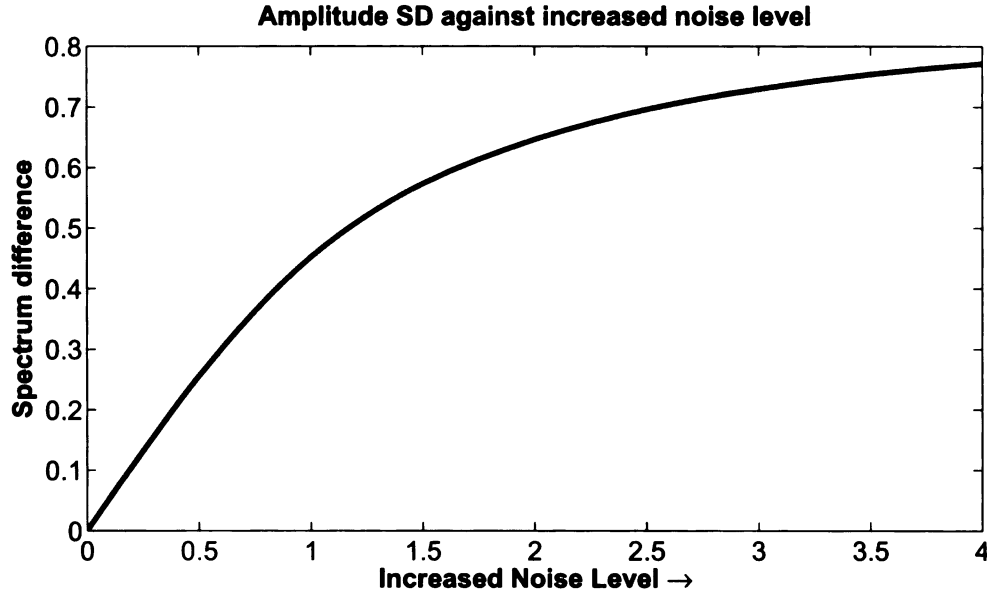


Figure 5.4: *The spectrum difference estimates for frequency identification for various levels of noise. The horizontal axis indicates the value ϑ representing the uniform random noise coefficient. When noise level increases, the estimates deteriorate.*

to indicate a close match if the frequency is identified correctly, and have low sensitivity to damping errors, unless the damping is greatly under estimated. Nonetheless, both SAC and spectrum difference seem to indicate a close match if the frequency is identified correctly, and have low sensitivity to damping errors. The complex SAC has a similar effect.

5.3.3 *Correct damping in both FRFs, with incorrect frequency in the tested FRF*

In general, many physical systems have low damping ratios, estimates of which may not always be of interest, so often the frequency estimates take the center stage. This case is similar to the previous case with the difference that now modal decomposition method has correctly identified damping estimates but errs in estimating the frequency estimates. We will explore the SAC and SD tools to observe their efficacy

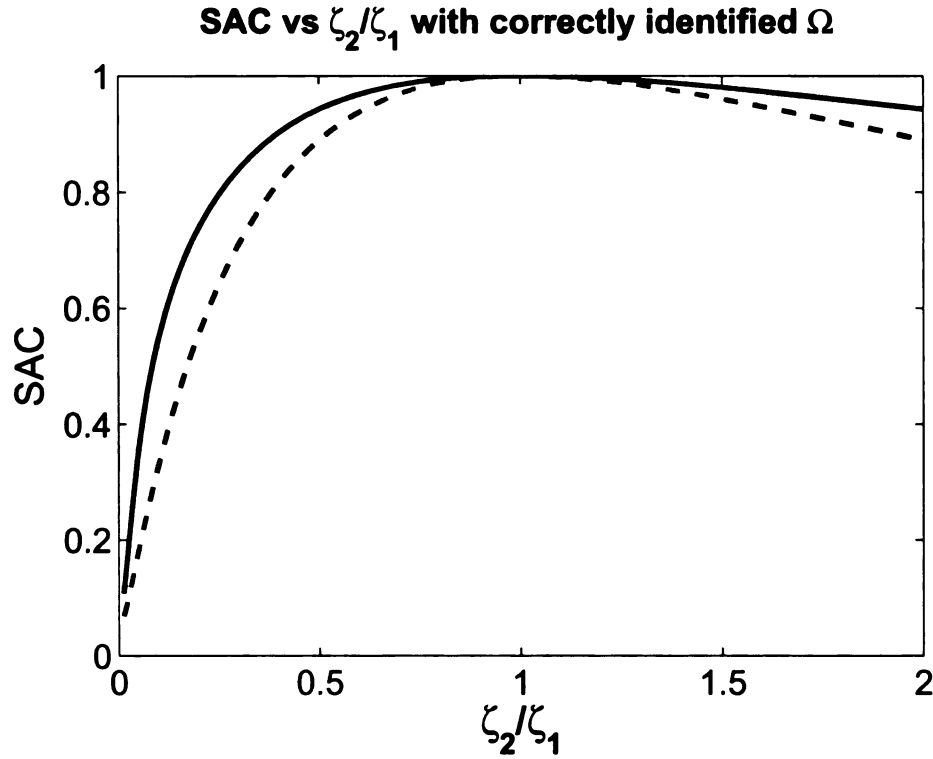


Figure 5.5: The SAC values for various estimates of identified damping ratios. The solid line (—) shows the amplitude SAC while dashed line (--) presents the amplitude of complex version of SAC. The damping estimate error ratio ζ_2/ζ_1 ranges from -100 % at 0.001 to +100 % at 2 with ζ_1 being 0.08 at 1.

in such condition.

In the plots of Fig. 5.7 and Fig. 5.8, the SAC and SD values are pictorially presented for various estimates of frequency values where the horizontal axis is non-dimensional frequency ratio of estimated over actual value. The SAC plot Fig. 5.7 that resembles a resonance curve shows the SAC value drop to ≈ 0.5 when the frequency estimate is “off” by 25 %. The spectrum difference value in Fig. 5.8 for the 25% difference in estimate is close to 0.35 corresponding to 35% error in SD value. The SD values decrease slightly as the frequency ratio increases near the frequency ratio 3, since the estimated frequency approaches the cutoff frequency at those values. This means for the SD computation in this range, the actual FRF vector $|\underline{H}_0|$ is only partially used by the SD scheme.

E

0,

0)

S,

5

In

an

th

to

at

cl

of

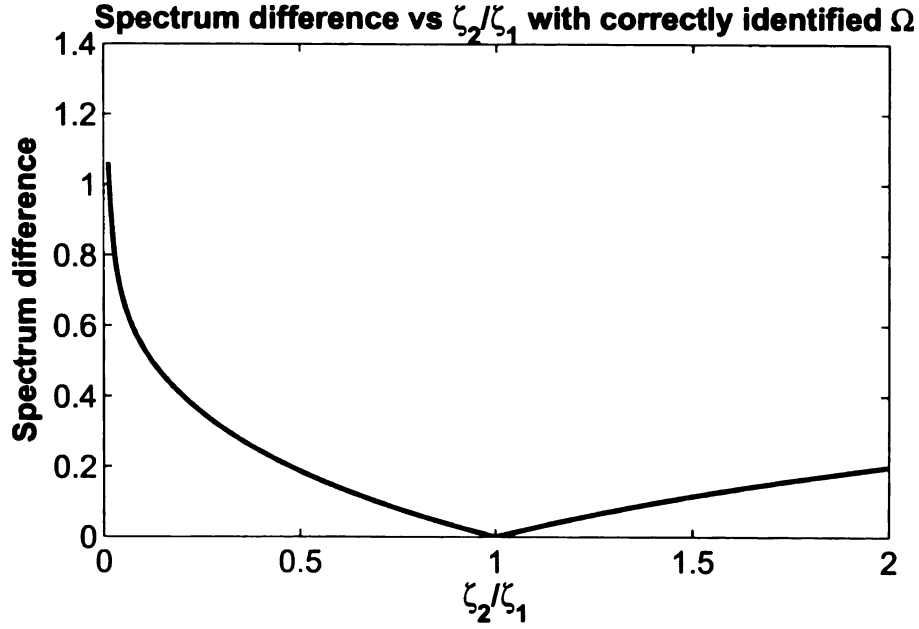


Figure 5.6: The spectrum difference values for various estimates of identified damping ratios. The damping estimate error ratio ζ_2/ζ_1 ranges from -100 % at 0.001 to +100 % at 2 with ζ_1 being 0.08 at 1.

From this study, we see that both the SAC and SD produce indicative values if only damping is identify correctly except for a small range of frequency values. Thus, only if frequency estimate errors are within 15 %, we could expect to see reasonable SAC and SD values.

5.3.4 *Lightly damped vs. heavily damped systems*

In this section, we want to study the behavior of the SAC and SD criteria in the low and high damped cases. The system frequency is assumed to be correctly identified by the decomposition method. We would like to see whether these methods are sensitive to reference damping ratios.

Here, we vary the damping ratio to observe SAC and SD values for both flat and peak responses. Two cases of light to high damping are considered. For lightly damped case, the value of ζ_1 was set to 0.02. For the highly damped case, the value of ζ_1 was set to 0.2. For the light damping case, the plots of both SAC and SD are

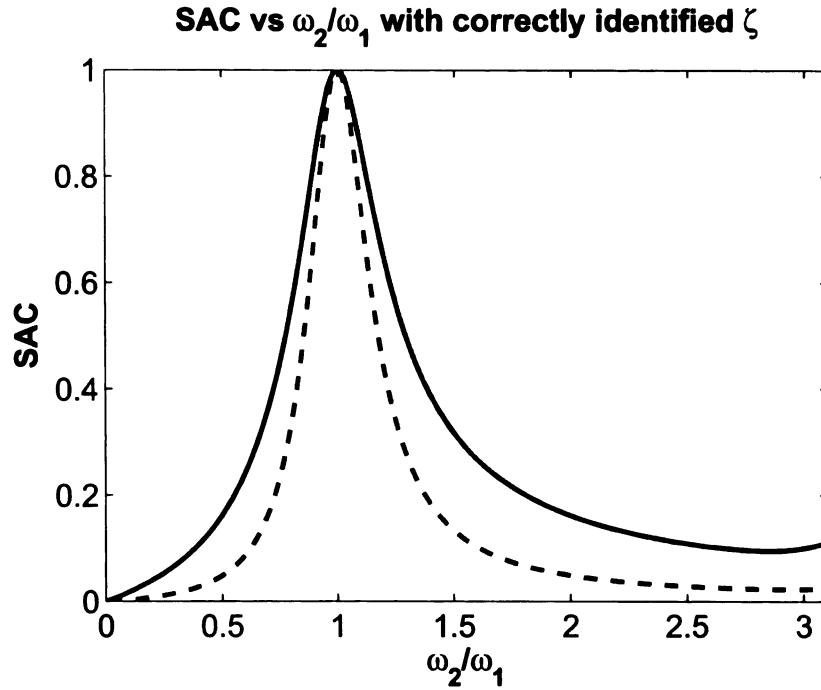


Figure 5.7: The SAC values for various estimates of identified frequency values. The solid line (—) shows the amplitude SAC while dashed line (- -) presents the amplitude of the complex version of SAC. The frequency estimate error ratio ω_2/ω_1 ranges from -100 % at 0.0 to +200 % at 3.

presented in Fig. 5.9 and Fig. 5.10 respectively.

For the high damping case, the plots of both SAC and SD are presented in Fig. 5.11 and Fig. 5.12 respectively.

These plots show that if the frequency content is identified correctly, erroneous damping values will not bear a large significance over both SAC and the SD criteria. Furthermore, the performance of both the SAC and SD is nearly independent of the level of damping in an underdamped reference system. This is fruitful since most of structural system have low damping values and hence for these quantification tools, the frequency estimates carry more importance.

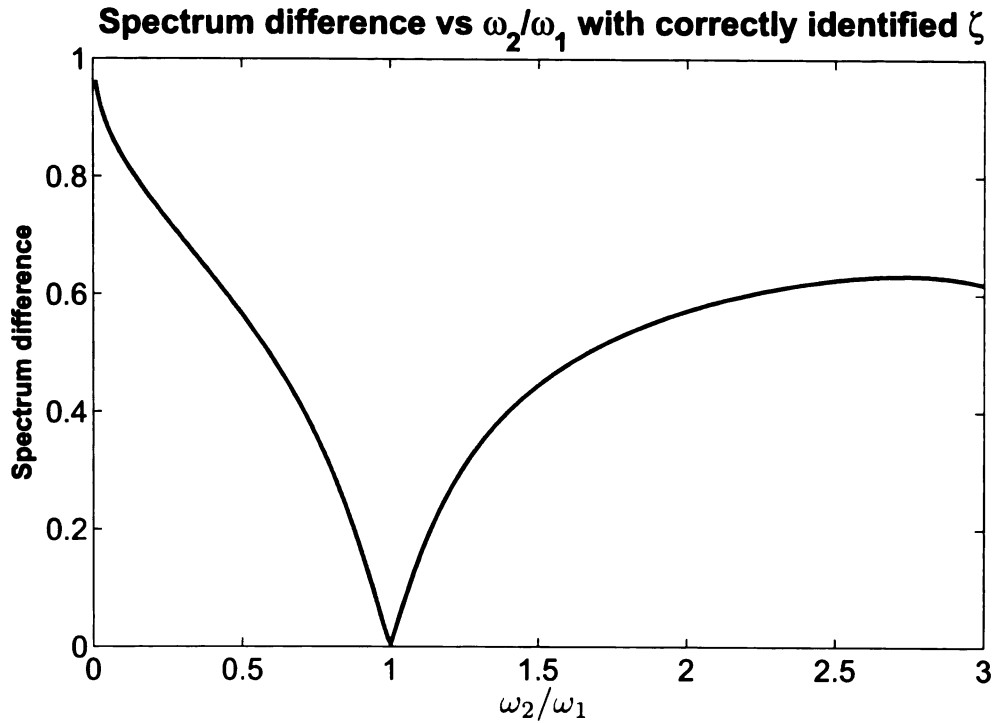


Figure 5.8: *The spectrum difference values for various estimates of identified frequency values. The frequency estimate error ratio ω_2/ω_1 ranges from -100 % at 0.0 to +200 % at 3.*

5.3.5 Summary of trends

We have now explored the SAC and SD criteria for various test cases. Both criteria require generation of the FRFs from system parameters. Based on these numerical studies, we see that these tools could be used for quantitative assessment of identification results. From the numerical studies presented above, we gather the following information.

1. The complex SAC appears to be more sensitive than the normal SAC amplitude in both frequency and damping estimations and is similar to the SD.
2. The noise and frequency errors are well expressed using both SD and SAC criteria.

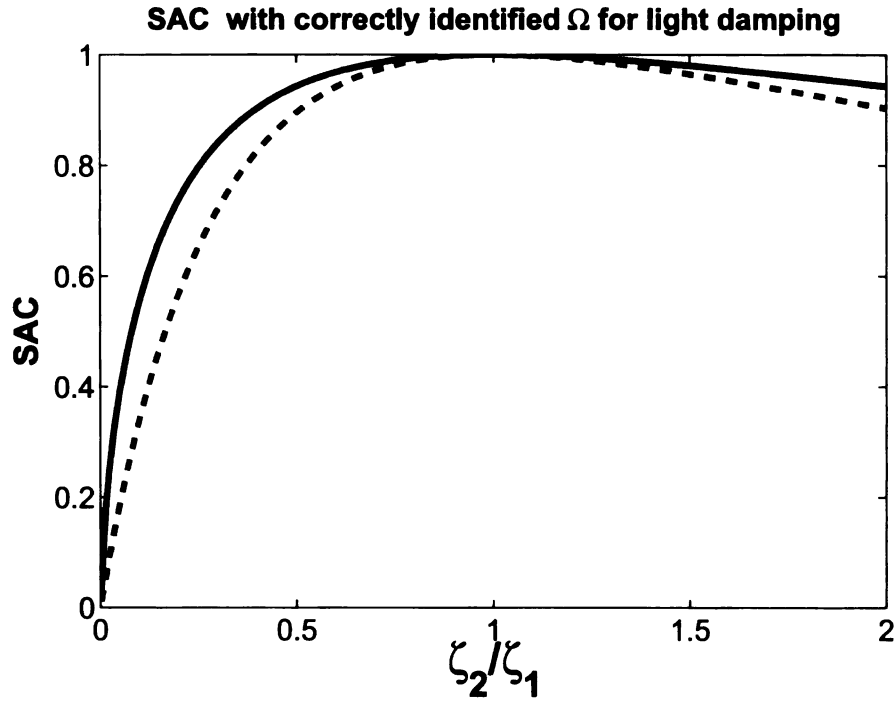


Figure 5.9: The amplitude SAC values for various estimates of identified damping values. The solid line (—) shows the amplitude SAC while dashed line (- -) presents the amplitude of the complex version of SAC. The reference system damping ratio is chosen as $\zeta_1 = 0.02$

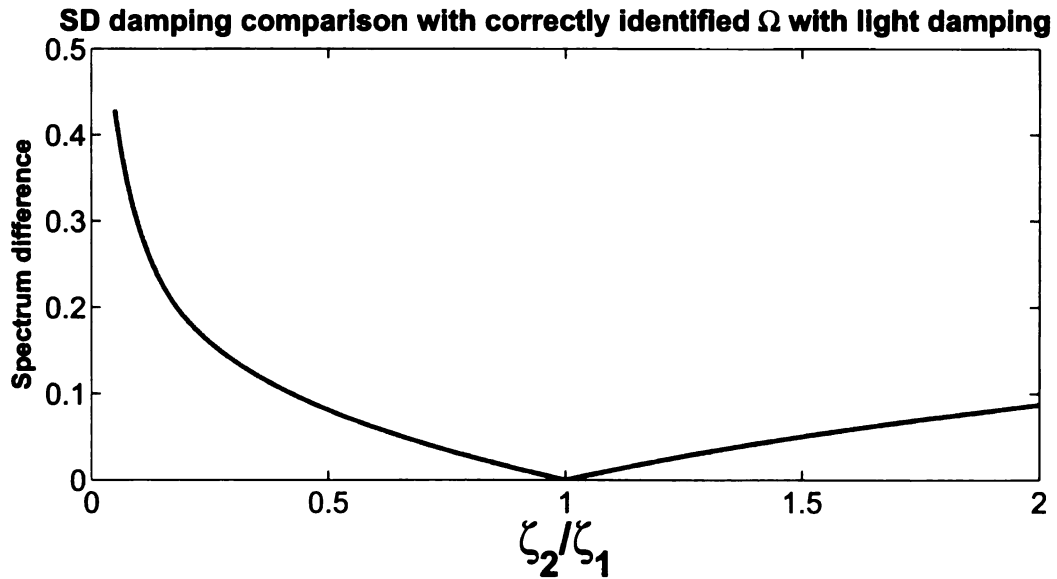


Figure 5.10: The spectrum difference values for various estimates of identified damping ratios. The reference system damping ratio is chosen as $\zeta_1 = 0.02$

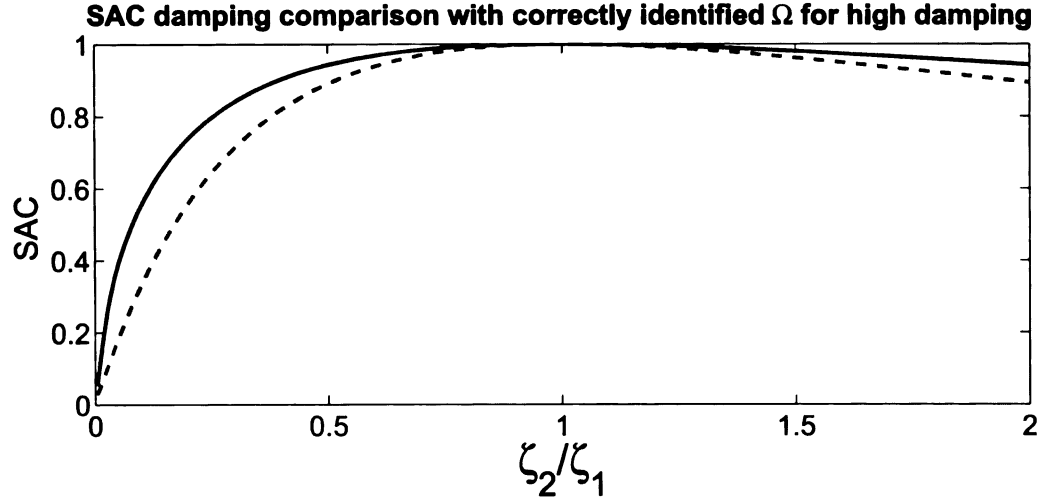


Figure 5.11: The SAC values for various estimates of identified damping values. The solid line (—) shows the amplitude SAC while dashed line (- -) presents the amplitude of the complex version of SAC. The reference system damping ratio is chosen as $\zeta_1 = 0.2$

3. Both the SAC and SD are less sensitive to damping errors than other types of errors in underdamped systems.

5.4 Experimental data

Next, we will use the established criteria on actual test data and detail an example to distinguish spurious modes from actual modes.

The fixed-free steel beam experiment conducted in chapter 4 is used here to evaluate the efficacy of the SAC and SD criterion for real-life experiments. The reference and actual FRFs are generated as follows. The reference FRF is generated from the estimates of system parameters obtained by the decomposition method. Similarly, for comparison another set of reference FRFs is generated from the first five frequency estimates using the FFT of the acceleration time signal. Since we do not have the damping estimates from the FFT, the damping estimates from decomposition method are used instead in generating these FRFs. The actual FRF is obtained

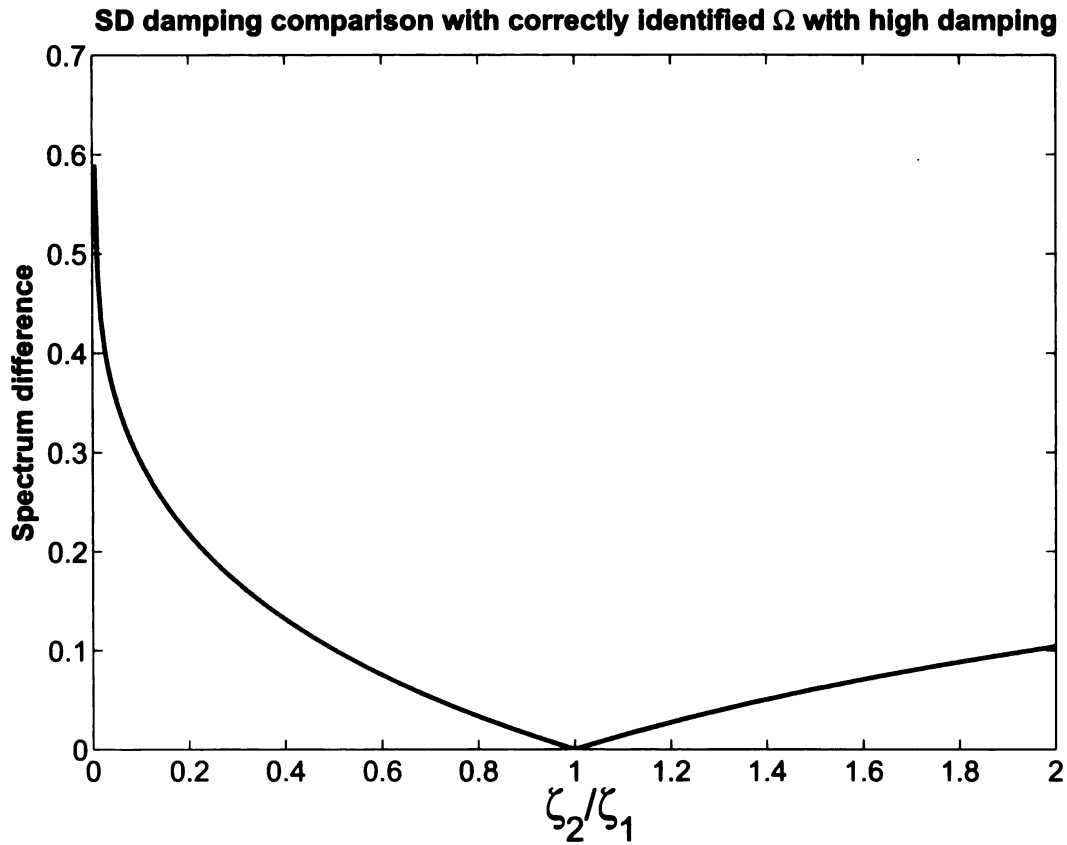


Figure 5.12: *The spectrum difference (SD) values for various estimates of identified damping ratios. The reference system damping ratio is chosen as $\zeta_1 = 0.2$*

from the modal coordinate. From the modal coordinate time history, we select the part that starts at the first upward zero crossing. This corresponds to a zero displacement and a positive velocity initial condition. This in turn could be associated with an equivalent impulse response with zero initial conditions proportional to an ideal impulse response, whence we obtain the approximate FRF.

Two data sets are used for the SAC and SD comparisons. The first data set is comprised of approximately 12,000 points and the second one has only 1000 data points. As observed in chapter 4, longer sampling improves quality in lower mode estimates whereas shorter sampling improves the higher modes.

5.4.1 Large sampling $\mathcal{N}=12,000$

In this case, the SVMD was clearly able to estimate system parameters of the first two modes. However, it is conceivable that in experiments, some of the spurious modal frequencies could be “close enough” to be mistaken for an actual mode. In this case, for both modes, some of the identified frequency and damping pairs are shown in Table 5.1. The first estimate corresponding to each mode is real while the others are spurious.

Table 5.1: *Estimated modal parameters from the decomposition method for a linear beam free response for first $N = 12,000$ sample values.*

Mode	FFT Frequency	Damping	Frequency
1	2.74	0.0033	2.7896
1	-	0.1590	3.0831
1	-	0.0263	2.2690
2	17.20	0.0035	17.174
2	-	0.0113	18.406

For each mode, the reference and actual FRFs were generated in the way described above. By computing the SAC and SD values between FRFs from each modal coordinate history, and each set of estimated modal parameters, we have two $n \times n$ matrices of complex amplitude SAC and SD values with n representing the total number of modes. These are plotted in Figures 5.13 and 5.14. The SD values are subtracted from 1 and thus plotted as $r = 1 - SD$ to aid the visualization by representing positive outcomes with tall bars.

The SAC values seem to point to pairs (2,2) estimated by SVMD as the second modal parameter; and (10,10), (12,12), (13,13) and (14,14) estimated by SVMD as *the* first modal parameter. The SD values seem to point to pairs (2,2) estimated by SVMD as the second modal parameter; and (10,10), (12,13), and (13,13) estimated by SVMD as the first modal parameter. In short, the common candidates are (2,2) for *second* mode and either (10,10) or (13,13) for the first mode.

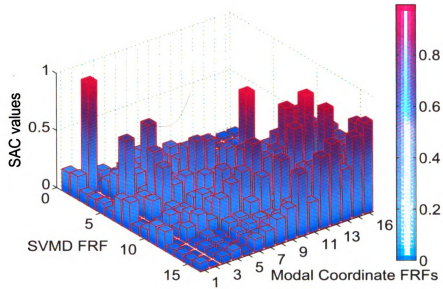


Figure 5.13: The amplitudes of complex SAC values computed for each FRF generated from the SVMD estimates compared against FRFs from modal coordinates.

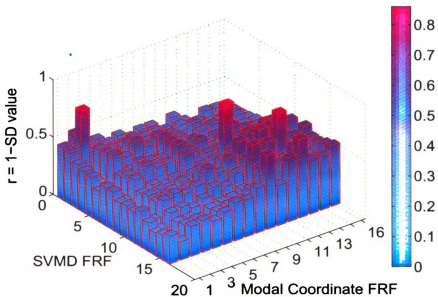


Figure 5.14: The $r = 1 - SD$ values computed for each FRF generated from the SVMD estimates compared against FRFs from modal coordinates. For ease of visualization, values of SD subtracted from 1 are plotted instead.

We also generated reference FRFs from the frequency estimates of FFT of the acceleration ensemble and these are shown in Figures 5.15 and 5.16. The FFT based FRFs were ordered to match the SVMD based FRFs to ease the visual comparison. The FFT generated SAC values seem to point to (2,2) identified by FFT as first modal parameter; (13,13) identified by FFT as first modal parameter. The FFT generated SD values show the same trend.

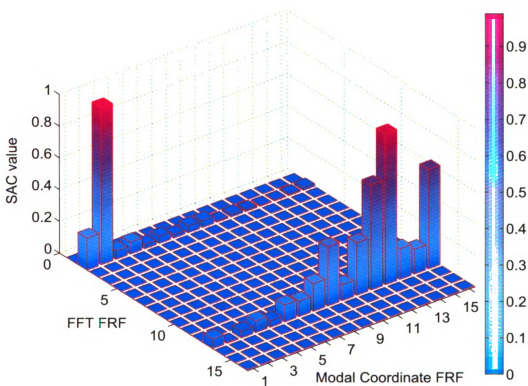


Figure 5.15: The amplitudes of complex SAC values computed for each FRF generated from the FFT estimates compared against FRFs from modal coordinates. The estimates are ordered to match sequence by SVMD for ease of comparison.

It is clear from the above plots that the modal pair of (13,13) that corresponds to the first mode as estimated by SVMD along with the modal pair (2,2) that corresponds to the second mode are the true system modes. This can be seen from all four plots where these values are maximum. Note that, these indicated modes from (2,2) and (13,13) agree with the qualitative results obtained via modal coordinates in section

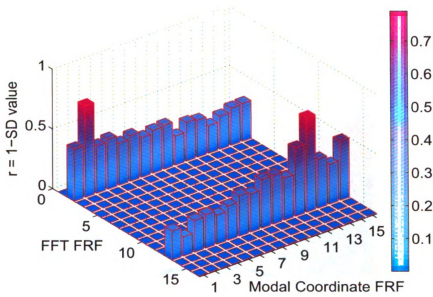


Figure 5.16: The $r = 1 - SD$ values computed for each FRF generated from the FFT estimates compared against FRFs from modal coordinates. The estimates are ordered to match the sequence of SVMd. For ease of visualization, values of SD subtracted from 1 are plotted instead.

4.3.2.

5.4.2 Smaller sampling $N=1000$

We turn our attention to a smaller sampling size which thereby results in the estimation of higher modes by the SVMd. The same procedure as described above is repeated to generate FRFs from modal coordinates which are then matched against FRFs from SVMd and FFT estimates respectively. The only difference is that for the FFT generated FRFs, only the first five estimates are used since SVMd was able to estimate the first five modes. The complex amplitude SAC comparison of SVMd estimates with modal coordinates is presented in Fig. 5.17.

The SAC values seem to point to pairs (1,1) estimated by SVMd as the fifth modal parameter; (2,2) estimated by SVMd as the fourth modal parameter; (5,5) estimated by SVMd as the third modal parameter; (11,10), (11,11), (11,12), and

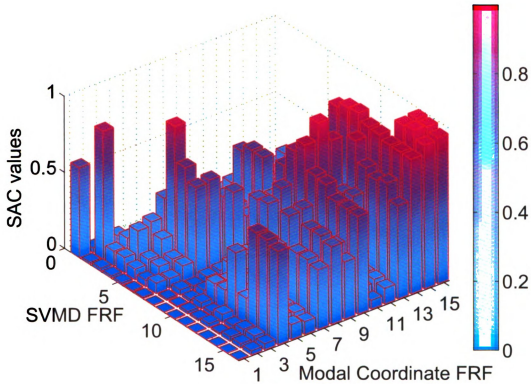


Figure 5.17: *The amplitude of complex SAC values computed for each FRF generated from the SVMD estimates compared against FRFs from modal coordinates.*

(12,13) estimated by SVMD as the second modal parameter; and (10,14), (11,14), (12,14), (13,14), (14,15), (15,15), and (15,16) estimated by SVMD as the first modal parameter.

Similarly, the SD values are computed from SVMD and modal coordinates generated FRFs. Again to aid visualization, values are subtracted from 1 and then shown in Fig. 5.18. The SD values seem to point to pairs (1,1) estimated by SVMD as fifth modal parameter; (2,2) estimated by SVMD as fourth modal parameter; (5,5), and (7,5) estimated by SVMD as third modal parameter; (11,11) estimated by SVMD as the second modal parameter; and (14,15), and (15,15) estimated by SVMD as the first modal parameter.

For the FRFs generated via FFT, the complex SAC and SD values are calculated with SAC values shown in Fig. 5.19 and SD subtracted from 1 are shown in Fig. 5.20.

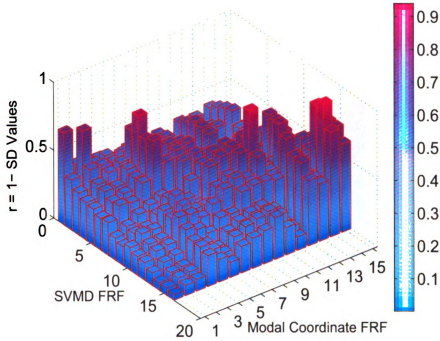


Figure 5.18: *The $r=1-SD$ values computed for each FRF generated from the SVMd estimates compared against FRFs from modal coordinates. The estimates are not ordered in any particular sequence. For ease of visualization, values of SD subtracted from 1 are plotted instead.*

The SAC values here seem to point to pairs (1,1) estimated by FFT as the fifth modal parameter; (2,2) estimated by FFT as the fourth modal parameter; (5,5) estimated by FFT as the third modal parameter; (11,11), and (11,14) estimated by FFT as the second modal parameter; and (15,14), (15,15), and (15,16) estimated by FFT as the first modal parameter.

The SD values in this case seem to point to the pairs (1,1) estimated by FFT as the fifth modal parameter; (2,2) estimated by FFT as the fourth modal parameter; (5,5) estimated by FFT as the third modal parameter; (11,11) estimated by FFT as the second modal parameter; (15,15) or may be (15,16) estimated by FFT as the first modal parameter.

If we combine all the results, these indicate that the pairs (1,1), (2,2), (5,5), (11,11) and (15,15) are the most common candidates for real modes. Note that the indicated

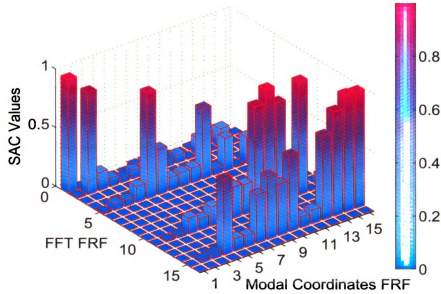


Figure 5.19: The amplitude of complex SAC values computed for each FRF generated from the FFT estimates compared against FRFs from modal coordinates. The estimates are ordered to match sequence by SVMd for ease of comparison.

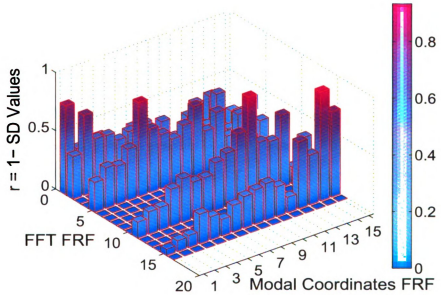


Figure 5.20: The $r=1-SD$ values computed for each FRF generated from the FFT estimates compared against FRFs from modal coordinates. The estimates are ordered to match the sequence of SVMd. For ease of visualization, values of SD subtracted from 1 are plotted instead.

modes from (1,1), (5,5), (11,11) and (15,15) are in complete agreement with the “nice looking” plots visualized in section 4.3.2. Also note that the mode from (2,2) augments the “borderline” mode candidate described in section 4.3.3 and confirms its status as a real mode.

5.4.3 Comments and summary

The SAC and SD criteria are evaluated for an experimental data set. We found both tools to be quite effective in evaluating the identification results. Both utilize FRFs to generate values that help assess the quality of an extracted mode. This quantitative measure augments the qualitative arguments presented in section 4.3.3.

We noticed that the SAC can produce excess candidates but perhaps at the same time more clear candidates. We also see that using SAC together with SD is almost always better and hence recommended.

We summarize the observations and findings as follows.

1. The FFT frequency spikes are probably more accurate than the SVMD frequencies.
2. The SVMD damping values have to be used for both kinds of FRF generations since the damping values were not obtained from the FFT generated FRFs. This may not adversely affect the purpose of evaluating modal coordinates since the damping errors have a weak effect on both SAC and SD values as shown in section 5.3.2.
3. It is likely that a spurious mode will have a bad modal coordinate and that this will produce a complex amplitude SAC far away from 1 or a SD value far from 0.

5.5 Time record length

We observed from the experimental data that for short time histories, higher modes were extracted, and for longer time histories, lower modes were extracted. We hypothesize that if the data record is too short, low frequency modes may not be fully represented and therefore not accurately extracted, and that if the data record is long, quickly damped modes will become dominated by noise for much of the signal, and will not be accurately extracted. We test these ideas, next, by looking at the effect of time record on modal identifications in a simulation study.

This section involves a numerical study on a three-degree-of-freedom system with added noise. We will use the numerical example presented in section 2.3. The system parameters are reproduced here which are

$$\mathbf{M} = \begin{bmatrix} 2 & 0 & 0 \\ 0 & 1 & 0 \\ 0 & 0 & 1 \end{bmatrix}, \mathbf{K} = \begin{bmatrix} 2 & -1 & 0 \\ -1 & 2 & -1 \\ 0 & -1 & 1 \end{bmatrix} \quad (5.7)$$

with the initial conditions $\mathbf{x}(0) = (1, 0, 0)^T$, and $\mathbf{v}(0) = (0, 0, 0)^T$. The undamped natural frequencies of the system are $\omega_1 = 0.4209$, $\omega_2 = 1.000$, and $\omega_3 = 1.6801$.

We are interested in exploring a couple of options. We want to study the effect of low and moderately high noise as well as the effect of high and low damping values in this time length study. In this study, the frequency and damping estimates are associated with the same eigenvalue, so an error in estimate of one may effect error in the other. The cases that cover the damping and noise ranges are described as follows.

The system damping is chosen to be proportional to mass $\mathbf{C} = c\mathbf{M}$. We will only test the underdamped systems for this study. Since the damping is proportional to the mass matrix, all modes have the same settling time, T_s . To have a constant modal settling time was primarily intended for the ease of analysis. While other system damping values could certainly be explored, in this study we wanted to exclude

any possible results misleading us away from the actual subject of interest. Those explorations may be subject of a future study.

By choosing two values $c = 0.5$ and $c = 0.01$, the range of damping ratios lays between 0.003 (low) to 0.59 (high). The individual damping ratios for each mode will be presented the results section.

In accordance with section 2.4, quantization noise was added to the system. The two noise levels were selected to be 6 bits (high) and 10 bits (low). The random noise ensemble was added to the displacement matrix \mathbf{X} . We then took numerical derivatives of the new \mathbf{X} to build \mathbf{V} and subsequently our ensemble matrices. The derivative step size was selected as $n_d = 16$ and $\Delta t = 0.01$ for all the studies detailed herein.

The time period of the lowest mode was equal to 14.93 seconds or 1493 data points, similarly the second lowest mode time period was approximated at 6.28 seconds (628 data points) and the highest at 3.74 seconds (374 data points). The simulation was run for the data record sweeping from one tenth of each mode time period to ten times the modal period. From the decomposition, identification results were computed and stored for each run. Then the difference between identified and actual system parameters was calculated. These error results are plotted for frequency and damping differences against the stated dimensionless time record length normalized for each modal period.

5.5.1 *Results*

5.5.1.1 **High damping**

For the case where $c = 0.5$, the system damping ratios are $\zeta_1 = 0.594$, $\zeta_2 = 0.25$, and $\zeta_3 = 0.1488$. These ratios represent the relatively high values as would be seen in some physical experiments. In this case, the 2 % settling time is $T_s = 16$ seconds, which is about 1.07, 2.54, and 4.27 modal periods for the first, second, and third

modes, respectively.

First, we employed the 10 bit or low level quantization noise. The error results in both damping and frequency estimates are shown in Fig. 5.21 and Fig. 5.22 respectively.

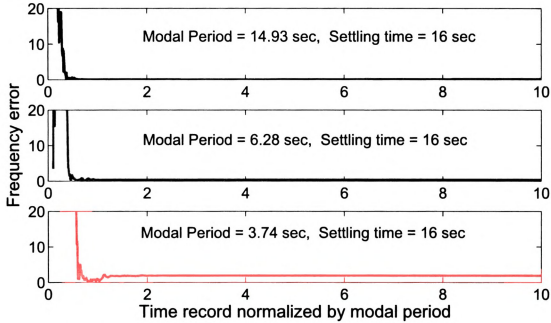


Figure 5.21: The percent error in estimation of frequency parameters against various lengths of data for a 3 DOF underdamped system. Each time record is normalized by its modal period. The quantization noise level is 10 bits.

Next, we increased the quantization noise to 6 bits and reran the simulation. The error results are shown in Fig. 5.23 and Fig. 5.24.

From the plots, a consistent trend can be observed. With a small time record, for all modes the error is huge in both frequency and damping estimates. As the data lengths approach roughly a modal period, the error values are greatly reduced. For the higher-noise case, the error values are minimum at about the modal settling time. In such case, as the time record continues to increase, the noise begins to dominate the response, and hence the correlation signals, and the results start to diverge.

Since all modes have the same settling time, the lower modes settle more quickly

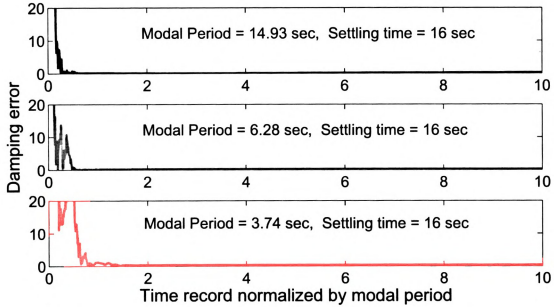


Figure 5.22: The percent error in estimation of damping values against various lengths of data for a 3 DOF underdamped system. Each time record is normalized by its modal period. The quantization noise level is 10 bits.

peak to peak (higher ζ), or in other words more quickly with respect to their modal-period normalized time variables. Thus with the modal period normalized time plots, we expect the lower modes to diverge more quickly, as observed in the plots.

5.5.1.2 Low damping

For the case where $c = 0.01$, the system damping ratios are $\zeta_1 = 0.0119$, $\zeta_2 = 0.005$, and $\zeta_3 = 0.003$. These ratios represent the relatively low damping values as would be seen in physical experiments. Here again, all modes have the same settling time, T_s . In this case, the 2 % settling time is $T_s = 800$ seconds, which is about 53.5, 127.4, and 213.9 modal periods for the first, second, and third modes, respectively.

In the Figs. 5.25 and 5.26, 6 bit quantization noise was employed and error values plotted. In Figs. 5.27 and 5.28, 10 bit quantization noise was used and the identification error results plotted.

In low damping cases, the results seem to imply that as long as the data length is

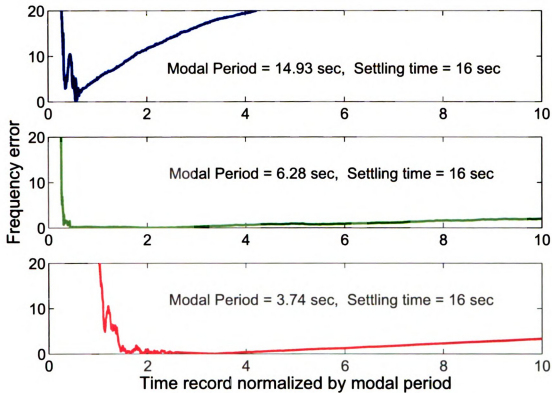


Figure 5.23: The percent error in estimation of frequency parameters against various lengths of data for a 3 DOF underdamped system. Each time record is normalized by its modal period. The maximum error appears in the first mode. The quantization noise level is 6 bits.

less than the modal settling time and that about two modal period oscillations have been captured, errors associated with parameter estimation would be negligible.

5.5.2 Summary of trends

We evaluated two cases that incorporate moderately “high” and low damping ratios, via a numerical example. The effect of inclusion of 10 bit and 6 bit quantization noise values on the signals was studied. Time record was normalized by the modal period in each case. We summarize the observations and findings as below.

- Two important features are modal time period and modal settling time. When time record is short, that is a small multiple or fraction of the modal time

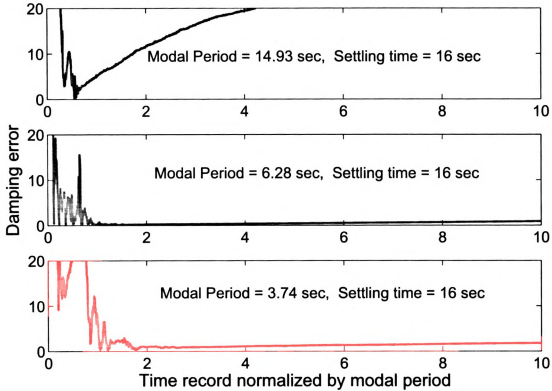


Figure 5.24: *The percent error in estimation of damping values against various lengths of data for a 3 DOF underdamped system. Each time record is normalized by its modal period and the maximum error appears in the first mode. The quantization noise level employed is 6 bits.*

period, estimates are expected to be erroneous. Likewise, when time period is long, that is greater than modal settling time, it also results in estimation errors which are attributed to noise dominance in the correlation signals.

- For estimating frequencies, we might expect to have at least one modal period, in low-noise simulations we saw good results at about two periods.
- For damping estimates, log decrement might lead us to think that at least a couple oscillation peaks are required, but our low noise simulations indicate that the data between peaks holds the information in it, too.
- Based on simulations, the “optimal” time record length seems between modal

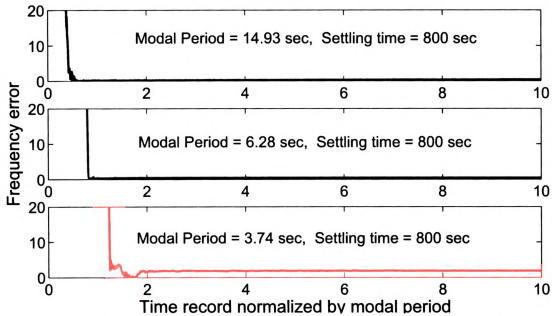


Figure 5.25: *The percent error in estimation of frequency parameters against various lengths of data for a 3 DOF underdamped system. Each time record is normalized by its modal period. The quantization noise level employed is 6 bits.*

period and modal settling time, a window where the estimation results have minimum errors.

5.6 Summary

We have evaluated the limitations of the identification quality of the decomposition method in this chapter. We have quantitatively examined the modal coordinates that determine the decomposition quality. Two criteria were developed that help assess the quality of decomposition using frequency response functions. Various cases that emulate non-ideal identification circumstances were numerically studied using the proposed criteria. Furthermore, experimental data were also analyzed using these methods. The criteria were applied on FRFs generated by decomposition methods and compared with FRFs generated from the FFT identification.

The spectrum assurance and the spectrum difference criteria used together prove

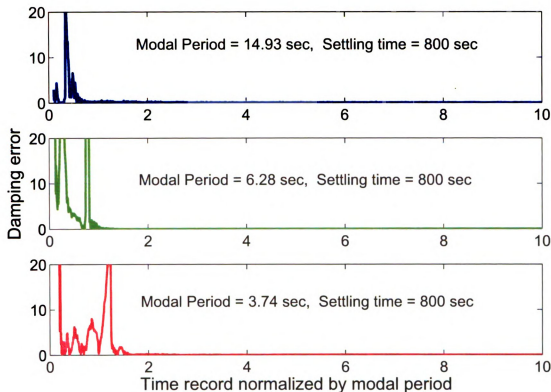


Figure 5.26: The percent error in estimation of damping values against various lengths of data for a 3 DOF underdamped system. Each time record is normalized by its modal period. The quantization noise level employed is 6 bits.

to be very useful in evaluating the identification results. These criteria quantify an actual mode when spurious results appear in identification. From both numerical and experimental case studies, we see that these criteria are robust even in presence of non-ideal damping identification.

Lastly, we addressed the effect of data length on the identification. This was studied via a numerical simulation. It was observed that identification results are best in a time record window associated with the modal time period and modal settling time.

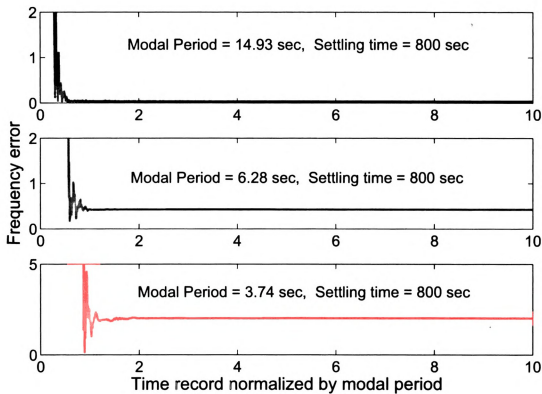


Figure 5.27: The percent error in estimation of frequency parameters against various lengths of data for a 3 DOF underdamped system. Each time record is normalized by its modal period. The quantization noise level employed is 10 bits.

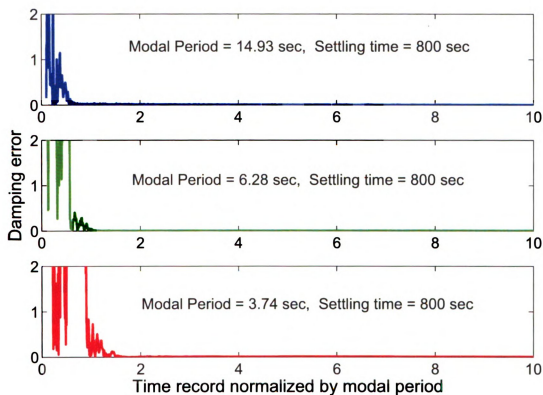


Figure 5.28: The percent error in estimation of damping values against various lengths of data for a 3 DOF underdamped system. Each time record is normalized by its modal period. The quantization noise level employed is 10 bits.

Comparison with Other Identification Methods

6.1 Introduction

In this chapter, comparison between various decomposition methods and selected time domain modal identification techniques is discussed. The list of time domain techniques for modal identification of linear systems is non-exhaustive and is probably well beyond the scope of this work. Consequently, the comparison made here presents a rather small but representative portion of the research in the area of system characterization and identification of structural systems. For a list of other comparison methods see for example the works of [43, 48–50, 99].

In this work, we would like to compare methods that are either most popular, accurate or practical. Specifically, the comparison of the state-variable modal decomposition (SVMD), the proper orthogonal decomposition (POD), and the smooth orthogonal decomposition (SOD) is being made with the Ibrahim time domain method (ITD) [27, 37, 40] and the eigensystem realization algorithm (ERA) [31, 44, 45]. These are the commonly applied methods in the output-only area of modal identification. For most cases, the identified system modes will also be matched against the POD generated modes (POMs) for verification of results. This would serve dual purpose as the POD comparison would also be employed for tying up the gap as mentioned

earlier in section 1.4.

We begin by summarizing the derivations of the ITD and the ERA. The interested reader is referred to the original works for detailed discussions. Here, the idea is to highlight the basis of formulating the eigenvalue problem. Next, we conduct a numerical simulation for a three-degrees-of-freedom (DOF) problem and then another simulation study for a sixteen DOF system. Both systems are then also subjected to quantization noise [91]. For the former case, extracted modes are easily verified by direct comparison with the linear normal modes of the system, whereas for the latter system, identified modes are compared to the linear normal modes via the modal assurance criterion [111]. Next, all of the identification schemes are compared in the experimental clamped-free beam studied in section (4.3). Comparisons are made between methods for frequency and damping estimations. Mode shapes corresponding to respective modal frequencies are also matched and plotted for most schemes. We conclude the chapter by some observations obtained through the experiments.

6.2 Time-domain modal identification methods

6.2.1 *Ibrahim time domain method*

One of the earliest time domain methods for modal analysis, the Ibrahim time domain (ITD) method was introduced in 1973 [27], with subsequent improvements following in later years [37, 40]. ITD is a single-input-multiple-output (SIMO) method, generally assuming the solution of an n DOF vibration system Eq. (2.1) to be of the form

$$x_i(t) = \sum_{k=1}^{2n} \phi_{ik} e^{s_k t}, i = 1, \dots, n \quad (6.1)$$

where ϕ_k is a $2n \times 1$ vector that forms the normal mode shape and $s_k = -\zeta\omega_n \pm \omega_d j$ provides the system frequencies and damping ratios for k th element.

Expanding Eq. (6.1) for n outputs obtained through n sensors with a sampling time record equaling $2n\Delta t$, with Δt being the sampling time step, we get

$$\begin{bmatrix} x_1(t_0) & x_1(t_1) & \dots & x_1(t_{2n-1}) \\ x_2(t_0) & x_2(t_1) & \dots & x_2(t_{2n-1}) \\ \vdots & \ddots & \ddots & \vdots \\ x_n(t_0) & x_n(t_1) & \dots & x_n(t_{2n-1}) \end{bmatrix} = \begin{bmatrix} \phi_{11} & \phi_{12} & \dots & \phi_{12n} \\ \phi_{21} & \phi_{22} & \dots & \phi_{22n} \\ \vdots & \ddots & \ddots & \vdots \\ \phi_{n1} & \phi_{n2} & \dots & \phi_{n2n} \end{bmatrix} \begin{bmatrix} e^{s_1 t_0} & e^{s_1 t_1} & \dots & e^{s_1 t_{2n-1}} \\ e^{s_2 t_0} & e^{s_2 t_1} & \dots & e^{s_2 t_{2n-1}} \\ \vdots & \ddots & \ddots & \vdots \\ e^{s_{2n} t_0} & e^{s_{2n} t_1} & \dots & e^{s_{2n} t_{2n-1}} \end{bmatrix} \quad (6.2)$$

In short form

$$\mathbf{X} = \Phi \mathbf{e}^{\mathbf{st}} \quad (6.3)$$

Here, \mathbf{X} is a $n \times 2n$ matrix of free response measurements from the structure and is known, Φ is an $n \times 2n$ matrix of unknown eigenvectors; and $\mathbf{e}^{\mathbf{st}}$ is a matrix containing unknown complex eigenvalues and known response measurement times.

ITD requires the time shifting of the displacement ensemble by one sampling step (sampling time steps can be chosen), for example $t_1 = t_0 + \Delta t$, to generate a new ensemble, termed the shifted matrix, as

$$\begin{bmatrix} x_1(t_1) & x_1(t_2) & \dots & x_1(t_{2n}) \\ x_2(t_1) & x_2(t_2) & \dots & x_2(t_{2n}) \\ \vdots & \ddots & \ddots & \vdots \\ x_n(t_1) & x_n(t_2) & \dots & x_n(t_{2n}) \end{bmatrix} = \begin{bmatrix} \phi_{11} & \phi_{12} & \dots & \phi_{12n} \\ \phi_{21} & \phi_{22} & \dots & \phi_{22n} \\ \vdots & \ddots & \ddots & \vdots \\ \phi_{n1} & \phi_{n2} & \dots & \phi_{n2n} \end{bmatrix} \Lambda \begin{bmatrix} e^{s_1 t_0} & e^{s_1 t_1} & \dots & e^{s_1 t_{2n-1}} \\ e^{s_2 t_0} & e^{s_2 t_1} & \dots & e^{s_2 t_{2n-1}} \\ \vdots & \ddots & \ddots & \vdots \\ e^{s_{2n} t_0} & e^{s_{2n} t_1} & \dots & e^{s_{2n} t_{2n-1}} \end{bmatrix} \quad (6.4)$$

or in short from as

$$\mathbf{X}_{1\tau} = \Phi \Lambda \mathbf{e}^{\text{st}} \quad (6.5)$$

where

$$\Lambda = \begin{bmatrix} e^{s_1 \Delta t} & 0 & \dots & 0 \\ 0 & e^{s_2 \Delta t} & \dots & 0 \\ \vdots & \ddots & \ddots & \vdots \\ 0 & 0 & \dots & e^{s_{2n} \Delta t} \end{bmatrix}$$

The shifted matrix has the same dimensions as \mathbf{X} and the same is true for the rest of the matrices in Eq. (6.5) in comparison with Eq. (6.3).

Another time shift, this time on $\mathbf{X}_{1\tau}$, would generate the second time shift matrix as

$$\mathbf{X}_{2\tau} = \Phi \Lambda^2 \mathbf{e}^{\text{st}} \quad (6.6)$$

Stacking Eqs. (6.3)-(6.6) together, we form

$$\begin{bmatrix} \mathbf{X} \\ \mathbf{X}_{1\tau} \end{bmatrix} = \begin{bmatrix} \Phi \\ \Phi \Lambda \end{bmatrix} \mathbf{e}^{\text{st}} \quad \text{or} \quad \bar{\mathbf{X}} = \Psi \mathbf{e}^{\text{st}} \quad (6.7)$$

and

$$\begin{bmatrix} \mathbf{X}_{1\tau} \\ \mathbf{X}_{2\tau} \end{bmatrix} = \begin{bmatrix} \Phi \Lambda \\ \Phi \Lambda^2 \end{bmatrix} \mathbf{e}^{\text{st}} \quad \text{or} \quad \hat{\mathbf{X}} = \Psi \Lambda \mathbf{e}^{\text{st}} \quad (6.8)$$

The Eqs. (6.7) and (6.8) are restructured to form the eigenvalue problem as

$$\bar{\mathbf{A}} \Psi = \Psi \Lambda \quad \text{where} \quad \bar{\mathbf{A}} = \hat{\mathbf{X}} \bar{\mathbf{X}}^{-1} \quad (6.9)$$

Solution of the eigenvalue problem of Eq. (6.9) yields the system modal parameters. System frequencies can be obtained by taking the logarithm of the eigenvalues obtained in Λ scaled by the sampling time, whereas the mode shapes are obtained from the columns of Ψ .

In essence, ITD requires the user to obtain displacement ensemble for a MDOF system and from that generate the two ensembles $\hat{\mathbf{X}}$ and $\bar{\mathbf{X}}^{-1}$. These ensembles

are then structured into the eigenvalue problem of Eq. (6.9), solution of which yields modal parameters.

6.2.2 *Eigensystem realization algorithm*

Deemed as one of the most accurate and practical methods [127] for modal parameter estimation, the eigensystem realization algorithm (ERA) was developed in 1985 [31] and then improved in following years [44, 128–131]. ERA is a multi-input-multi-output (MIMO) method that requires constituting a *Hankel* matrix which contains the *Markov* parameters. This method utilizes singular value decomposition to extend the Ho-Kalman algorithm [132] for realizing a state-variable system model. After obtaining the system model, the model is then transformed to the modal space for modal parameter estimation. Even though the realized system matrix \mathbf{A}_c is enough for frequencies and damping estimates, an additional step is required for the mode shape estimation. Following are the salient steps of the ERA method.

Consider the state-variable equations of a finite dimensional, discrete time, linear, time invariant dynamical system as

$$\mathbf{x}(k+1) = \mathbf{A}_d \mathbf{x}(k) + \mathbf{B}_d \mathbf{u}(k) \quad (6.10)$$

$$\mathbf{y}(k) = \mathbf{C}_d \mathbf{x}(k) \quad (6.11)$$

where \mathbf{x} is an n -dimensional state vector, \mathbf{u} is an m -dimensional control input, and \mathbf{y} is a p -dimensional output or measurement vector and k indicates discrete samples. The matrices $\mathbf{A}_d, \mathbf{B}_d, \mathbf{C}_d$ are the state, the input and the output matrices respectively, of the discrete model. These are different from the ones shown in section 2.2.

From the free response, functions that provide the system time domain description are termed Markov parameters, given by

$$\mathbf{Y}(k) = \mathbf{C}_d \mathbf{A}_d^{k-1} \mathbf{B}_d \quad (6.12)$$

The ERA method begins by forming a generalized block Hankel matrix of order $r \times s$, where r and s are some “optimally” chosen numbers [99], as

$$\mathbf{H}(k-1) = \begin{bmatrix} \mathbf{Y}(k) & \mathbf{Y}(k+1) & \dots & \mathbf{Y}(k+s) \\ \mathbf{Y}(k+1) & \mathbf{Y}(k+2) & \dots & \mathbf{Y}(k+s+1) \\ \vdots & \ddots & \ddots & \vdots \\ \mathbf{Y}(k+r) & \mathbf{Y}(k+r+1) & \dots & \mathbf{Y}(k+s+r) \end{bmatrix} \quad (6.13)$$

The singular value decomposition on the matrix $\mathbf{H}(0)$ yields

$$\mathbf{H}(0) = \mathbf{U} \Sigma \mathbf{V}^T \quad (6.14)$$

Keeping the “desired” singular values (usually $2n$ [99]) and truncating the matrices \mathbf{U} and \mathbf{V} to keep the same first dimensions, the realization triple is obtained as

$$\mathbf{A} = \Sigma^{-1/2} \mathbf{U}^T \mathbf{H}(1) \mathbf{V} \Sigma^{-1/2}, \quad \mathbf{B} = \Sigma^{1/2} \mathbf{V}^T \mathbf{E}_m, \quad \mathbf{C} = \mathbf{E}_p^T \mathbf{U} \Sigma^{1/2} \quad (6.15)$$

where

$$\mathbf{E}_p^T = [\mathbf{I}_n, 0, \dots, 0], \quad \mathbf{E}_m^T = [\mathbf{I}_m, 0, \dots, 0]$$

Modal frequencies and modal damping ratios can then be obtained from real and imaginary parts of eigenvalues of \mathbf{A}_c after the transition from discrete to continuous system as

$$\mathbf{A}_c = [\ln(\mathbf{A}) \pm 2\pi i] / k \Delta\tau, i = \sqrt{-1} \quad (6.16)$$

with $\Delta\tau$ being the sampling interval.

To obtain the mode shapes, the following transformation is used

$$\Phi = \mathbf{E}_p^T \mathbf{U} \Sigma^{1/2} \Gamma \quad (6.17)$$

where Γ is the matrix of eigenvectors of the identified system matrix \mathbf{A} .

6.2.2.1 A note on obtaining Markov parameters in ERA

The ERA requires using Markov parameters to construct the Hankel matrices whose correct order is difficult to obtain. A trial and error based approach employed earlier [44] was improved by a procedure that uses an observer based Kalman filter for Markov estimation (OKID), suggested by [133] with further improvements shown in [134]. However, these procedures are complicated and suffer from many difficulties from the identification perspective, as cited in [135]. These are listed as: (I) The initial conditions used in these procedures are typically unknown. (II) The number of Markov parameters in the model increase with the number of discrete samples k . (III) It is required to keep all the non-zero Markov parameter coefficients in the model and this number can be quite large for a lightly damped system. This makes the algorithm computationally expensive.

In present work, for the ERA, the required Hankel matrices were obtained in a different way as follows. Using only one sensor (as opposed to the original ERA) with the time series data acquired by that sensor, the square Hankel matrix was obtained by employing the Matlab function “hankel”. This matrix was then pared down to have only nonzero (nonsingular) entries. It was observed that this resulted in a clear distinction between the “strong” and the “weak” singular values when SVD was applied to the Hankel matrix $H(0)$, thereby verifying the efficacy of proposed approach. After these steps, the remaining ERA steps shown in section 6.2.2 can be easily followed. We will now refer to this approach as modified ERA. Even with this approach, the modified ERA still remains expensive since it uses all the time series data for that particular sensor and thus it may not be an ideal choice for the case where large data is unavoidable. Further study on the subject is required for improved performance. This may require use of stabilization diagrams as frequently used in the SSI methods [32] for model order determination or selecting appropriate rows and columns of the Hankel matrix.

6.3 Numerical simulations

Structural system models are now numerically simulated and compared using the mentioned identification schemes. Two example models are used to explore both free and forced response cases.

6.3.1 *Free response: A three DOF discrete system example*

We begin with the simple three DOF mass-spring-dashpot system example investigated in [136] for POD, [95] for SOD and [100] for SVMD, and also reported in section 2.3 for free response analysis. The system mass and stiffness parameters are given in Eq. (2.12) and are reproduced here as

$$\mathbf{M} = \begin{bmatrix} 2 & 0 & 0 \\ 0 & 1 & 0 \\ 0 & 0 & 1 \end{bmatrix}, \mathbf{K} = \begin{bmatrix} 2 & -1 & 0 \\ -1 & 2 & -1 \\ 0 & -1 & 1 \end{bmatrix} \quad (6.18)$$

with the reported initial conditions $\mathbf{x}(0) = (1, 0, 0)^T$, and $\mathbf{v}(0) = (0, 0, 0)^T$. The undamped natural frequencies of the system are $\omega_1 = 0.4209$, $\omega_2 = 1.000$, and $\omega_3 = 1.6801$.

In each simulation, the time responses for each mass displacement and velocity were numerically computed. Here, we used a step size $\Delta t = 0.01$ and a sample size $N = 2000$. The derivative step size was $n_d = 1$, and for ITD $\tau = 0.01$. The system damping was selected to be mass proportional as $\mathbf{C} = c\mathbf{M}$ where c was chosen as 0.01. This results in lightly damped modes shown in Table 6.1.

All of the identification schemes are seen to match up with the system eigenvalues to the 4th decimal place except SOD. The SOD is reasonably good but fails to perfectly identify the system frequencies. Nonetheless it is expected to improve if a larger data set is used for identification purposes. (It was verified that the largest error in identifying the system frequencies lay within $\approx 2\%$ for $N = 10,000$ data points).

Table 6.1: *Estimated modal parameters from various decomposition methods compared against the theoretical eigenvalue problem for a 3 DOF discrete system example*

Method	System		ITD		SVMD		ERA		SOD	
Ω_i	Freq.	Damp.	Freq.	Damp.	Freq.	Damp.	Freq.	Damp.	Freq.	Damp.
ω_1	0.4209	0.0119	0.4209	0.0119	0.4209	0.0119	0.4209	0.0119	0.4595	-
ω_2	1.0000	0.0050	1.0000	0.0050	1.0000	0.0050	1.0000	0.0050	0.9869	-
ω_3	1.6801	0.0030	1.6801	0.0030	1.6801	0.0030	1.6801	0.0030	1.6654	-

The normalized values of the displacement partitions of the three independent eigenvectors are $\mathbf{w}_1^T = (0.3602, 0.5928, 0.7204)^T$, $\mathbf{w}_2^T = (-0.7071, 0, 0.7071)^T$, $\mathbf{w}_3^T = (0.2338, -0.8524, 0.4676)^T$. For ITD and SVMD, the mode shapes matched up to the 4th decimal place with the LNMs. The SOD resulted in $\mathbf{w}_1^T = (0.6859, 0.6165, 0.3867)^T$, $\mathbf{w}_2^T = (0.6980, 0.0036, -0.7161)^T$, $\mathbf{w}_3^T = (0.2036, -0.8348, 0.5114)^T$. However, it was verified that the modes produced from the SOD were orthogonal as $\Psi^T \mathbf{R} \Psi = \mathbf{I}$, where $\mathbf{R} = \mathbf{X} \mathbf{X}^T$ (see section 3.2).

Assuming that the mass distribution was known, the mass weighted POD [136] was formulated by using $\hat{\mathbf{R}} = \mathbf{R} \mathbf{M}$ as

$$\frac{1}{N} \mathbf{X} \mathbf{X}^T \Phi = \frac{1}{N} \Lambda \Phi \quad (6.19)$$

where Φ is a matrix of eigenvectors that in this case would correspond to LNMs and Λ is the matrix of eigenvalues that corresponds to mean signal energy distribution in the usual POD manner. Φ results in $\mathbf{w}_1^T = (0.3470, 0.6034, 0.7179)^T$, $\mathbf{w}_2^T = (-0.7106, -0.0196, 0.7034)^T$, $\mathbf{w}_3^T = (-0.2459, 0.8459, -0.4733)^T$. Results from the modified ERA are not comparable as it used only mode and could not generate mode shapes since only one sensor output with “strong” signal strength [99] was utilized.

6.3.1.1 Noise effects

Next, the same system was subjected to an 8-bit quantization noise which is a typical value considered in reference [91]. Proceeding exactly the same way as explained in section 2.4, random noise was added to the system. The only difference here is that the differentiation step size was chosen to be $n_d = 16$ and $\tau = 16$ to ensure compatibility for ITD. Also, the step and sample sizes were the same as shown in the example above. Modal parameter estimation is presented in Table 6.2. SVMd gets good estimates in both frequency and damping values and has about 1% of maximum frequency error and about 5% maximum damping estimate error. The ITD results in almost identical frequency values with the system frequency values and also shows good damping estimates except the first mode for which the damping estimate is off by $\approx 35\%$. The ERA has the best estimates both in terms of frequency and damping with almost no errors and up to 4th decimal place accuracy in estimation but did not generate any mode shapes. The SOD has maximum error of about 9% in the frequency estimates.

Table 6.2: *Modal parameters estimation from various decomposition methods compared against the theoretical eigenvalue problem for a 3 DOF discrete system with 8-bit quantization noise.*

Method	System		ITD		SVMd		ERA		SOD	
	Ω_i									
	<i>Freq.</i>	<i>Damp.</i>	<i>Freq.</i>	<i>Damp.</i>	<i>Freq.</i>	<i>Damp.</i>	<i>Freq.</i>	<i>Damp.</i>	<i>Freq.</i>	<i>Damp.</i>
ω_1	0.4209	0.0119	0.4210	0.0161	0.4208	0.0125	0.4208	0.0118	0.4625	-
ω_2	1.0000	0.0050	1.0000	0.0050	0.9958	0.0050	1.0000	0.0050	0.9877	-
ω_3	1.6801	0.0030	1.6802	0.0031	1.6601	0.0029	1.6801	0.0030	1.6441	-

The eigenvectors obtained by SVMd and ITD match the system modes to the 4th decimal place. The modes estimated by SOD are also reasonably close to the LNMs as can be seen in $\mathbf{w}_1^T = (0.7003, 0.6180, 0.3573)^T$, $\mathbf{w}_2^T = (0.6987, 0.0019, -0.7154)^T$, $\mathbf{w}_3^T = (0.2148, -0.8358, 0.5053)^T$. The mass weighted POD shows similar trends without considerable deviation from the noise-free case

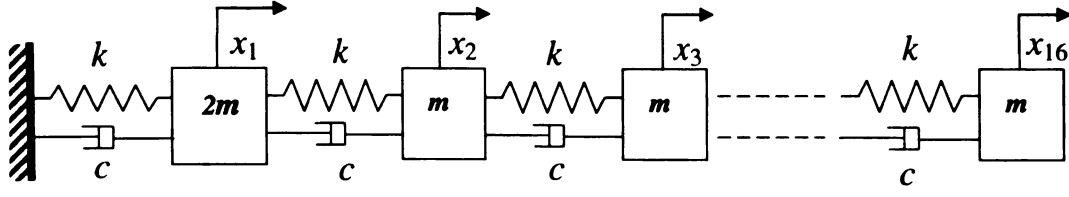


Figure 6.1: The mass-spring-damper model. The dashpots are figurative to represent the presence of damping, and do not accurately correspond to the example damping matrix.

and resulted in $\mathbf{w}_1^T = (0.3428, 0.6128, 0.7121)^T$, $\mathbf{w}_2^T = (-0.7121, -0.0188, 0.7018)^T$, $\mathbf{w}_3^T = (-0.2490, 0.8396, -0.4828)^T$.

In summary, all the decomposition methods work very well for both noise-free and noise contaminated cases for frequency estimations. In the noisy case, performance in the ITD can be improved; that is, to get a better damping estimate for the first mode, a larger differentiation step size (for instance $n_d = 32$) can be employed, but that results in somewhat decreased performance for all of the other identification schemes.

6.3.2 Forced response: A sixteen DOF system example

For randomly forced response, a sixteen DOF mass-spring-dashpot system shown in Fig. 6.1 is explored. In this example, the same mass and stiffness matrices as presented in [137] and also shown in section (3.3) are utilized. These are given as

$$\mathbf{M} = \begin{bmatrix} 2 & 0 & 0 & \dots & 0 \\ 0 & 1 & 0 & \dots & 0 \\ \vdots & \ddots & \ddots & \ddots & \vdots \\ 0 & \vdots & \dots & 0 & 1 \end{bmatrix}_{16 \times 16}, \quad \mathbf{K} = \begin{bmatrix} 2 & -1 & 0 & 0 & \dots & 0 \\ -1 & 2 & -1 & 0 & \dots & 0 \\ 0 & -1 & 2 & -1 & \ddots & 0 \\ \vdots & \vdots & \ddots & \ddots & \ddots & \vdots \\ 0 & \dots & \dots & 0 & -1 & 1 \end{bmatrix}_{16 \times 16} \quad (6.20)$$

and the damping matrix is chosen to be $\mathbf{C} = c\mathbf{M}$, where $c = 0.01$. In this example we considered the system already contaminated with measurement noise as explained in the following section.

6.3.2.1 Noise effects

The current example is similar to that of reference [102] except that the current system is a sixteen DOF system and is excited by two *independent* Gaussian white noise excitations. These forcing functions are applied at the first and sixteenth masses. In addition, the displacement output ensemble is corrupted with additional sensor noise having the signal to noise ratio (SNR) of 40 dB.

The system was simulated for 1000 seconds (later we found out it was about 15 modal periods of first frequency) with SIMULINK toolbox in Matlab, with a fixed-step Dormand Prince (a member of family of Runge-Kutta methods) differential equation solver [109] was used to evaluate the response of system. The programs default error tolerances were used (10^3 for relative error and 10^6 for absolute error). White noise forcing was generated using the Gaussian white noise generator function that produces discrete-time normally distributed random numbers with sampling time step matching the solver step size chosen as 0.1, resulting in generation of 10,000 data points. The forcing was observed to have a mean approaching zero. Both displacement and forcing matrices were saved to the Matlab workspace for further processing.

In the decomposition, the \mathbf{V} ensemble was formed with centered finite differences with a total step of two samples, such that difference matrix \mathbf{D} was $N_v \times N$, and $\mathbf{V} = \mathbf{X}\mathbf{D}^T$ was $n \times N_v$, where $N_v = N - 2$. From the data decomposition eigenvalues, estimates of the natural frequencies are compared to the true modal frequencies in Table 6.3. As mentioned earlier in section 6.2.2.1, for this large data set the SVD of the Hankel matrix was too large and was problematic to obtain. Cast this way, ERA is an expensive method and estimates were not computable. Reduction in the data set resulted in significant estimation errors and thus is not reported.

The system frequency estimates for all schemes are good. The error estimates for ω_{16} (which contains the largest error) reduced to about 2% for all methods when $N = 100,000$ points were used. Nonetheless, all schemes show similar trends and work

Table 6.3: *System frequencies estimated from decomposition methods with white noise forcing compared against structural eigen frequencies*

Method	System		ITD		SVMD		SOD	
Ω_i	<i>Freq.</i>	<i>Error</i>	<i>Freq.</i>	<i>Error</i>	<i>Freq.</i>	<i>Error</i>	<i>Freq.</i>	<i>Error</i>
ω_1	0.0951	-	0.0926	2.60%	0.0926	2.60%	0.0934	1.76%
ω_2	0.2832	-	0.2847	0.55%	0.2847	0.54%	0.2840	0.29%
ω_3	0.4644	-	0.4708	1.37%	0.4705	1.31%	0.4704	1.27%
ω_4	0.6345	-	0.6358	0.21%	0.6354	0.14%	0.6354	0.14%
ω_5	0.7933	-	0.7883	0.62%	0.7874	0.73%	0.7874	0.74%
ω_6	0.9482	-	0.9456	0.27%	0.9441	0.42%	0.9440	0.44%
ω_7	1.1035	-	1.1045	0.09%	1.1022	0.11%	1.1023	0.10%
ω_8	1.2557	-	1.2557	0.00%	1.2524	0.26%	1.2511	0.36%
ω_9	1.4000	-	1.4039	0.27%	1.3993	0.05%	1.3991	0.06%
ω_{10}	1.5330	-	1.5337	0.04%	1.5278	0.34%	1.5279	0.33%
ω_{11}	1.6522	-	1.6453	0.41%	1.6391	0.79%	1.6392	0.79%
ω_{12}	1.7558	-	1.7559	0.00%	1.7481	0.44%	1.7482	0.42%
ω_{13}	1.8423	-	1.8470	0.25%	1.8378	0.24%	1.8377	0.24%
ω_{14}	1.9107	-	1.9147	0.20%	1.9044	0.32%	1.9039	0.35%
ω_{15}	1.9601	-	1.9698	0.49%	1.9635	0.17%	1.9622	0.10%
ω_{16}	1.9900	-	2.0898	5.01%	2.1181	6.40%	2.1072	5.89%

well for all the modes (even those with closely spaced frequencies, in this case the last three). The ability to work well in closely spaced frequencies is a basic advantage of time-domain methods over the frequency domain based identification schemes.

The modal assurance criterion (MAC) [110, 111] is now applied to evaluate consistency of the estimated modes with the system modes. The normalized inner products (squared) between estimated and true modes are computed using the method. Values of near unit magnitude indicate modal vectors that nearly line up. For visualization, the modal vectors from the state-variable modal decomposition and the structural eigenvalue problem using the modal assurance criterion are compared in Fig. 6.2. Al-

though all modes estimates are quite good, two of the modes do not show the MAC value of identity, these are the same modes which had higher errors in frequency estimates, too.

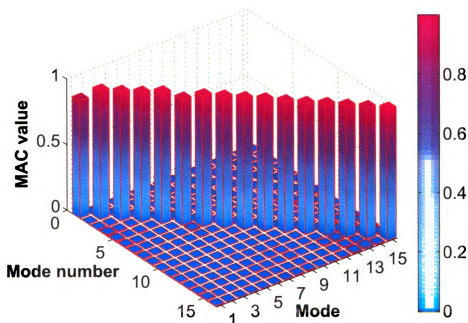


Figure 6.2: The MAC values for all SVMD modes. MAC value of 1 shows vectors match up. Modes are not in any particular sequence

Modes from other schemes (SOD, ITD and mass weighted POD) are also shown in figures 6.3, 6.4 and 6.5. Barring POD, all the modes are identified well in all schemes. POD has good values except may be 3-4 modes that may be due to noise in the system (this requires further investigation).

6.4 Clamped-free cantilever beam experiment

Though numerical simulations provide a good picture of the theoretical framework, theoretical assumptions may not always hold and the system may have features such as non-stationary signals, nonlinearity, effects of filtering, spurious modes, contamination due to noise, unknown model order, and reduced observability, which can only

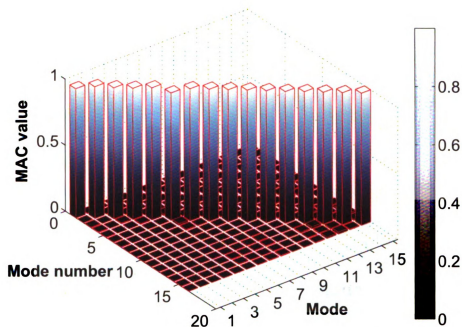


Figure 6.3: *The MAC values for all sixteen modes for SOD. MAC value of 1 shows vectors match up. Modes are not in any particular sequence*

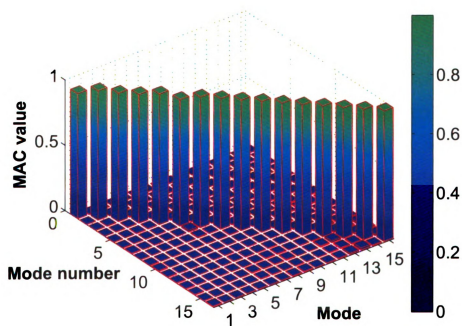


Figure 6.4: *The MAC values for all ITD modes. MAC value of 1 shows vectors match up. Modes are not in any particular sequence*

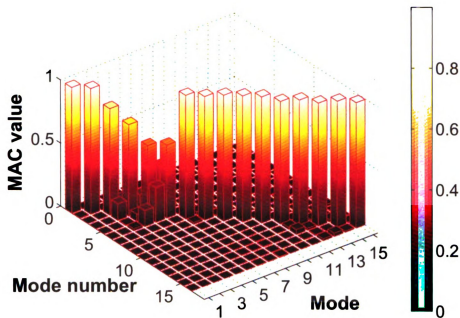


Figure 6.5: The MAC values for all mass-weighted POD modes. MAC value of 1 shows vectors match up. Modes are not in any particular sequence

be properly understood by thorough testing. Nonetheless, the experimental beam studied in section 4.3 is investigated using the stated modal identification schemes.

6.4.1 Identification results

In order to accurately compare the experimental results for SVMD, ITD, ERA, SOD and POD, the number of samples were reduced to the first $N = 1000$ samples. The data were then high-pass filtered at 0.5 Hz. These values were selected based on discussions in section 4.3.1. For SVMD, the correlation matrices $\mathbf{P} = \mathbf{Y}\mathbf{Y}^T/N_d$ and $\mathbf{Q} = \mathbf{Y}\mathbf{W}^T/N_d$ were then formed, and the SVOMs and SVOVs were extracted. The two delayed ensemble matrices were obtained from the \mathbf{Y} matrix ensemble for ITD. Extraction of SOMs and SOVs was accomplished by forming the two correlation matrices $\mathbf{V}\mathbf{V}^T$ and $\mathbf{X}\mathbf{X}^T$. For ERA, only one of the displacement time histories was employed (the time history of the 8th sensor was used here, the choice being completely arbitrary). The obtained frequency identification results for the first five modes are

shown in the Table 6.4. Damping estimates for the first three modes were computed using the log decrement method applied to carefully excited, dominantly single-mode responses, and are compared against the identification schemes in Table 6.5.

Table 6.4: *Experimental system frequencies (Hz.) estimated from various decomposition methods for a linear beam free response compared against the undamped structural eigen frequencies*

Parameter	Theoretical	FFT	ITD	SVMD	ERA	SOD
ω_1	2.74	2.75	2.93	2.78	3.04	2.23
ω_2	17.16	17.20	17.18	17.18	17.17	17.49
ω_3	48.05	47.21	47.52	47.91	47.43	49.53
ω_4	94.16	94.28	92.17	93.55	96.83	56.97
ω_5	156.68	155.9	153.57	153.96	156.05	144.47

Frequency identification for all schemes is relatively good with the exception of some estimates by SOD, in particular the 4th modal frequency. Note that the data set used in this estimation does not cover the entire first modal period, hence errors are expected as discussed in section 5.5. ERA was also able to estimate the sixth frequency as 228 Hz (where the theoretical undamped frequency and the FFT frequency peaks are 233.7 Hz and 230.7 Hz respectively) but was somewhat erroneous in estimating the first frequency. ITD and SVMD were relatively consistent for all modes and their estimates were matching the most among all.

Table 6.5: *Experimental modal damping estimated from various decomposition methods for the linear beam free response. Only first three damping estimates are computed by using dominantly single mode log decrement method*

Parameter	Theoretical	ITD	SVMD	ERA
ζ_1	0.0048	-0.042	-0.057	-0.1069
ζ_2	0.0040	0.0039	0.0039	0.0035
ζ_3	0.0036	0.0029	0.0028	0.0038
ζ_4	-	0.0506	0.0097	0.024
ζ_5	-	0.0055	0.0016	0.0015

The damping estimate for the first mode is poor for all of the schemes (again, this is because the time record only covers about half of the first modal period). (While

using a larger set of data points for the same test run with 12,000 sample points, the estimates were recorded as 0.0051 and 0.0049 for ITD and SVMD respectively. However, in that case only the first two modal frequencies were identifiable, a discussion of this can be seen in section (4.3.2). The second and third modes are very good for all schemes. ERA also computed the damping estimate for the sixth mode at 0.0022.

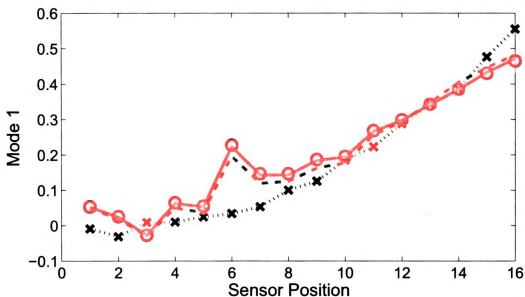


Figure 6.6: Identification methods are compared for the first beam mode. POD is shown with dotted line --, SOD is shown with crosses \times , SVMD with circles \circ , and ITD with the solid line —.

Mode shapes are now compared primarily for the SVMD, SOD, and ITD methods along with POD shown in some plots. The eigenvectors obtained from these methods are normalized and are plotted separately for each mode in Figures 6.6, 6.7, 6.8, 6.9, and 6.10. These plots, in general, accord with the frequency estimates, with ITD and SVMD showing almost identical plots. SOD shows good results for lower modes since the lower modes were dominant, but errs at higher mode shape estimates. POD has the same trend and is only shown for the lower modes. For higher modes, it has huge error and thus is not reported. The log plot of POVs is shown in Fig. 6.11 that shows

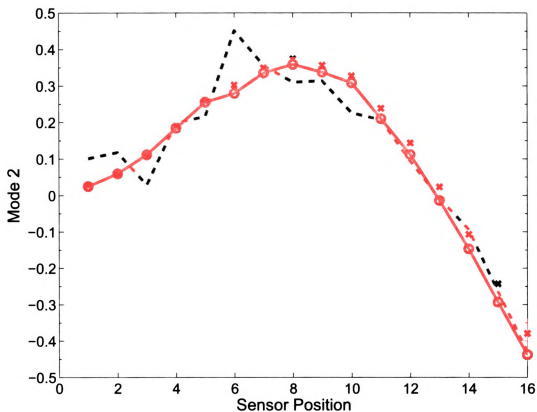


Figure 6.7: Identification methods are compared for the second beam mode. POD is shown with dotted line --, SOD is shown with crosses \times , SVMd with circles \circ , and ITD with the solid line —.

about four significant modes. This however, does not mean that POD and SOD in general cannot estimate higher modes. For instance, when the same beam was excited with a different response that showed a higher mode (in that case a dominant third mode), both POD and SOD were indeed able to get a good mode shape estimate for the third mode as shown in Fig. 6.12.

In essence, SVMd and ITD are able to estimate modal parameters up to the first five frequencies and five mode shapes very well in this experimental setup for the given set of data samples. ERA for the same data set was able to estimate the first five frequencies as well as a sixth frequency but at the cost of almost missing the lowest frequency, and was unable to estimate mode shapes. SOD was good for lower

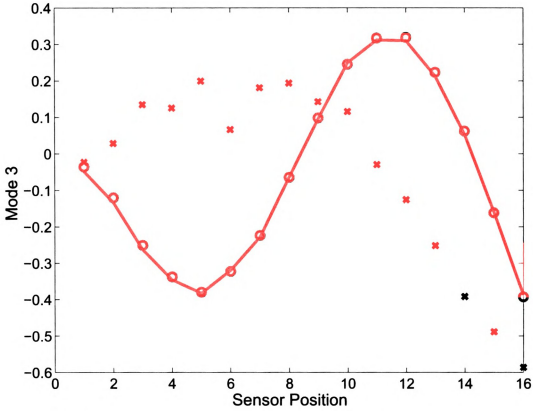


Figure 6.8: Identification methods are compared for the third beam mode. SOD is shown with crosses \times , SVMD with circles \circ , and ITD with the solid line $—$.

modal frequencies and associated mode shapes but did poorly for the higher ones. It was however, verified that the SOD produced modes were orthogonal $\Psi^T \mathbf{R} \Psi = \mathbf{I}$.

In general, for all identification schemes, it was observed that when larger data were used, lower modal estimates improved but high mode estimates degraded and vice-versa. (A complete discussion on effects of time record lengths is presented in section 5.5). The particular data set was selected to get reasonably high modes without degrading performance too much for the lower modes for most schemes, and to be able to compare all schemes (hence the 1000 sample points). Tests were also done on other beam samples (not shown). Results with those cases contribute to our general assessment of the methods.

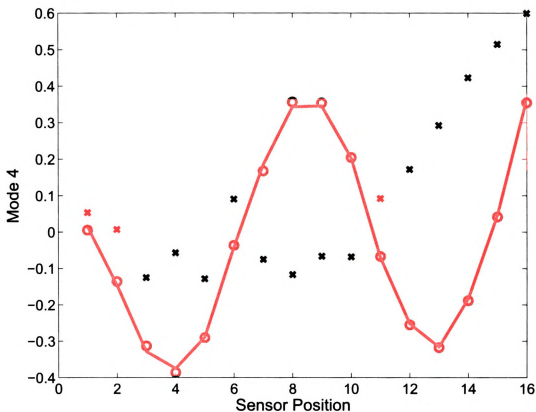


Figure 6.9: Identification methods are compared for the fourth beam mode. SOD is shown with crosses \times , SVM with circles \circ , and ITD with the solid line $—$.

6.5 Summary

We have made comparisons for various time-domain and decomposition based modal identification methods that extract modal information from responses of generally damped linear multi-degree-of-freedom systems. In each case, input to the system was not measured and only the response was measured. For each method, an eigenvalue problem was constructed, and the resulting eigenvalues and eigenvectors contained frequency plus damping and mode shape information, respectively.

Three kinds of systems were evaluated. The two numerical simulations were compared for free and random response cases that also involved quantization noise studies. Lastly, we performed an experiment on a real life structure and observed modal pa-

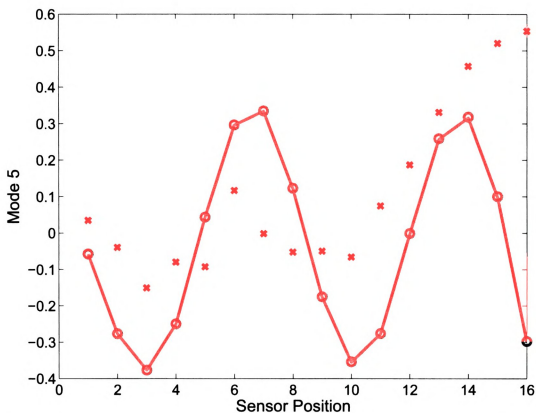


Figure 6.10: Identification methods are compared for the fifth beam mode. SOD is shown with crosses \times , SVM with circles \circ , and ITD with the solid line $—$.

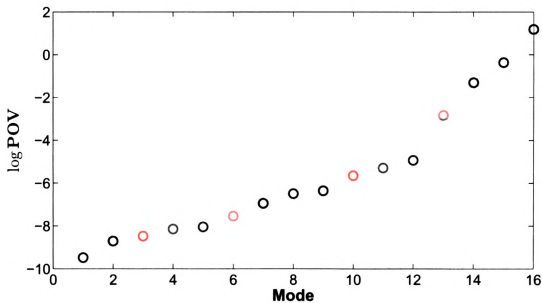


Figure 6.11: The log plot of POVs shown. The plot shows about 4 significant modes.

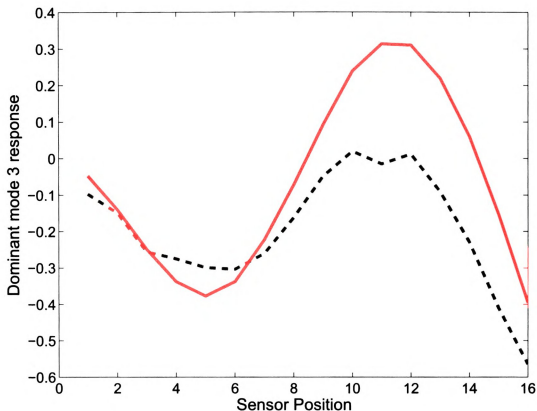


Figure 6.12: *SOD and POD mode shape identification for a higher mode with the system excited in a way to get a dominant 3rd order beam mode response. SOD is shown with the solid line —, and POD is shown with a dotted line - -.*

parameter estimates obtained through identical circumstances (same number of samples employed, filter conditions, etc.).

Among all the methods, SVM and ITD show closest resemblance in parameter estimation. Their frequency and mode shape estimates are reasonably good and the methods work very well in low noise conditions. SOD generally requires a larger data set, in particular for estimations of higher modes, and works well for lightly damped cases. ERA is a reliable but computationally expensive method and it would be interesting to be able to use ERA with more sensor histories for mode shape estimates (as original ERA is conducted). There is a trade-off between number of modal parameters to be estimated and their accuracy: and in general, accuracy of

lower modes increases with increasing number of sampling points, at the cost of the higher modes. These observations were also based on tests with other beams, which were not presented.

7.1 Synopsis

O*rthogonal* decomposition methods for experimental modal analysis have been presented in this work. A novel approach called the state-variable modal decomposition (SVMD) was analyzed for free and random response cases for linear multi-degree-of-freedom structural problems. Also addressed was the extension of smooth orthogonal decomposition (SOD) for random response. These methods fall under the output-only time-domain category of modal analysis that does not require measuring the input forces. Both methods are extensions of the well known proper orthogonal decomposition method (POD) and overcome some of the inherent limitations of the POD. These methods tie up the gap between current time-domain schemes and the POD. We will briefly summarize work presented in each chapter and conclude with a discussion on potential future work.

7.1.1 *Free response*

A modal decomposition strategy based on state-variable ensembles was formulated. A nonsymmetric, generalized eigenvalue problem was constructed. The data-based eigenvalue problem was related to the generalized eigenvalue problem associated with

free-vibration solutions of the state-variable formulation of linear multi-degree-of-freedom systems. For linear free-response data, the inverse-transpose of the eigenvector matrix represents the state-variable modal eigenvectors, and the eigenvalues of the nonsymmetric eigenvalue problem approximate those of the state-variable model. As such, the eigenvalues lead to estimates of frequencies and modal damping. The interpretation holds for linear systems with multi-modal free responses without the need of input data, whether damping is large or small, or modal or nonmodal. Simulations for noise contaminated cases also showed satisfactory performance for underdamped system parameter estimations.

7.1.2 *Random response*

The smooth orthogonal decomposition (SOD) and the state-variable modal decomposition SVMD methods were extended for modal analysis of randomly excited systems. Modal parameter estimation in terms of natural frequencies and mode shapes was studied using the SOD method. We showed that under certain conditions, the SOD eigenvalue problem formulated from white noise excited response data could be tied to the unforced structural eigenvalue problem, and thus could be used for modal parameter estimation. Using output response ensembles only, the generalized eigenvalue problem was formed to estimate modal frequencies and modal vectors for an eight-degree-of-freedom lightly damped vibratory system. The estimated frequencies were compared against system frequencies obtained from the structural eigenvalue problem and estimated modal vectors were checked using the modal assurance criterion. Simulations showed that for light damping, satisfactory results were obtained for estimating both system frequencies and modal vectors even in the presence of sensor noise. While the work was primarily geared towards the SOD analysis, the SVMD was briefly touched upon to show a similar connotation as the SOD analysis.

7.1.3 *Experiments*

Since in general, real life systems can deviate considerably from ideal theoretical assumptions, applicability of SVMD method was evaluated for free responses by multiple experimental setups. We evaluated the SVMD method for structures modeled as both single and multi-degree-of-freedom systems. Many beam structures were tested and we were successfully able to estimate modal parameters for multiple modes. This presents SVMD as a viable modal parameter estimation scheme.

We observed that the time record of the data plays critical role in the parameter estimation. The trend found was that shorter length data was good for estimating higher modes, while longer length data were good for estimating lower modes. Modal coordinates together with mode shapes and modal frequencies were found useful to determine the quality of the decomposition and also to distinguish actual modes from fictitious ones. Another important factor was appropriate filter selection. Filter cut-off frequency selected as half (or less) of the fundamental frequency (computed by FFT) removed low noise drifts that may otherwise appear in the response, and in integrations of measured accelerations.

The experimental investigation also revealed limitations of the SVMD method. It was observed that at best, the SVMD method is only as good as the number of sensors utilized for measurements. If the number of sensors is less than the active system modes, SVMD can only identify a few modes with accuracy.

7.1.4 *Quantitative evaluation*

In previous sections, we used information in modal coordinates qualitatively to examine the effectiveness of the decomposition results and to help separate spurious modes. In order to establish a more efficient way of addressing the decomposition quality, we developed two new tools. These tools quantify the decomposition effectiveness. The spectrum assurance and spectrum difference tools use the FRFs obtained from both

the modal coordinates and the identification results (from decomposition methods or FFT) to generate a number that ranges between 0 and 1. Both could be used together to eliminate a “close but spurious” candidate. These criteria were first explored using some numerical case studies. System parameters such as frequency and damping values were varied to establish any specific trends. It was seen that both criteria are less sensitive to changes in damping errors than to frequency errors. Then these tools were applied to experimental data to quantify the decomposition results.

Finally, we evaluated the data length effects on the identification. This was explained via a numerical study. It was observed that with addition of noise to the system, results suffered if the data length was either too short or too long. At least one modal period should be used for frequency identification. While the damping estimates showed similar trends, we found that useful information was contained within the oscillations peaks as well. Modal settling time was found to be the other useful measure. When time record was greater than modal settling time, the noise effects started to become significant and identification results were found to err.

7.1.5 Comparison to other methods

A number of common time-domain methods are available for modal parameter estimation. We compared the decomposition based methods SVMD, SOD and POD against the two methods of significant impact, the Ibrahim time domain method and the modified eigensystem realization algorithm. We simulated two numerical examples for free and random response cases. The free response case used a three DOF system whereas the random response case employed a sixteen DOF structural system. Both cases were contaminated with noise at the output. All methods were compared against the theoretical frequencies and damping ratios. In the free response case, mode shapes were directly matched while in the random response case the modal assurance criterion was used. Lastly, we made comparisons on the experimental beam

studied in the previous chapter.

In numerical simulations with light damping, all of the methods generally produced good estimates of the system frequencies even in the presence of noise. Also, mode shape estimates accorded well with the frequency estimates. The SVMD and ITD methods produced the most closely matching results, especially in the experiments. The estimation by using a modified ERA in the experimental test was slightly better for frequencies and damping estimates, but it was unable to produce any mode shapes. The SOD worked well for the lower modes but ran into issues at the higher mode estimations.

7.2 Recommendations for use of the decomposition methods

In this section, we will briefly describe the strategy for any interested user to implement the decomposition methods for physical experiments.

The decomposition methods are output-only methods so collection of “clean” data cannot be overemphasized. From numerous studies, we have established that the decomposition methods work very well for noise-free systems. Given that the physical systems would have some form of noise, every possible effort should be made to minimize the effects of noise on response data. Thus, use of noise filters, low sensitivity voltage amplifiers, proper selection and proper installation of accelerometers is highly recommended.

Decomposition methods are evaluated for free and random response cases. A near-ideal impulse or a broadband random excitation is required for methods to work the best. Care should be taken to implement the near-ideal excitation on the test structure.

To construct decomposition method ensembles, integrations should be preferred over differentiations where possible.

An FFT of the response data can establish a range of system frequencies of interest since FFT is regarded as more accurate for estimating frequencies, and useful in determining candidates for extracted true modes. If decomposition methods have frequencies that may be “in the neighborhood” of the probable mode, SAC and SD tools should be applied to distinguish the real and spurious modes. SAC in general, produces more clear candidates but SD narrows down the choice. It is perhaps best to use these together.

If the interest is in identification of lower modes, use of “longer” time record length (that is at least a modal period) is recommended. For low noise cases, the 2% settling time criterion of the lowest mode can be used as a guide for maximum time record length. In general, these criteria may not be a known priori but FFT can be used to estimate the lowest modal frequency.

If the interest is in higher modes, since these modes generally damp out quickly, a “shorter” time record can identify the higher modes. At least one modal period is required though for adequate estimates.

The decomposition methods estimate low to moderate damping in lower modes with relatively long data. High damping case or damping in higher modes were not verified experimentally in this work.

For very light damping, all decomposition methods work equally well. SVMD, ITD and ERA can estimate low to moderate damping estimates. ERA is the most expensive scheme but perhaps can identify higher modes. ITD and SVMD have the most common features and most matching results.

7.3 Future work

The SVMD method has been evaluated as a viable output-only time-domain modal identification scheme. The method is an extension of the POD method applied in

linear structural system analysis. The method has been analyzed in free response and random response cases. Below, we suggest some of the potential directions for broadening the capabilities of the method.

7.3.1 Damping estimation for random excitation

In section 3.4.1, we presented the analysis of the SVMD for MDOF systems subjected to random response. The analysis suggests that the SVMD should produce modal parameter estimates for randomly excited systems including frequencies, damping ratios and mode shapes. However, in section 3.4.2, we observed that this was not entirely true. Indeed, the SVMD method produced good estimates of modal frequencies and the mode shapes, but failed to pickup any damping ratio estimates. In the same section it was noted that this may be due to differentiation errors associated with the Euler derivative applied to generate ensemble matrices \mathbf{V} and \mathbf{A} . We also observed that by using the ensemble matrices that are generated by SIMULINK (that uses high order numerical integration schemes), accurate damping estimates were obtainable by the SVMD method. While it may be tempting to use a higher order (Newton-Cotes [138]) derivative scheme, the stated observations suggest that a higher derivative scheme may or may not work. A better way is to integrate the acceleration ensemble to obtain the velocity and displacement ensembles. This is especially easier in experiments. We also suggest experimental verification of the ideas presented in chapters 4 and 5 to verify applicability of both SOD and SVMD methods to responses to random excitation.

7.3.2 Continuous systems

In deriving the SVMD method for modal analysis of linear MDOF systems, we used discrete models. The ensembles, numerical derivatives, etc., were all discretized. However, in actual experiments we used continuous systems (beams). Even though the

decomposition worked well for such systems, it was never shown analytically that SVMD works well for a continuous system. Hence it would be useful to conduct an analytical study that addresses SVMD analysis for continuous systems. This can be done for both free responses as well as randomly excited systems.

7.3.3 *Nonlinear systems*

Throughout in the modal analysis by SVMD, we assumed the systems under study to be linear, time invariant, and causal. As mentioned in reference [3],

It is appropriate to include a consideration of the possibility that not all the systems or structures encountered in practice will be linear.

The SVMD can be used to identify the linearized frequency content present in a nonlinear system. To see this we consider a 2 DOF system that has an undamped harmonic oscillator attached to a Van der Pol oscillator [139]. The governing equations of motion are

$$\ddot{x}_1 + k(2x_1 - x_2) = 0 \quad (7.1)$$

$$\ddot{x}_2 + k(x_2 - x_1) - \epsilon \dot{x}_2(1 - x_2^2) = 0 \quad (7.2)$$

where the mass and stiffness parameters are all normalized to unity. Varying the parameter ϵ , the fixed point dynamics can be varied. However, we used small ϵ values, such that $0 < \epsilon < 0.5$, for the SVMD analysis.

The system was simulated using SIMULINK toolbox for 10 seconds. The step size was chosen as $\Delta t = 0.004977$, the sample size was $N = 2000$, and the initial conditions were $\mathbf{x}(0) = (0.000001, 0)^T$, and $\mathbf{v}(0) = (0, 0)^T$. The ϵ value for this particular case was chosen as 0.3. The time record approximately matches one period of the lowest-frequency mode of the linearized system. The undamped natural frequencies of the linearized system are $\omega_1 = 0.6205$, and $\omega_2 = 1.6116$.

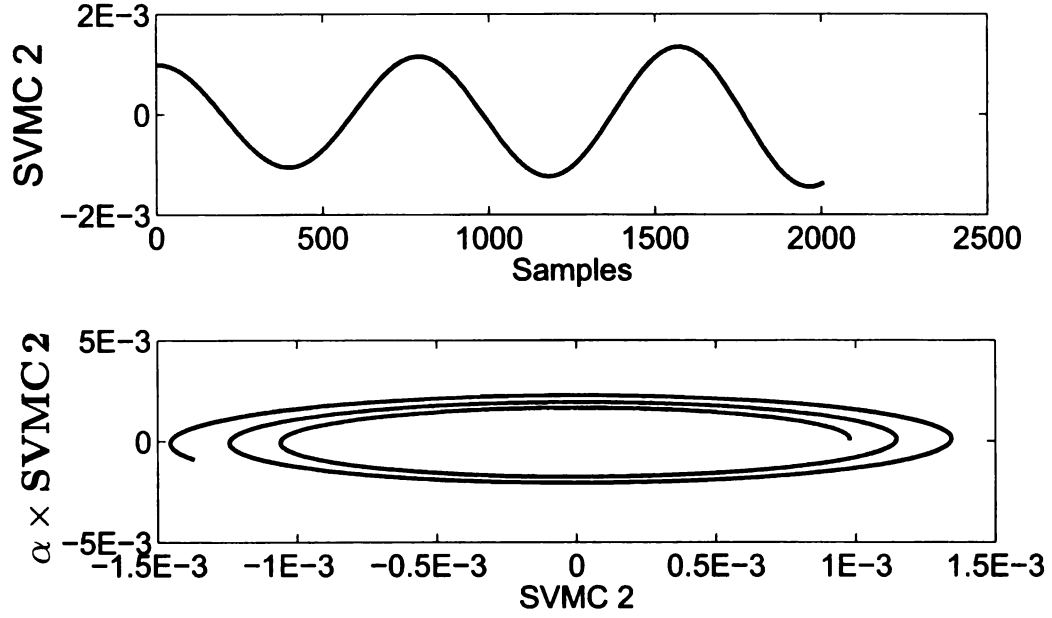


Figure 7.1: The modal coordinates plot for ω_2 and their phase space are plotted for 10 second simulation time.

The decomposition was performed in the usual manner on the collected data. We found that even for this small time period, the SVMD was able to perfectly estimate the system frequencies and the damping ratios. Note that SVMD was able to identify negative damping. The SVMD identified mode shapes (normalized) were $\mathbf{w}_1^T = \bar{\mathbf{w}}_2^T = (0.6354 - 0.1043i, 1.0554 - 0.058i)^T$, $\mathbf{w}_3^T = \bar{\mathbf{w}}_4^T = (-0.0671 - 0.6786i, -0.0487 + 0.4118i)^T$. These perfectly matched with those of the structural eigenvalue problem.

By construction, $\dot{\mathbf{Q}} = \alpha \mathbf{Q}$. Using this relationship, we took the real part of time history of modal coordinate corresponding to ω_2 , and plotted it against the real part of $\alpha_2 \times Q(\omega_2)$ (where α_2 corresponds to the eigenvalue associated with the second mode). This plot is shown in Fig. 7.1.

When the simulation time was increased to 400 seconds, the system response closely reaches the limit cycle, the SVMD identified the system frequencies as $\omega_1 = 0.6073$, and $\omega_2 = 1.8244$. The SVMD was able to identify the modal vector associated with the ω_1 as $\mathbf{w}_1^T = \bar{\mathbf{w}}_2^T = (0.6579 - 0.0016i, 1.0731 - 0.0013i)^T$, the real part being

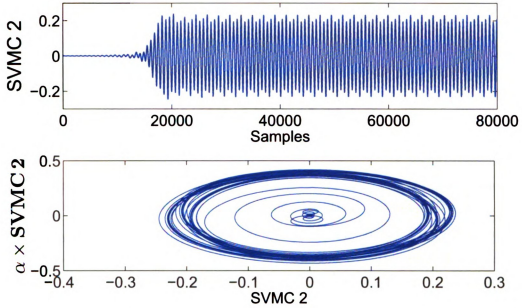


Figure 7.2: The modal coordinates plot for ω_2 and their phase space are plotted for simulation time of 400 seconds.

close to structural modal vector. However, the modal vector associated with ω_2 was erroneous. This vector was identified as $\mathbf{w}_3^T = \mathbf{w}_4^T = (-0.0014 - 0.3941i, -0.0001 + 0.5236i)^T$. That the modal vector of the large motion is not a good match with the linearized modal vector is not surprising, since with large motion the nonlinearities participate significantly.

Again, we took the real part of time history of modal coordinate corresponding to ω_2 , and plotted it against the $\alpha_2 \times Q(\omega_2)$ (where α_2 corresponds to the eigenvalue associated with the first mode). This plot is shown in Fig. 7.2. We see that response has reached a limit cycle.

These are early findings and we are unclear at this point whether the modal coordinates can contribute to dynamical phenomenon such as period doubling.

In essence, SVMd can identify the linearized frequencies hidden in a nonlinear system, but needs further exploration in identification of nonlinear systems.

BIBLIOGRAPHY

- [1] P. Avitabile, "Experimental modal analysis: A simple non-mathematical presentation," *Sound and Vibration*, vol. 35, pp. 20–31, January 2001.
- [2] N. Maia, J. M. M. Silva, J. He, N. A. J. Lieven, R. M. Lin, G. W. Skingle, W.-M. To, and A. P. Urgueira, *Theoretical and Experimental Modal Analysis*. Somerset, England: Research Studies Press Ltd, 1997.
- [3] D. J. Ewins, *Modal Testing: Theory and Practice*. Research Studies Press, Letchworth, UK., 1984.
- [4] D. Ewins, *Modal testing: Theory and Practice*. Brüel and Kjaer, 1986.
- [5] K. McConnell, *Vibration Testing: Theory and Practice*. New York: John Wiley and Sons, Inc., 1995.
- [6] J. He and Z. Fu, *Modal Analysis*. Oxford: Butterworth-Heinemann, 2001.
- [7] J. L. Doob, *Stochastic Processes*. New York: John Wiley & Sons, 1953.
- [8] S. H. Crandall, ed., *Random Vibration*, ch. 2, pp. 33–51. NewYork: Technology Press of the Massachusetts Institute of Technology and John Wiley & Sons, 1958.
- [9] L. L. Beranek, ed., *Noise and Vibration Control*, ch. 5, Data Analysis, pp. 100–137. NewYork: McGraw Hill, Inc, 1971.
- [10] S. H. Crandall and W. D. Mark, *Random Vibration in Mechanical Systems*. NewYork: Academic Press, 1963.
- [11] A. H. Jazwinski, *Stochastic Processes and Filtering Theory*, vol. 64 of *Mathematics in Science and Engineering*. NewYork: Academic Press, 1970.
- [12] N. E. Huang, Z. Shen, S. R. Long, M. L. C. Wu, H. H. Shih, Q. N. Zheng, N. C. Yen, C. C. Tung, and H. H. Liu, "The empirical mode decomposition and the hilbert spectrum for nonlinear and non-stationary time series analysis," *Proceedings of the Royal Society of London Series A—Mathematical Physical and Engineering Sciences*, vol. 454, no. 1971, pp. 903–995, 1998.

- [13] J. N. Yang and Y. Lei, "System identification of linear structures using hilbert transform and empirical mode decomposition," in *Proceedings of the 18th International Modal Analysis Conference: A Conference on Structural Dynamics*, vol. 1, (San Antonio, TX), pp. 213–219., Society for Experimental Mechanics Inc., Bethel, CT, 2000.
- [14] J. N. Yang and Y. Lei, "Identification of natural frequencies and damping ratios of linear structures via hilbert transform and empirical mode decomposition," in *Proceedings of the International Conference on Intelligent Systems and Control*, (IASTED/Acta Press, Anaheim, CA), pp. 310–315, 1999.
- [15] J. N. Yang, Y. Lei, S. Lin, and N. Huang, "Hilbert-huang based approach for structural damage detection," *Journal of engineering mechanics*, vol. 130, pp. 85–95, January 2004.
- [16] R. Yan and R. X. Gao, "Hilberthuang transform based vibration signal analysis for machine health monitoring," *IEEE Transactions On Instrumentation And Measurement*, vol. 55, pp. 2320–2329, Dec 2006.
- [17] S. G. Mallat, "A theory for multiresolution signal decomposition - the wavelet representation," *IEEE Transactions on Pattern Analysis and Machine Intelligence*, vol. 11, no. 7, pp. 674–693, 1989.
- [18] T. Önsay and A. G. Haddow, "Wavelet transform analysis of transient wave-propagation in a dispersive medium," *Journal of the Acoustical Society of America*, vol. 95, no. (3), pp. 1441–1449, 1994.
- [19] P. Argoul and P. Le, "Instantaneous indicators of structural behaviour based on the continuous cauchy wavelet analysis," *Mechanical Systems and Signal Processing*, vol. 17, no. (1), pp. 243–250, 2003.
- [20] D. Coca and S. A. Billings, "Continuous-time system identification for linear and nonlinear systems using wavelet decompositions," *International Journal of Bifurcation and Chaos*, vol. 7, no. 1, pp. 87–96, 1997.
- [21] K. H. Ip, P. W. Tse, and H. Y. Tam, "Extraction of patch-induced lamb waves using a wavelet transform," *Smart Materials and Structures*, vol. 13, no. (4), pp. 861–872., 2004.
- [22] F. L. di Scalea and J. McNamara, "Wavelet transform for characterizing longitudinal and lateral transient vibrations of railroad tracks," *Research in Nondestructive Evaluation*, vol. 15, no. (2), pp. 87–98., 2004,.

- [23] A. Roueff, J. Chanussot, J. I. Mars, and M. Q. Nguyen, "Unsupervised separation of seismic waves using the watershed algorithm on time-scale images," *Geophysical Prospecting*, vol. 52, no. (4), pp. 287–300., 2004.
- [24] H. S. Lee and S. H. Kwon, "Wave profile measurement by wavelet transform," *Ocean Engineering*, vol. 30, no. (18), pp. 2313–2328., 2003.
- [25] M. C. Huang, "Wave parameters and functions in wavelet analysis," *Ocean Engineering*, vol. 31, no. (1), pp. 111–125., 2004.
- [26] J.-W. Liang and B. F. Feeny, "Wavelet analysis of stick-slip signals in oscillators with dry-friction contact," *Journal of Vibration and Acoustics*, vol. 127, pp. 139–143, April 2005.
- [27] S. R. Ibrahim and E. C. Mikulcik, "A time domain modal vibration test technique," *Shock and Vibration Bulletin*, vol. 34, no. 4, pp. 21–37, 1973.
- [28] F. R. Spitznogle and A. H. Quazi, "Representation and analysis of time-limited signals using a complex exponential algorithm," *Journal of The Acoustical Society of America*, vol. 47, pp. 1150–1155, 1970.
- [29] D. L. Brown, R. J. Allemang, R. D. Zimmerman, and M. Mergeay, "Parameter estimation techniques for modal analysis," *SAE Transactions, SAE Paper Number 790221*, vol. 88, pp. 828–846, 1979.
- [30] H. Vold, J. Kundrat, G. Rocklin, and R. Russel, "A multi-input modal estimation algorithm for mini-computer," *SAE Technical Papers Series, No 820194*, vol. 91, pp. 815–821, 1982.
- [31] J.-N. Juang and R. S. Pappa, "An eigensystem realization algorithm for modal parameter identification and model reduction," *Journal of Guidance, Control and Dynamics*, vol. 8, no. 5, pp. 620–627, 1985.
- [32] P. V. Overschee and B. De Moor, *Subspace Identification for Linear Systems: Theory- Implementation- Applications*. Boston: Kluwer Academic Publishers, 1996.
- [33] H. Vold, "Orthogonal polynomials in the polyreference method," in *Proceedings of the International Seminar on Modal Analysis, Katholieke University of Leuven, Belgium*, 1986.
- [34] M. Richardson and D. L. Formenti, "Parameter estimation from frequency response measurements using rational fraction polynomials," in *Proceedings of the International Modal Analysis Conference*, pp. 167–182, 1982.

- [35] C. Y. Shih, Y. G. Tsuei, R. J. Allemang, and D. L. Brown, "Complex mode indication function and its application to spatial domain parameter estimation," *Mechanical System and Signal Processing*, vol. 2, pp. 367–377, 1988.
- [36] R. Brincker, L. Zhang, and P. Andersen, "Modal identification of output-only systems using frequency domain decomposition," *Smart Materials And Structures*, vol. 10, pp. 441–445, 2001.
- [37] S. R. Ibrahim and E. C. Mikulcik, "The experimental determination of vibration test parameters from time responses," *Shock and Vibration Bulletin*, vol. 46, pp. 187–196, 1976.
- [38] S. R. Ibrahim and E. C. Mikulcik, "A method for the direct identification of vibration parameters from the free response," *Shock and Vibration Bulletin*, vol. 47, no. 4, pp. 183–198, 1977.
- [39] R. Pappa and S. R. Ibrahim, "A parametric study of the ibrahim time domain modal identification algorithm," *The Shock and Vibration Bulletin*, vol. 51, no. 3, p. 4357, 1981.
- [40] S. R. Ibrahim and R. S. Pappa, "Large modal survey testing using the ibrahim time domain identification technique," *Journal of Spacecraft and Rockets*, vol. 19, no. 5, pp. 459–465, 1982.
- [41] P. Mohanty and D. J. Rixen, "A modified ibrahim time domain algorithm for operational modal analysis including harmonic excitation," *Journal of Sound and Vibration*, vol. 275, pp. 375–390, August 2004.
- [42] G. R. Prony, "Essai experimental et analytique: sur les lois de la dilatabilite des fluides elastiques et sur celles de la force expansive de la vapeur de l'eau et de la vapeur de l'alcool, a differentes temperatures," *Journal de L'Ecole Polytechnique, Floreal et Priarial, An III*, vol. 1, no. 2, pp. 24–76, 1795.
- [43] N. M. M. Maia and J. M. M. Silva, "Modal analysis identification techniques," *Philosophical Transactions of the Royal Society of London: Series A, Mathematical, Physical and Engineering Sciences*, vol. 359, no. 1778, pp. 29–40, 2001.
- [44] J.-N. Juang, *Applied System Identification*. Upper Saddle River, New Jersey: Prentice Hall, 1994.
- [45] J.-N. Juang and M. Q. Phan, *Identification and Control of Mechanical Systems*. New York, New York: Cambridge University Press, 2001.
- [46] G. Kerschen, F. Poncelet, and J. C. Golinval, "Physical interpretation of independent component analysis in structural dynamics," *Mechanical Systems and Signal Processing*, vol. 21, pp. 1561–1575, May 2007.

- [47] F. Poncelet, G. Kerschen, J. C. Golinval, and D. Verhelst, "Output-only modal analysis using blind source separation techniques," *Mechanical Systems and Signal Processing*, vol. 21, pp. 2335–2358, 2007.
- [48] M. Rades, "Literature review : Linear model parameter estimation," *The Shock and Vibration Digest*, vol. 25, no. 3, pp. 1–15, 1993.
- [49] R. Allemang and D. L. Brown, "A unified matrix polynomial approach to modal identification," *Journal of Sound and Vibration*, vol. 211, no. 3, pp. 301–322, 1998.
- [50] N. Lieven and D. Ewins, "The context of experimental modal analysis," *Philosophical Transactions of the Royal Society of London: Series A, Mathematical, Physical and Engineering Sciences*, vol. 359, no. 1778, pp. 5–10, 2001.
- [51] D. L. Brown and R. J. Allemang, "The modern era of experimental modal analysis one historical perspective," *Sound and Vibration*, vol. 40th Anniversary Issue, pp. 16–25, 2007.
- [52] C. C. Kennedy and C. D. P. Pancu, "Use of vectors in vibration measurement and analysis," *Journal of Aeronautical Sciences*, vol. 14, no. 11, pp. 603–625, 1947.
- [53] R. C. Lewis and D. L. Wrisley, "A system for the excitation of pure natural modes of complex structures," *Journal of Aeronautical Sciences*, vol. 17, no. 11, pp. 705–722, 1950.
- [54] G. W. Asher, "A method of normal mode excitation utilizing admittance measurements," in *Dynamics of Aeroelasticity, Proceedings, Institute of the Aeronautical Sciences*, pp. 69–76, 1958.
- [55] J. L. Lumley, "The structure of inhomogeneous turbulent flow," in *Atmospheric Turbulence and Radio Wave Propagation* (A. M. Yaglom and V. I. Tatarski, eds.), (Nauka, Moscow), 1967.
- [56] J. L. Lumley, *Stochastic Tools in Turbulence*. Academic Press, New York., 1970.
- [57] G. Berkooz, P. Holmes, and J. L. Lumley, "The proper orthogonal decomposition in the analysis of turbulent flows," *Annual reviews of Fluid mechanics*, vol. 25, pp. 539–575, 1993.
- [58] J. P. Cusumano and B. Y. Bai, "Period-infinity periodic motions, chaos and spatial coherence in a 10 degree of freedom impact oscillator," *Chaos, Solitons and Fractals*, vol. 3, no. 5, pp. 515–535, 1993.

- [59] J. P. Cusumano, M. T. Sharkady, and B. W. Kimble, "Spatial coherence measurements of a chaotic flexible-beam impact oscillator," in *Aerospace Structures: Nonlinear Dynamics and System Response*, vol. ASME AD-Vol. 33, pp. 13–22, 1993.
- [60] B. I. Epureanu, L. S. Tang, and M. P. Paidoussis, "Exploiting chaotic dynamics for detecting parametric variations in aeroselastic systems," *AIAA Journal*, vol. 42, no. 4, pp. 728–735, 2004.
- [61] L. Ukeiley, M. Varghese, M. Glauser, and D. Valentine, "Multifractal analysis of a lobed mixer flowfield utilizing the proper orthogonal decomposition," *AIAA Journal*, vol. 30, no. 5, pp. 1260–1267, 1993.
- [62] L. Ukeiley, M. Glauser, and D. Wick, "Downstream evolution of proper orthogonal decomposition eigenfunctions in a lobed mixer," *AIAA Journal*, vol. 31, no. 8, pp. 1392–1397, 1993.
- [63] M. A. Davies and F. C. Moon, "Solitons, chaos, and modal interactions in periodic structures," in *Nonlinear Dynamics: the Richard Rand 50th Anniversary Volume*, pp. 119–143, Singapore: World Scientific, 1997.
- [64] I. T. Georgiou, I. B. Schwartz, E. Emaci, and A. Vakakis, "Interaction between slow and fast oscillations in an infinite degree of freedom linear system coupled to a nonlinear subsystem," *Journal of Applied Mechanics*, vol. 66, no. (2), pp. 448–459., 1999.
- [65] P. M. FitzSimons and C. Rui, "Determining low dimensional models of distributed systems," *Advances in Robust and Nonlinear Control Systems*, vol. ASME-DSC53, pp. 9–15, 1993.
- [66] G. Kerschen, J. Golinval, A. Vakakis, and L. Bergman, "The method of proper orthogonal decomposition for dynamical characterization and order reduction of mechanical systems: an overview," *Nonlinear Dynamics. Special issue: Dimension Reduction of Dynamical Systems: Methods, Models, Applications.*, vol. 41, pp. 141–170, 2005.
- [67] R. V. Kappagantu and B. F. Feeny, "Part 2: Proper orthogonal modal modeling of a frictionally excited beam," *Nonlinear Dynamics*, vol. 23, no. 1, pp. 1–11, 2000.
- [68] R. Kappagantu and B. Feeny, "An "optimal" modal reduction of a system with frictional excitation," *Journal of Sound and Vibration*, vol. 224, no. 5, pp. 863–877, 1999.

- [69] B. I. Epureanu, E. H. Dowell, and K. C. Hall, "Reduced-order models of unsteady transonic viscous flows in turbomachinery," *Journal of Fluids and Structures*, vol. 14, pp. 1215–1234, 2000.
- [70] B. I. Epureanu, "A parametric analysis of reduced order models of viscous flows in turbomachinery," *Journal of Fluids and Structures*, vol. 17, pp. 971–982., 2003.
- [71] G. Kerschen, B. F. Feeny, and J. C. Golinval, "On the exploitation of chaos to produce reduced order models," *Computer Methods in Applied Mechanics and Engineering*, vol. 192, pp. 1785–1795, 2003.
- [72] K. Yasuda and K. Kamiya, "Experimental identification technique of nonlinear beams in time domain," in *ASME Design Engineering Technical Conferences*, (Sacramento), 1997. on CD-ROM.
- [73] X. Ma and A. F. Vakakis, "Karhunen-loève decomposition of the transient dynamics of a multibay truss," *AIAA Journal*, vol. 37, no. (8), pp. 939–946., 1999.
- [74] X. Ma, M. A. F. Azeez, and A. F. Vakakis, "Nonlinear normal modes and non-parametric system identification of nonlinear oscillators," *Mechanical Systems and Signal Processing*, vol. 14, no. (1), pp. 37–48., 2000.
- [75] V. Lanaerts, G. Kerschen, and J. C. Golinval, "Parameter identification of nonlinear mechanical systems using proper orthogonal decomposition," in *Proceedings of the IMAC XVIII*, (San Antonio.), 2000.
- [76] K. Karhunen, "Zur Spektral Theorie Stochastischer Prozesse," *Ann. Acad. Sci. Fennicae*, vol. A, pp. 1–34, 1946.
- [77] M. Loeve, *Probability Theory*. Princeton, NJ: Van Nostrand, 1955.
- [78] D. Kosambi, "Statistics in function space," *Journal of Indian Mathematical Society*, vol. 7, pp. 76–88, 1943.
- [79] K. Pearson, "On lines and planes of closest fit to systems of points in space," *Philosophical Magazine*, vol. 2, no. 6, pp. 559–572, 1901.
- [80] V. Klema and A. Laub, "The singular value decomposition: Its computation and some applications," *IEEE Transactions on Automatic Control*, vol. 25, no. 2, pp. 164–176, 1980.
- [81] Y. C. Liang, H. P. Lee, S. P. Lim, W. Z. Lin, K. H. Lee, and C. G. Wu, "Proper orthogonal decomposition and its applications—part 1: Theory," *Journal of Sound and Vibration*, vol. 252(3), pp. 527–544, 2002.

- [82] N. Aubry, R. Guyonnet, and R. Lima, "Spatiotemporal analysis of complex signals: Theory and applications," *Journal of Statistical Physics*, vol. 64, no. (3-5), pp. 683–739, 1991.
- [83] T. D. Dewit, A. L. Pecquet, and J. C. Vallet, "The biorthogonal decomposition as a tool for investigation fluctuations in plasmas," *Physics of Plasmas*, vol. 1, no. 10, pp. 3288–3300, 1994.
- [84] B. F. Feeny and R. Kappagantu, "On the physical interpretation of proper orthogonal modes in vibrations," *Journal of Sound and Vibration*, vol. 211, no. 4, pp. 607–616, 1998.
- [85] B. F. Feeny, "On proper orthogonal coordinates as indicators of modal activity," *Journal of Sound and Vibration*, vol. 255, no. 5, pp. 805–817., 2002.
- [86] S. Han and B. F. Feeny, "Application of proper orthogonal decomposition to structural vibration analysis," *Mechanical Systems and Signal Processing*, vol. 17, no. (5), pp. 989–1001., 2003.
- [87] G. Kerschen and J. C. Golinval, "Physical interpretation of the proper orthogonal modes using the singular value decomposition," *Journal of Sound and Vibration*, vol. 249, no. 5, pp. 849–865., 2002.
- [88] U. Iemma, L. Morino, and M. Diez, "Digital holography and karhunen-loeve decomposition for the modal analysis of two-dimensional vibrating structures," *Journal of Sound and Vibration*, vol. 291, pp. 107–131, 2006.
- [89] B. F. Feeny and Y. Liang, "Interpreting proper orthogonal modes in randomly excited vibration systems," *Journal of Sound and Vibration*, vol. 265, no. 5, pp. 953–966., 2003.
- [90] B. F. Feeny, "A complex orthogonal decomposition for wave motion analysis," *Journal of Sound and Vibration*, vol. 310, pp. 77–90, Feb 2008.
- [91] A. V. Oppenheim and R. W. Schaffer, *Discrete-Time Signal Processing*. Prentice Hall, Englewood Cliffs, NJ., 1989.
- [92] J. Cooley and J. Tukey, "An algorithm for the machine calculation of complex fourier series," *Math. Computation*, vol. 19, pp. 297–301, 1965.
- [93] R. Gilmore and M. Lefranc, *The Topology of Chaos*. Wiley, New York., 2002.
- [94] I. T. Georgiou and C. I. Papadopoulos, "Developing pod over the complex plane to form a data processing tool for finite element simulations of steady state structural dynamics," in *International Mechanical Engineering Congress and Exposition*, p. on DVD ROM, November 5-10 2006.

- [95] D. Chelidze and W. Zhou, "Smooth orthogonal decomposition-based vibration mode identification," *Journal of Sound and Vibration*, vol. 292, pp. 461–473, 2006.
- [96] W. Zhou and D. Chelidze, "Blind source separation based vibration mode identification," *Mechanical systems and signal processing*, vol. 21, pp. 3072–3087, Feb 2007.
- [97] D. Chelidze and M. Liu, "Dynamical systems approach to fatigue damage identification," *Journal of Sound and Vibration*, vol. 281, no. 3–5, pp. 887–904, 2005.
- [98] D. Chelidze and M. Liu, "Multidimensional damage identification based on phase space warping: An experimental study," *Nonlinear Dynamics*, vol. 46, pp. 61–72, Oct 2006.
- [99] W. Zhou and D. Chelidze, "Generalized eigenvalue decomposition in time domain modal parameter identification," *Journal of Vibration and Acoustics*, vol. 130, pp. 1–6, Feb 2008.
- [100] B. F. Feeny and U. Farooq, "A nonsymmetric state-variable decomposition for modal analysis," *Journal of Sound and Vibration*, vol. 310, pp. 792–800, March 2008.
- [101] B. F. Feeny and U. Farooq, "A state-variable decomposition method for estimating modal parameters," in *ASME International Design Engineering Technical Conferences*, Sep 2007.
- [102] U. Farooq and B. F. Feeny, "Smooth orthogonal decomposition for randomly excited systems," *Journal of Sound and Vibration*, vol. 316, pp. 137–146, Sep 2008.
- [103] L. Rayleigh, *The Theory of Sound*, vol. 1. New York: reprinted by Dover 1945, 1877.
- [104] T. K. Caughey, "Classical normal modes in damped linear systems.," *Journal of Applied Mechanics*, vol. 27, pp. 269–271, 1960. Transactions of the ASME 82, series E.
- [105] L. Meirovitch, *Principles and Techniques of Vibrations*. NewYork: Prentice Hall., 1997.
- [106] J. Ginsberg, *Mechanical and Structural Vibrations*,. Wiley, New York., 2001.

- [107] G. James, T. Carne, and J. Lauffer, "The natural excitation technique (next) for modal parameter extraction from operating structures," *International Journal of Analytical and Experimental Modal Analysis*, vol. 10, pp. 260–277, Oct 1995.
- [108] C. R. Farrar and G. H. James III, "System identification from ambient vibration measurements on a bridge," *Journal of Sound and Vibration*, vol. 205, no. 1, pp. 1–18, 1997.
- [109] J. Dormand and P. Prince, "A family of embedded runge-kutta formulae," *Journal of Computational and Applied Mathematics*, vol. 6, pp. 19–26, 1980.
- [110] R. J. Allemang and D. Brown, "A correlation coefficient for modal vector analysis," in *Proceedings, International Modal Analysis Conference*, pp. 110–116, 1982.
- [111] R. Allemang, "The modal assurance criterion twenty years of use and abuse," *Sound and Vibration*, vol. August, pp. 14–21, 2003.
- [112] S. Han and B. F. Feeny, "Enhanced proper orthogonal decomposition for the modal analysis of homogeneous structures," *Journal of Vibration and Control*, vol. 8, no. (1), pp. 19–40., 2002.
- [113] J. S. Bendat and A. G. Piersol, *Random Data : Analysis and Measurement Procedures*. New York: John Wiley & Sons, 1971.
- [114] J. S. Bendat and A. G. Piersol, *Random Data : Analysis and Measurement Procedures*. New York: John Wiley & Sons, 2nd ed., 1986.
- [115] T. Kailath, *Linear Systems*. Englewood Cliffs, NJ: Prentice Hall, 1980.
- [116] W. J. Rugh, *Linear System Theory*. Englewood Cliffs, NJ: Prentice Hall, 2 ed., 1995.
- [117] C.-T. Chen, *Linear System Theory and Design*. New York: Oxford University Press, 3rd ed., Aug 1998.
- [118] S. Skogestad and I. Postlethwaite, *Multivariable Feedback Control: Analysis and Design*. New York: John Wiley and Sons, Sep 2005.
- [119] H. K. Khalil, *Nonlinear Systems*. Upper Saddle River, New Jersey: Prentice Hall, 3rd ed., 2002.
- [120] J. S. Bendat and A. G. Piersol, *Engineering Applications Of Correlation And Spectral Analysis*. New York: John Wiley & Sons, 1980.
- [121] P. J. Antsaklis and A. J. Michel, *Linear Systems*. New York: Birkhäuser, 2006.

- [122] J. F. Rhoads, N. J. Miller, S. W. Shaw, and B. F. Feeny, "Mechanical domain parametric amplification," in *ASME International Design Engineering Technical Conferences*, pp. DvD -ROM, 2007.
- [123] J. Dally and W. Riley, *Experimental Stress Analysis*. Knoxville,TN: College House Enterprise, 1991.
- [124] B. F. Feeny and J. W. Liang, "A decrement method for the simultaneous estimation of coulomb and viscous friction," *Journal of Sound and Vibration*, vol. 195, no. 1, pp. 149–154, 1996.
- [125] W. T. Thomson and M. D. Dahleh, *Theory of Vibration with Applications*. Upper Saddle River, NJ: Prentice Hall, 1998.
- [126] B. Balachandran and E. Magrab, *Vibrations*. Belmont, CA: Thomson Brooks/Cole, 2004.
- [127] F. Bazán, "Eigensystem realization algorithm (era): reformulation and system pole perturbation analysis," *Journal of Sound and Vibration*, vol. 274, pp. 433–444, July 2004.
- [128] J.-N. Juang, "Mathematical correlation of modal parameter identification methods via system realization theory," *International journal of analytical and experimental modal analysis*, vol. 2, no. 1, pp. 1–18, 1987.
- [129] J. N. Juang and H. Suzuki, "An eigensystem realization in frequency domain for modal parameter identification," *Journal of Vibration, Acoustic, Stress, and Reliability in design*, vol. 110, no. 1, pp. 24–29, 1988.
- [130] J.-N. Juang and R. Pappa, "A comparative overview of modal testing and system identification for control of structures," *Shock and Vibration Digest*, vol. 20, no. 5, pp. 4–15, 1988.
- [131] J.-N. Juang, J. E. Cooper, and J. R. Wright, "An eigensystem realization algorithm using data correlations (ERA/DC) for modal parameter identification," *Contrl theory and advanced technology*, vol. 4, no. 1, pp. 5–14, 1988.
- [132] B. L. Ho and R. E. Kalman, "Effective contruction of linear state-variable models from input/output data," *Regelungestechnik*, vol. 14, pp. 545–548, 1966.
- [133] J.-N. Juang, M. Phan, L. Horta, and R. Longman, "Identification of observer/kalman filter markov parameters: Theory and experiments," *Journal of Guidance, Control, and Dynamics*, vol. 16, no. 2, pp. 320–329, 1993.

- [134] M. Phan, L. Horta, J.-N. Juang, and R. Longman, "Improvement of observer/kalman filter identification (okid) by residual whitening," *Journal of Vibrations and Acoustics*, vol. 117, pp. 232–239, 1995.
- [135] R. K. Lim, M. Q. Phan, and L. R. W., "State-space system identification with identified hankel matrix," Tech. Rep. Technical Report No.3045,, Department of Mechanical and Aerospace Engineering, Princeton University,, Princeton, NJ., 1998.
- [136] B. Feeny and R. Kappagantu, "On the physical interpretation of proper orthogonal modes in vibrations," *Journal of Sound and Vibration*, vol. 211, no. 4, pp. 607–616, 1998.
- [137] U. Farooq and B. . F. Feeny, "Output-only modal analysis of randomly excited systems using smooth orthogonal decomposition," in *1st Annual Dynamic Systems and Control Conference*, (Ann Arbor, Michigan, USA), October 20-22 2008.
- [138] E. Kreyszig, *Advanced Engineering Mathematics*. John Wiley & Sons, 9th ed., 2006.
- [139] B. V. der Pol, "A theory of the amplitude of free and forced triode vibrations," *Radio Review*, vol. 1, pp. 754–762, 1920.

MICHIGAN STATE UNIVERSITY LIBRARIES



3 1293 03063 2800